UNIVERSITY OF CALIFORNIA SAN DIEGO

Characterizing the Organic Composition of Marine Aerosol from the North Atlantic to the Oceano Dunes

A Dissertation submitted in partial satisfaction of the requirements
for the degree Doctor of Philosophy

in

Oceanography

by

Savannah L. Lewis

Committee in charge:

Professor Lynn M. Russell, Chair
Professor Lihini I. Aluwihare Co-Chair
Professor Andrew E. Allen
Professor Andrew C. Kummel
Professor Greg C. Roberts

2022

The Dissertation of Savannah L. Lewis is approved, and it is acceptable in quality and form for publication on microfilm and electronically.

University of California San Diego

2022

DEDICATION

This doctoral dissertation is dedicated to my husband, Erin Patrick Lewis. Your encouragement, constant supply of tea, and unwavering belief in my abilities has been instrumental in my academic journey.

TABLE OF CONTENTS

LIST OF FIGURES

LIST OF TABLES

ACKNOWLEDGEMENTS

First, I would like to thank Professor Lynn Russell for her guidance and mentorship as my graduate advisor and thesis chair. I appreciate the countless hours that have been spent teaching me how to be a scientist and editing many drafts of my papers. These will be lessons I carry throughout my career. I would like to thank the previous and present members of the Russell group, as well as the many collaborators I have had the pleasure of working with for their assistance, comradery, guidance, and support. Lastly, I thank my family and friends for their steadfast support and encouragement.

Chapter 1, in full, is a reprint of the material as it appears in *Frontiers in Marine Science* 2021. Lewis, S.L.; G. Saliba, L.M. Russell, P.K. Quinn, T.S. Bates, M.J. Behrenfeld, 2021 "Seasonal Differences in Submicron Marine Aerosol Particle Organic Composition in the North Atlantic". *8,* doi:10.3389/fmars.2021.720208. The dissertation author was the primary investigator and author of this paper.

Chapter 2, in full, has been submitted for publication to *American Chemical Society: Earth and Space Chemistry.* Lewis, S. L., L.M. Russell, G. Saliba, P.K. Quinn, T.S. Bates, C.A. Carlson, N. Baetge, L.I. Aluwihare, E. Boss, A.A. Frossard, T.G. Bell, and M.J. Behrenfeld, (2022). "Characterization of Sea Surface Microlayer and Marine Aerosol Organic Composition using STXM-NEXAFS Microscopy and FTIR Spectroscopy". *American Chemical Society: Earth and Space Chemistry* (In Review). The dissertation author was the primary investigator and author of this paper.

Chapter 3, in full has been submitted for publication to *Atmospheric Environment.* Lewis, S.L.; L.M. Russell; J.A. McKinsey, W.J. Harris, (2022) *Atmospheric Environment*

“Contributions of Dust and Other Chemical Components to PM2.5 and PM10 Concentrations at Oceano Dunes”. The dissertation author was the primary researcher and author of this material.

VITA

2016 B.S. in Biochemistry, *magna cum laude,* California State University, Fullerton

2017 Graduate Teaching Assistant, University of California, San Diego

2022 Ph.D. in Oceanography, University of California, San Diego

PUBLICATIONS

Lewis, S. L., L.M. Russell, G. Saliba, P.K. Quinn, T.S. Bates, C.A. Carlson, N. Baetge, L.I. Aluwihare, E. Boss, A.A. Frossard, T.G. Bell, and M.J. Behrenfeld (in review), Characterization of Sea Surface Microlayer and Marine Aerosol Organic Composition using STXM-NEXAFS Microscopy and FTIR Spectroscopy, *American Chemical Society: Earth and Space Chemistry*

Lewis, S.L.; L.M. Russell; J.A. McKinsey, W.J. Harris (in review), Contributions of Dust and Other Chemical Components to PM2.5 and PM10 Concentrations at Oceano Dunes, *Atmospheric Environment*

Lewis, S.L., G. Saliba, L. M. Russell, P. K. Quinn, T. S. Bates, and M. J. Behrenfeld (2021), Seasonal Differences in Submicron Marine Aerosol Particle Organic Composition in the North Atlantic, *Frontiers in Marine Science*, *8*, doi:10.3389/fmars.2021.720208

Lawler, M. J., **S.L. Lewis**, L. M. Russell, P. K. Quinn, T. S. Bates, D. J. Coffman, L. M. Upchurch, and E. S. Saltzman (2020), North Atlantic marine organic aerosol characterized by novel offline thermal desorption mass spectrometry: polysaccharides, recalcitrant material, and secondary organics, *Atmos. Chem. Phys.*, *20*(24), 16007-16022, doi:10.5194/acp-20-16007-2020.

Saliba, G., C. Chen, **S.L. Lewis**, L. Russell, L.H. Rivellini, A.K.Y. Lee, P.K. Quinn, T.S. Bates, N. Haëntjens, E.S. Boss, L. Karp-Boss, N. Baetge, C.A. Carlson, M.J. Behrenfeld. (2019), Factors driving the seasonal and hourly variability of sea-spray aerosol number in the North Atlantic, *Proceedings of the National Academy of Sciences*, 116(41), 20309, doi:10.1073/pnas.1907574116.

Saliba, G., C. Chen, **S.L. Lewis**, L. Russell, P.K. Quinn, T.S. Bates, T.G. Bell, M.J. Lawler, E.S. Saltzman, K.J. Sanchez, R. Moore, M. Shook, L.H. Rivellini, A.K.Y. Lee, N. Baetge, C.A. Carlson, M.J. Behrenfeld. (2020), Seasonal Differences and Variability of Concentrations, Chemical Composition, and Cloud Condensation Nuclei of Marine Aerosol Over the North Atlantic, *Journal of Geophysical Research: Atmospheres*, 125(19), e2020JD033145, doi:10.1029/2020JD033145.

Saliba, G., K.J. Sanchez, L. Russell, C.H. Twohy, G.C. Roberts, **S.L. Lewis**, J. Dedrick, C.S. McCluskey, K. Moore, P.J. DeMott, D.W. Toohey (2021), Organic composition of three different size ranges of aerosol particles over the Southern Ocean, *Aerosol Science and Technology*, 55(3), 268-288, doi:10.1080/02786826.2020.1845296.

Sanchez, K. J., B. Zhang, H. Liu, G. Saliba, C. Chen, **S.L. Lewis**, L.M. Russell, M.A. Shook, E.C. Crosbie, L.D. Ziemba, M.D. Brown, T.J. Shingler, C.E. Robinson, E.B. Wiggins, K.L. Thornhill, E.L. Winstead, C. Jordan, P.K. Quinn, T.S. Bates, J. Porter, T.G. Bell, E.S. Saltzman, M.J. Behrenfeld, R.H. Moore (2021), Linking marine phytoplankton emissions, meteorological processes, and downwind particle properties with FLEXPART, *Atmos. Chem. Phys.*, 21(2), 831-851, doi:10.5194/acp-21-831-2021.

Bates, T. S., P. K. Quinn, D. J. Coffman, J. E. Johnson, L. Upchurch, G. Saliba, **S.L. Lewis**, J. Graff, L. M. Russell, and M. J. Behrenfeld (2020), Variability in Marine Plankton Ecosystems Are Not Observed in Freshly Emitted Sea Spray Aerosol Over the North Atlantic Ocean, *Geophysical Research Letters*, 47(1), e2019GL085938, doi:10.1029/2019GL085938.

Twohy, C. H., P.J. DeMott, L.M. Russell, D.W. Toohey, B. Rainwater, R. Geiss, K.J. Sanchez, **S.L. Lewis**, G.C. Roberts, R.S. Humphries, C.S. McCluskey, K.A. Moore, P.W. Selleck, M.D. Keywood, J.P. Ward, I.M. McRobert. (2021), Cloud-Nucleating Particles Over the Southern Ocean in a Changing Climate, *Earth's Future*, *9*(3), e2020EF001673, doi: 10.1029/2020EF001673.

Sanchez, K. J., B. Zhang, H. Liu, M.D. Brown, E.C. Crosbie, F. Gallo, J.W. Hair, C.A. Hostetler, C.E. Jordan, C.E. Robinson, A.J. Scarino, T.J. Shingler, M.A. Shook, K.L. Thornhill, E.B. Wiggins, E.L. Winstead, L.D. Ziemba, G. Saliba, **S.L. Lewis**, L.M. Russell, P.K. Quinn, T.S. Bates, J. Porter, T.G. Bell, P. Gaube, E.S. Saltzman, M.J. Behrenfeld, R.H. Moore (2022), North Atlantic Ocean SST-gradient-driven variations in aerosol and cloud evolution along Lagrangian cold-air outbreak trajectories, *Atmos. Chem. Phys.*, *22*(4), 2795-2815, doi:10.5194/acp-22-2795-2022.

ABSTRACT OF THE DISSERTATION

Characterizing the Composition and Source of Marine Aerosol from the North Atlantic to the Dunes of Pismo Beach

by

Savannah L. Lewis

Doctor of Philosophy in Oceanography

University of California San Diego, 2022

Professor Lynn M. Russell, Chair
Professor Lihini I. Aluwihare, Co-Chair

Atmospheric aerosol particles in the marine environment play an important role in the Earth's radiative budget which are affected by the sources and compositions of the aerosol particles. Atmospheric aerosol particles were collected over four cruises in the remote regions of the North Atlantic Ocean and one field experiment from a stationary platform in the Oceano Dunes and were quantified using Fourier Transform Infrared (FTIR) spectroscopy and Scanning Transmission X-Ray Microscopy with Near-Edge Absorption Fine Structure (STXM-NEXAFS) for organic functional groups. X-ray fluorescence (XRF) analyses were used to understand the elemental composition of the Oceano Dunes samples. The four cruises' atmospheric primary marine aerosol (aPMA) organic functional group composition was compared to see whether seasonal and biological changes had an effect. The average composition was 78% hydroxyl, 10%

alkane, 6% amine, and 7% carboxylic acid groups, which was consistent with previous marine studies with sources including marine saccharides and amino sugars. The standard deviation within each season was greater than the differences between seasons, showing a limited seasonal response in the organic fraction. Generated primary marine aerosol particles (gPMA), atmospheric aerosol particles, sea-surface microlayer samples, and seawater samples were collected to compare the particle and bulk organic compositional differences as organics rise through the water column and are ejected into the marine boundary layer. The bulk organic composition consisted of the same three organic functional groups (hydroxyl, alkane, and amine groups) that comprised 50-90% of the quantified organic mass, though STXM-NEXAFS did illuminate the particle-to-particle diversity in all sample sources. The sea-surface microlayer and atmospheric aerosol particles were found to have far more variability in composition than generated primary marine aerosol and seawater, which could be attributed to a closer linkage between the organic sources and greater secondary processing within these sample sources than either generated primary marine aerosol or seawater. Coastal aerosol from Oceano Dunes showed a mixture of sources, with the dominant sources being wind-driven dust from the Oceano Dunes, sea salt from sea spray, and marine-derived organics. While this coastal location has recorded PM10 exceedances, the natural sources are unlikely to be a health-risk because they have not been shown to include toxic components.

Introduction

Aerosol particles, solid or liquid particles suspended in air, play an important role in the global radiative balance and influence atmospheric properties in a variety of ways including absorbing and scattering solar radiation directly (Yu et al., 2006) and acting as a nucleating source for water vapor (Lohmann & Feichter, 2005; Twomey, 1974). Marine aerosol particles are particularly important to study due to the large effect the ocean has on regulating the energy budget and encompassing over 70% of the earth's surface. Organic components, mixed with salt, in atmospheric marine aerosol particles (aMA) (Blanchard, 1964) can reduce the cooling effect (Randles, Russell, & Ramaswamy, 2004). The composition of the organic components plays a role in the hygroscopicity of the particle and, ultimately, how the cloud interacts with solar radiation. Due to marine clouds having a significant effect on the global radiative balance, it is critical to understand the composition of marine aerosol.

The composition of aerosol particles is controlled by the source and atmospheric processing that occurs after emission (Russell, Bahadur, & Ziemann, 2011). Quantifying the organic composition of aMA and identifying the sources is important to better understand and predict aerosol climate forcing, which still has a large amount of uncertainty. Primary marine aerosol, PMA, are defined as particles that are directly emitted from the ocean prior to undergoing chemical reactions. Crashing surface waves create bubbles by entrapping air that proceeds to rise as bubbles. Organic components from biological activity can become incorporated into the surface of newly created bubbles, resulting in a layer of organic compounds that can affect particle formation and CCN properties (Cunliffe et al., 2013; Engel et al., 2017; Long et al., 2014). Once the bubbles reach the sea surface, they burst and produce two types of

droplets: small film droplets, enriched in organic material, and larger jet droplets that contain mostly sea salt in addition to a smaller fraction of organic components (Wang et al., 2017; Woolf, Bowyer, & Monahan, 1987). The organic film on the ocean surface, known as the microlayer, may play a critical role in the atmospheric chemistry and affects both particle formation and composition (Adamson & Gast, 1990; E. R. Lewis & Schwartz, 2004; Long et al., 2014; Modini, Russell, Deane, & Stokes, 2013). The composition of particles can change as they travel through the water column and are ejected by bubble bursting.

Phytoplankton and their by-products are a large component of primary sea spray in remote ocean regions (E. R. Lewis & Schwartz, 2004). As ocean conditions continue to change, it is likely that the phytoplankton populations may change and impact the resulting aerosol properties. Diatoms, one of the most common type of phytoplankton, have decreased at a rate of 1% from 1998 to 2012 globally (Rousseaux & Gregg, 2015). It is also plausible that heterotrophic bacteria are driving the organic enrichment in particles, as seen in Prather et al. (2013), which could be why there are so many mixed results from using chlorophyll-a as a proxy for phytoplankton activity (O'Dowd et al., 2015; Quinn et al., 2014; Schwier et al., 2017). Many have studied the chemical and biological relationships individually, however there are few measurements that allows explicit comparison of the changing phytoplankton populations and the chemical composition of the resulting aerosol particles.

Aerosol particles not only have an impact on climate, but they can impact human health by decreasing air quality and decreasing the average human lifespan (Dockery et al., 1993; Pope, Ezzati, & Dockery, 2009). The Environmental Protection Agency (EPA) and other regulatory bodies regulates PM2.5 and PM10 concentrations (EPA, 2022), however it is well-established that the toxicity of the particles varies with its composition (Duan, Tan, Wang, Hao, & Chail,

2012; Seagrave et al., 2006). In particular, rural locations have been shown to have less toxic particles than urban locations that have a higher concentration of combustion by-products (Duan et al., 2012; Lighty, Veranth, & Sarofim, 2000; Rogula-Kozłowska et al., 2014). It is important for aerosol particles to be chemically speciated so that the source can be identified and, therefore, toxicity can be understood, rather than assuming the same toxicity of all measured compounds, as is common practice in governmental regulations.

Chapter 1 presents measurements of ambient atmospheric and generated aerosol particles from four research cruises in the North Atlantic Ocean during the four seasons to capture the different phytoplankton phases. The seasonality of both atmospheric primary marine aerosol particles and generated primary marine aerosol particles showed more variability within each season than between seasons, which shows the influence of a consistent seawater organic source (S. Lewis et al., 2021).

Chapter 2 presents measurements of seawater, generated primary marine aerosol, seawater microlayer, and ambient atmospheric aerosol that were collected during two of the research cruises in the North Atlantic Ocean to investigate how organics are transferred from the ocean to the marine atmosphere. FTIR and STXM-NEXAFS measurements showed the organics between the seawater microlayer and ambient atmospheric aerosol appear to be more closely linked than seawater and generated primary marine aerosol.

Chapter 3 presents measurements of atmospheric aerosol at the Oceano Dunes to identify the sources and composition to help inform local policy. The major sources appeared to be wind-driven dust from the sand dunes and both salts and organics from sea spray with an unidentified source likely an artifact of the state's instrumentation susceptibility to semivolatiles.

Together, this work investigates how the organic composition of marine aerosol changes with regards to season, atmospheric processing, production mechanism, and whether the marine ecosystem affects this relationship. The coastal study found a more diverse range of sources, though the most substantial influence on the organic composition was marine. The composition and sources of atmospheric marine aerosol are summarized in the conclusion section, where future studies that could help improve our understanding of the complex relationship between marine aerosol and the ocean are discussed.

References

Adamson, A. W., & Gast, A. P. (1990). *Physical Chemistry of Surfaces*: Wiley.

Blanchard, D. C. (1964). Sea-to-Air Transport of Surface Active Material. *Science, 146*(3642), 396. doi:10.1126/science.146.3642.396

Cunliffe, M., Engel, A., Frka, S., Gašparović, B., Guitart, C., Murrell, J. C., . . . Wurl, O. (2013). Sea surface microlayers: A unified physicochemical and biological perspective of the air–ocean interface. *Progress in Oceanography, 109*, 104-116. doi:https://doi.org/10.1016/j.pocean.2012.08.004

Dockery, D. W., Pope, C. A., Xu, X., Spengler, J. D., Ware, J. H., Fay, M. E., . . . Speizer, F. E. (1993). An Association between Air Pollution and Mortality in Six U.S. Cities. *New England Journal of Medicine, 329*(24), 1753-1759. doi:10.1056/nejm199312093292401

Duan, J. C., Tan, J. H., Wang, S. L., Hao, J. M., & Chail, F. H. (2012). Size distributions and sources of elements in particulate matter at curbside, urban and rural sites in Beijing. *Journal of Environmental Sciences, 24*(1), 87-94. doi:10.1016/s1001-0742(11)60731-6

Engel, A., Bange, H. W., Cunliffe, M., Burrows, S. M., Friedrichs, G., Galgani, L., . . . Zäncker, B. (2017). The Ocean's Vital Skin: Toward an Integrated Understanding of the Sea Surface Microlayer. *Frontiers in Marine Science, 4*. doi:10.3389/fmars.2017.00165

EPA. (2022). Summary of the Clean Air Act. Retrieved from https://www.epa.gov/laws-regulations/summary-clean-air-act

Lewis, E. R., & Schwartz, S. E. (2004). *Sea Salt Aerosol Production: Mechanisms, Methods, Measurements, and Models - A Critical Review*. Washington, D.C.: AGU.

Lewis, S., Saliba, G., Russell, L., Quinn, P., Bates, T., & Behrenfeld, M. (2021). Seasonal Differences in Submicron Marine Aerosol Particle Organic Composition in the North Atlantic. *Frontiers in Marine Science, 8*. doi:10.3389/fmars.2021.720208

Lighty, J. S., Veranth, J. M., & Sarofim, A. F. (2000). Combustion aerosols: Factors governing their size and composition and implications to human health. *Journal of the Air & Waste Management Association, 50*(9), 1565-1618. doi:10.1080/10473289.2000.10464197

Lohmann, U., & Feichter, J. (2005). Global indirect aerosol effects: a review. *Atmos. Chem. Phys., 5*(3), 715-737. doi:10.5194/acp-5-715-2005

Long, M. S., Keene, W. C., Kieber, D. J., Frossard, A. A., Russell, L. M., Maben, J. R., . . . Bates, T. S. (2014). Light-enhanced primary marine aerosol production from biologically productive seawater. *Geophysical Research Letters, 41*(7), 2661-2670. doi:10.1002/2014gl059436

Modini, R. L., Russell, L. M., Deane, G. B., & Stokes, M. D. (2013). Effect of soluble surfactant on bubble persistence and bubble-produced aerosol particles. *Journal of Geophysical Research-Atmospheres, 118*(3), 1388-1400. doi:10.1002/jgrd.50186

O'Dowd, C., Ceburnis, D., Ovadnevaite, J., Bialek, J., Stengel, D. B., Zacharias, M., . . . Danovaro, R. (2015). Connecting marine productivity to sea-spray via nanoscale biological processes: Phytoplankton Dance or Death Disco? *Scientific Reports, 5*(1), 14883. doi:10.1038/srep14883

Pope, C. A., Ezzati, M., & Dockery, D. W. (2009). Fine-Particulate Air Pollution and Life Expectancy in the United States. *New England Journal of Medicine, 360*(4), 376-386. doi:10.1056/nejmsa0805646

Prather, K. A., Bertram, T. H., Grassian, V. H., Deane, G. B., Stokes, M. D., DeMott, P. J., . . . Zhao, D. (2013). Bringing the ocean into the laboratory to probe the chemical complexity of sea spray aerosol. *Proceedings of the National Academy of Sciences of the United States of America, 110*(19), 7550-7555. doi:10.1073/pnas.1300262110

Quinn, P. K., Bates, T. S., Schulz, K. S., Coffman, D. J., Frossard, A. A., Russell, L. M., . . . Kieber, D. J. (2014). Contribution of sea surface carbon pool to organic matter enrichment in sea spray aerosol. *Nature Geoscience, 7*(3), 228-232. doi:10.1038/ngeo2092

Randles, C., Russell, L., & Ramaswamy, V. (2004). Hygroscopic and optical properties organic sea salt aerosol and consequences for climate forcing. *Geophys. Res. Lett, 31*. doi:10.1029/2004GL020628

Rogula-Kozłowska, W., Klejnowski, K., Rogula-Kopiec, P., Ośródka, L., Krajny, E., Błaszczak, B., & Mathews, B. (2014). Spatial and seasonal variability of the mass concentration and chemical composition of PM2.5 in Poland. *Air Quality, Atmosphere & Health, 7*(1), 41-58. doi:10.1007/s11869-013-0222-y

Rousseaux, C. S., & Gregg, W. W. (2015). Recent decadal trends in global phytoplankton composition. *Global Biogeochemical Cycles, 29*(10), 1674-1688. doi:10.1002/2015GB005139

Russell, L. M., Bahadur, R., & Ziemann, P. J. (2011). Identifying organic aerosol sources by comparing functional group composition in chamber and atmospheric particles. *Proceedings of the National Academy of Sciences, 108*(9), 3516. doi:10.1073/pnas.1006461108

Schwier, A. N., Sellegri, K., Mas, S., Charrière, B., Pey, J., Rose, C., . . . D'Anna, B. (2017). Primary marine aerosol physical flux and chemical composition during a nutrient enrichment experiment in mesocosms in the Mediterranean Sea. *Atmos. Chem. Phys., 17*(23), 14645-14660. doi:10.5194/acp-17-14645-2017

Seagrave, J., McDonald, J. D., Bedrick, E., Edgerton, E. S., Gigliotti, A. P., Jansen, J. J., . . . Mauderly, J. L. (2006). Lung Toxicity of Ambient Particulate Matter from Southeastern

U.S. Sites with Different Contributing Sources: Relationships between Composition and Effects. *Environmental Health Perspectives, 114*(9), 1387-1393. doi:doi:10.1289/ehp.9234

Twomey, S. (1974). Pollution and the planetary albedo. *Atmospheric Environment (1967), 8*(12), 1251-1256. doi:10.1016/0004-6981(74)90004-3

Wang, X., Deane, G. B., Moore, K. A., Ryder, O. S., Stokes, M. D., Beall, C. M., . . . Prather, K. A. (2017). The role of jet and film drops in controlling the mixing state of submicron sea spray aerosol particles. *Proceedings of the National Academy of Sciences, 114*(27), 6978-6983. doi:10.1073/pnas.1702420114

Woolf, D. K., Bowyer, P. A., & Monahan, E. C. (1987). Discriminating between the film drops and jet drops produced by a simulated whitecap. *Journal of Geophysical Research: Oceans, 92*(C5), 5142-5150. doi:https://doi.org/10.1029/JC092iC05p05142

Yu, H., Kaufman, Y. J., Chin, M., Feingold, G., Remer, L. A., Anderson, T. L., . . . Zhou, M. (2006). A review of measurement-based assessments of the aerosol direct radiative effect and forcing. *Atmospheric Chemistry and Physics, 6*(3), 613-666. doi:10.5194/acp-6-613-2006

Chapter 1 Seasonal Differences in Submicron Marine Aerosol Particle Organic Composition in the North Atlantic

Submicron atmospheric primary marine aerosol (aPMA) were collected during four North Atlantic Aerosol and Marine Ecosystem Study (NAAMES) research cruises between November 2015 and March 2018. The average organic functional group (OFG) composition of the aPMA samples was 72-85% hydroxyl group mass, 6-13% alkane group mass, and 5-8% amine group mass, which is similar to prior observations and to aerosol generated from Sea Sweep. The carboxylic acid group had seasonal averages that ranged from 1% for Winter, 8% for Late Spring, and 10% for Autumn. The carboxylic acid group mass concentration correlated with nitrate mass concentration and weakly with PAR above 100 W m^{-2}, suggesting a substantial secondary organic aerosol contribution in sunnier months. The three sizes of aPMA aerosol particles (<0.18, <0.5, and <1 μm) had the same four organic functional groups (hydroxyl, alkane, amine, and carboxylic acid groups). The aPMA spectra of the three sizes showed more variability (higher standard deviations of cosine similarity) within each size than between the sizes. The ratio of organic mass (OM) to sodium (OM/Na) of submicron generated primary marine aerosol (gPMA) was larger for Autumn with project average of 0.93 ± 0.3 compared to 0.55 ± 0.27 for Winter, 0.47 ± 0.16 for Late Spring, and 0.53 ± 0.24 for Early Spring. When the gPMA samples were separated by latitude (47 - 60N and 18 - 47N), the median OM/Na concentration ratio for Autumn was higher than the other seasons by more than the project

standard deviations for latitudes north of 47N but not for those south of 47N, indicating that the seasonal differences are stronger at higher latitudes. However, the high variability of day-to-day differences in aPMA and gPMA composition within each season meant that seasonal trends in organic composition were generally not statistically distinguishable.

1.1 Introduction

Composition of the organic components of atmospheric marine aerosol (aMA) particles can influence aerosol direct and indirect effects on radiative budgets (Tsigaridis, Koch, & Menon, 2013). This influence makes the quantification of the organic fraction an important property for accurately modeling aerosol effects in the marine environment (Randles, Russell, & Ramaswamy, 2004). Sea spray aerosol is a mixture of water and sea salt and contains a significant fraction of organic material (Blanchard, 1964). The composition and concentration of the organic mass (OM) can vary between different ocean basins and seasons (S. Liu et al., 2021), but observations constraining these seasonal differences are rare (Saliba et al., 2020).

There are a few coastal sites with multiple seasons of observations of organic aerosol mass concentrations and one of the most studied is Mace Head, a coastal site in the eastern North Atlantic. Three years of continuous measurements showed that the aerosol non-refractory organic mass observed in polar air masses arriving at Mace Head is highest in summer (0.36 μg m^{-3}) and reaches a minimum in winter (0.05 μg m^{-3}) (Ovadnevaite et al., 2014). At the same site, the organic mass fraction of submicron marine aerosol varied from 15% during low chlorophyll periods (winter) to 63% during high chlorophyll periods (spring through autumn) (O'Dowd et al., 2004). Sea salt was the largest signal, regardless of chlorophyll concentrations, in sizes larger than 1 μm, but the organic fraction was consistently the largest component in the smaller sizes. During high chlorophyll periods, the organic signal was up to 80% of the total mass for particles <0.25 μm diameter (O'Dowd et al., 2004).

Biological activity (often represented by chlorophyll-*a* (Chl *a*) concentration) has been shown to covary with the organic composition of seawater (Carlson, Ducklow, & Michaels, 1994; Collins et al., 2013; Gaston et al., 2011; Prather et al., 2013; Rinaldi et al., 2013; Wang et al., 2015), but the extent to which these changes are reflected in ambient sea spray composition is an open question (Meskhidze et al., 2013). Actively bubbling seawater during open ocean studies provides one technique for linking seawater properties to emitted sea spray aerosol (Bates et al., 2012; Keene et al., 2007). Sea Sweep (Bates et al., 2012) is a commonly deployed seawater bubbling system and, here, we refer to aerosol particles produced by this system as 'generated primary marine aerosol' (gPMA). Observations during previous deployments of Sea Sweep showed that the organic functional group composition of both seawater and gPMA were similar in the Atlantic, Arctic, and Pacific during spring and summer (Frossard et al., 2014) and that no significant differences exist between submicron organic mass fractions for five separate cruises in the North Atlantic (Bates et al., 2020). In all, while there are coastal observations that have shown links between marine biological activity and atmospheric organic aerosol (Mansour et al., 2020; O'Dowd et al., 2004; Sciare et al., 2009), there are very few remote marine observations that show a difference in the organic composition of gPMA under different biological conditions (Facchini et al., 2008).

There is even less information about changes in the composition of marine aerosol organic mass over the seasonal cycle. The composition of atmospheric primary marine aerosol (aPMA) in the Arctic, Atlantic, and coastal Pacific has been found to be remarkably consistent, with the hydroxyl organic functional group being the largest by mass followed by roughly equivalent contributions of alkane and amine groups (Frossard et al., 2014; L. M. Russell, Hawkins, Frossard, Quinn, & Bates, 2010). Saliba et al. (2020) used the contribution of the

hydroxyl group as a marker of seawater organics in ambient aerosol and showed a difference in the fraction of organic components by season. Higher sea spray organic mass was present when wind speed and sea salt concentration were higher. However, their work did not assess the seasonal differences in contributions of other organic functional groups.

The size distribution of marine particles is well-documented (Hoppel, Fitzgerald, Frick, Larson, & Mack, 1990; Meskhidze et al., 2013; Lynn M. Russell, Huebert, Flagan, & Seinfeld, 1996), but there is very limited size-dependent composition information. The organic mass fraction has been shown to increase with decreasing particle diameter (Facchini et al., 2008; Keene et al., 2007; O'Dowd et al., 2004; Prather et al., 2013). One of the few seasonal marine studies that included size resolved information showed that water soluble organic carbon and total carbon in fine mode particles have maximum concentrations in early- to mid-summer, which coincides with the typical time for high biological activity (Yoon et al., 2007). Different particle sizes have also been shown to be chemically distinct from each other, such as the bimodal distribution of transparent exopolymer particles (<180 nm and >5000 nm) and size-specific saccharides (Aller et al., 2017; Leck, Gao, Mashayekhy Rad, & Nilsson, 2013).

There is very limited information on seasonal differences in particle composition, the relationship of seawater source to primary aerosol, or differences in organic composition of marine aerosol particles with size, all of which have an influence on the direct and indirect effects of aerosol particles (Tsigaridis et al., 2013). For the current study, co-located atmospheric and seawater measurements were conducted to examine how ocean properties and atmospheric aerosols are linked. Samples were collected during four research cruises corresponding to four different seasons as part of the North Atlantic Aerosols and Marine Ecosystems Study (NAAMES) (Behrenfeld et al., 2019). Understanding how the organic fraction and composition

of ambient and bubbling-generated marine aerosol particles change with size and season is an important first step in assessing these linkages. This study shows the dependence of marine organic composition on size and season by comparing organic compositions from Fourier Transform Infrared spectroscopy (FTIR) for generated and ambient aerosols under clean marine conditions.

1.2 Methods

1.2.1 NAAMES

NAAMES was an interdisciplinary investigation conducted in the western North Atlantic to improve understanding of Earth's ocean ecosystem-aerosol-cloud system. NAAMES consisted of four 26-day cruises on the R/V *Atlantis* occurring in November 2015 (NAAMES 1, Winter), May-June 2016 (NAAMES 2, Late Spring), September 2017 (NAAMES 3, Autumn), and March-April 2018 (NAAMES 4, Early Spring). The ship traveled from Woods Hole, MA, to ~ 55°N for the first three cruises and returned again to Woods Hole (Figure 1.1). For the last cruise, the ship traveled from San Juan, Puerto Rico, to ~44.5°N and finished at Woods Hole. During each cruise, the ship occupied 5-7 multi-day sampling stations to conduct ecological and atmospheric measurements.

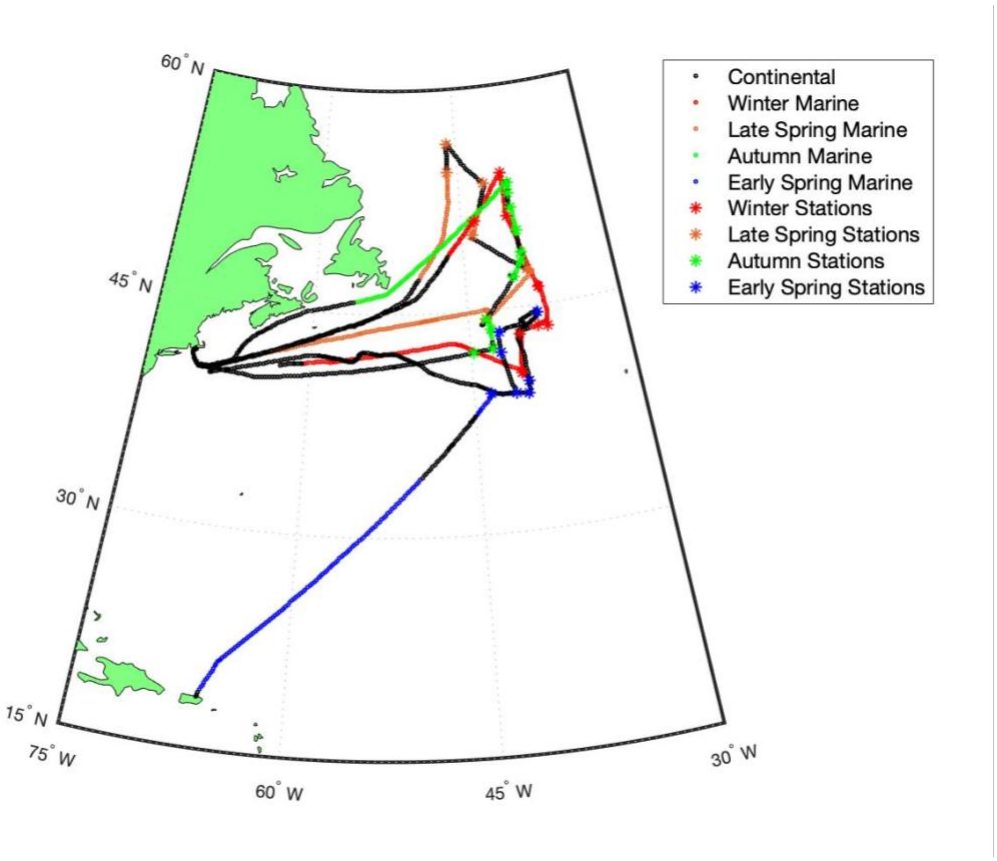

Figure 1.1: Map of the NAAMES study region with intensives sampling locations indicated with asterisks. The air mass categories are shown for each cruise with continental air masses (black) and marine air masses (Winter (red), Late Spring (orange), Autumn (green), and Early Spring (blue)). The Winter, Late Spring, and Autumn cruises departed from Woods Hole, MA and the Early Spring cruise departed from San Juan, Puerto Rico.

1.2.2 Sea Sweep

Sea Sweep is a marine aerosol generator that has been used to simulate bubble bursting at the ocean surface and identify properties of primary marine aerosol (Bates et al., 2012). Aerosols produced by Sea Sweep are identified here as gPMA to distinguish them from naturally occurring sea spray. Sea Sweep consists of a stainless-steel frame attached to two inflatable pontoon floats and was deployed off the port bow of the R/V *Atlantis*. A stainless-steel hood on

top of the Sea Sweep frame maintains a laminar flow air curtain of particle-free air (charcoal and HEPA filtered) at the bow and stern ends of the frame (Bates et al., 2012). Stainless steel frits, 200 μm in size, were positioned below the sea surface at approximately 0.75 m. The resulting particles were then transported to a variety of instruments for analysis.

1.2.3 Filter Collection

Ambient and Sea Sweep (gPMA) aerosol particles were collected through a temperature- and humidity-controlled inlet during NAAMES. Ambient and gPMA particles were dried using diffusion driers filled with silica gel and collected on 37 mm Teflon filters (Pall Inc., 1 μm pore size) at a sample flow rate of 8.3 L min^{-1} (1 μm) or 10 L min^{-1} (0.18, 0.5, and 1.1 μm size cut). The total <1 μm cyclone flow was 16.7 L min^{-1}. The <0.18, <0.5, and <1.1 μm Berner impactor total flows were 30 L min^{-1}. Filters were collected for 12-23 hours for ambient samples (<0.18, <0.5, and <1 μm) and 2 hours for Sea Sweep samples (<0.18, <1, and <1.1 μm), resulting in filtered air volumes of 1.0 -13.8 m^3. After collection, the filters were immediately unloaded, stored in petri dishes, and frozen for offline analysis at Scripps Institution of Oceanography.

1.2.4 FTIR Spectroscopy and Algorithm

Field samples were analyzed using FTIR spectroscopy (Bruker Tensor 27 spectrometer with a deuterated triglycine sulfate, DTGS, detector) to measure the infrared transmission using 2 cm^{-1} resolution (Takahama, Johnson, & Russell, 2013). Sea Sweep filters that showed hydrate peaks were dehydrated in a temperature and humidity controlled clean room (between 2 and 5 weeks) until the hydrate signature was no longer present (Frossard & Russell, 2012). Dehydration was required for 17 Sea Sweep (gPMA) filters from Winter, 27 from Late Spring, none for Autumn, and 10 from Early Spring. The FTIR spectrum for each filter was analyzed using an automated fitting algorithm (Maria, Russell, Turpin, & Porcja, 2002; L. M. Russell et

al., 2009; Takahama et al., 2013). When the baselining procedure resulted in degenerate spectra (defined as spectra that have no discernable peaks and low signal to noise), they were excluded from further analysis. Five organic functional groups were quantified from these mixtures (alkane, hydroxyl, amine, carboxylic acid, and non-acidic carbonyl) and summed together to quantify organic mass (OM) concentration, with groups below detection limits excluded. Organic mass group concentrations were considered above detection if they met three criteria: 1) the fitted peak area for the individual functional group exceeded the minimum observable peak area (defined below), 2) the fitted peak area for the individual functional group exceeded twice the standard deviation of the pre-scan background area, and 3) the alkane functional group was one of the groups that met the first two criteria. 44% of <0.18 μm, 77% of <0.5 μm, and 63% of <1 μm ambient samples were above the detection limit. The low percentage of above detection limit <0.18 μm filters is due to the low mass collected in this size range.

The minimum observable peak areas for the five functional groups reported here were determined based on comparison of peak areas fitted by the algorithm to visual determination of which peaks could be distinguished from the noise by trained analysts (L. M. Russell et al., 2009). Alkenes, aromatic compounds, and organo-sulfates were below detection limit for 90% of the samples and, thus, are not included in our analysis. Organic mass from this technique has an uncertainty of ± 20% due to functional groups that overlap the Teflon absorption, unquantified functional groups, and semi-volatile properties (Maria et al., 2002; Lynn M. Russell, 2003; Lynn M. Russell et al., 2009; L. M. Russell et al., 2009; Takahama et al., 2013). To account for different bubbling rates, OM concentrations from Sea Sweep samples are reported here as normalized to Na mass concentrations from IC measurements on synchronous samples.

1.2.5 Marine Air Mass Criteria

Ambient samples were divided into three main categories: continental, mixed, and marine. A solenoid valve was used to redirect flow from the sample filters when particle counts exceeded thresholds set between 1000 and 2000 particles cm^{-3}, depending on proximity to the port. This conditioned sampling was used to ensure that filters were not contaminated by local shipboard emissions. Ambient samples were considered to be "marine" when 90% or more of the filter sampling time met the following criteria from *Saliba et al.,* (2020): 1) HYSPLIT 48 hour back trajectories (Draxler & Hess, 1998) originated from the North or tropical Atlantic and did not pass over land during that time, 2) ammonium (NH_4^+) concentrations were below 0.1 µg m^{-3}, 3) particle concentrations were below 2000 particles cm^{-3}, 4) the relative wind direction was within 90° of the bow and 5.) 50% or more of the filter sampling time must not exceed a black carbon (BC) threshold of 50 ng m^{-3}. Forty-eight hour back trajectories were used because they provide the best tradeoff between longer time-periods with higher uncertainty and shorter time periods showing fewer upwind contributions (P. K. Quinn et al., 2019; Saliba et al., 2020). Sampling time was defined as the time between the start and stop time of the filtration, excluding times when filter sampling was shut off by the solenoid valve. This resulted in categorizing 19 <1 µm filters as aMA during the four NAAMES cruises. Continental filters were defined as times when 48-hour HYSPLIT back trajectories originated from North America, a relative wind direction within 90° of the bow, and sampling 10% or less during marine periods. Fourteen <1 µm filters were categorized as continental for the four NAAMES cruises. Eleven <1 µm filters fell between the 'marine' and 'continental' categories and were thus categorized as 'mixed filters'. These 'mixed filters' corresponded to sampling for 10% to 90% under marine conditions and the remaining time under continental conditions. These aMA samples include contributions

from other sources present in marine areas, such as ship emissions and transported constituents from coastal or continental emissions (Frossard et al., 2014).

Atmospheric primary marine aerosol (aPMA), a sub-category of aMA, was defined to better isolate ocean sources of particles that result from bubble bursting at the sea surface. aPMA filters were defined as <1 μm aMA filters that had cosine similarity values >0.9 with the aPMA spectrum from Frossard et al.(2014) (Figure 1.2a). The aPMA sub-category represented more than half of the aMA samples overall, including 8 of 8 samples in Winter, none of 1 in Early Spring, 3 of 6 in Late Spring, and 3 of 6 in Autumn. Similarity to the Frossard et al.(2014) aPMA spectra was used as a criterion because that spectrum had a high cosine similarity to the gPMA of that earlier study and that observed during NAAMES. This similarity provides a strong indication that aPMA samples are largely "primary" because they have a composition similar to bubbled seawater previously measured during 5 separate campaigns in different clean marine regions (Frossard et al., 2014). Cosine similarity (namely the dot-product cosine of two normalized spectra) was used to quantify spectral similarity because it has been shown to be sensitive to small spectral differences in FTIR (Frossard et al., 2014; J. Liu et al., 2017; Stein & Scott, 1994; Wan, Vidavsky, & Gross, 2002). Filters for size cutoffs smaller than 1 μm (<0.5 and <0.18 μm) were defined as aPMA if their start and stop time was within 2 hours of<1 μm aPMA filters. There are no filters that met the aPMA criteria during Early Spring, likely due to substantial continental influences at the lower latitudes sampled during this cruise. A similar issue was not encountered during the other three seasons (Figure 1.1).

1.3 Results

1.3.1 aMA Composition and Seasonal Differences

The aMA filters had variable spectra, and therefore variable OFG composition, that may have reflected the different aerosol transport patterns sampled during each cruise (Behrenfeld et al., 2019). The aMA category includes aPMA filters and other filters that fulfilled the marine airmass trajectory and low continental tracer concentration requirements (see Methods).

Organic composition of <1 μm aMA samples for the four cruises are summarized in Table 1.1. Winter aMA had the highest average OM concentration (0.30 ± 0.22 μg m^{-3}) when average wind speed was high and there were minimal contributions from other sources. These conditions generally corresponded to sampling of air masses of polar origin. Winter samples had the highest hydroxyl group mass (85 ± 5%) of the four cruises (Table 1.1) and had similar composition to a previous cruise in the Arctic (ICEALOT) (Frossard et al., 2014).

Early Spring had one aMA filter above the detection limit with an OM concentration of 0.1 μg m^{-3} (Table 1.1). The number of aMA samples during Early Spring was limited because the majority of the ship time was sampling continental air masses (69%) (Table 1.2). Early Spring aMA filters had a higher alkane group amount (35%) than the other campaigns, which is likely due to the persistent continental influence in the marine environment during this campaign (Table 1.1, Table 1.2).

Table 1.1: Average organic functional group composition and organic mass (OM) averages of <1 µm filters from 4 different air mass categories during the four NAAMES campaigns. Numbers in parentheses after the OM average concentrations indicate the number of samples available for each average.

	Winter	**Late Spring**	**Autumn**	**Early Spring**
aPMA OM (µg m^{-3})	0.3 ± 0.22 (8)	0.37± 0.08 (3)	0.12 ± 0.04 (3)	NA
Hydroxyl Fraction (%)	85 ± 5	78 ± 9	72 ± 20	
Alkane (%)	9 ± 3	6 ± 4	13 ± 5	
Amine (%)	5 ± 4	8 ± 3	5	
Acid (%)	1 ± 4	8 ± 7	10 ± 17	
Carbonyl (%)	0	0	0	
aMA OM (µg m^{-3})	0.30 ± 0.22 (8)	0.25 ± 0.17 (5)	0.23 ± 0.17 (5)	0.1 (1)
Hydroxyl Fraction (%)	85 ± 5	58 ± 28	56 ± 26	65
Alkane (%)	9 ± 3	15 ± 13	25 ± 21	35
Amine (%)	5 ± 4	9 ± 8	4 ± 6	0
Acid (%)	1 ± 4	18 ± 20	15 ± 22	0
Carbonyl (%)	0	0	0	0
Mixed OM (µg m^{-3})	0.30 ± 0.1 (3)	0.31 ± 0.13 (4)	0.22 ± 0.01 (2)	0.24 ± 0.05 (2)
Hydroxyl Fraction (%)	56 ± 42	50 ± 16	72 ± 1	58 ± 9
Alkane (%)	21 ± 18	25 ± 10	5 ± 1	30 ± 4
Amine (%)	6 ± 4	5 ± 1	11 ± 5	10 ± 2
Acid (%)	17 ± 23	12 ± 11	12 ± 6	2 ± 4
Carbonyl (%)	0	8 ± 16	0	0
Continental OM excluding winds abaft periods (µg m^{-3})	0.42 ± 0.25 (6)	0.46 ± 0.48 (4)	0.68 ± 0.43 (1)	0.48 ± 0.45 (3)
Hydroxyl Fraction (%)	63 ± 14	30 ± 27	28	60 ± 6
Alkane (%)	18 ± 6	39 ± 21	38	25 ± 16
Amine (%)	6 ± 5	4 ± 4	5	11 ± 7
Acid (%)	1 ± 4	19 ± 17	29	4 ± 7
Carbonyl (%)	12 ± 14	8 ± 16	0	0
gPMA OM/Na (µg m^{-3})	0.55 ± 0.27 (5)	0.47 ± 0.16 (6)	0.93 ± 0.3 (7)	0.53 ± 0.24 (4)
Hydroxyl Fraction (%)	75 ± 9	85 ± 1	87 ± 5	61 ± 22
Alkane (%)	13 ± 5	8 ± 4	8 ± 6	27 ± 15
Amine (%)	12 ± 7	7 ± 4	5 ± 3	12 ± 7
Acid (%)	0	0	0	0
Carbonyl (%)	0	0	0	0

The Late Spring campaign coincided with the climax of the annual phytoplankton bloom and samples collected during this period had the second highest average OM during clean marine periods (0.25 ± 0.17 μg m^{-3}) (Table 1.1). The contribution of carboxylic acid group to aMA OM was substantially higher during this cruise than in Winter or Early Spring (18% vs. 1 and 0% respectively), but similar to Autumn (Table 1.1).

The Autumn campaign corresponded to the declining phase of the phytoplankton bloom. Samples collected during this period had an aMA OM average of 0.23 ± 0.17 μg m^{-3} (Table 1.1) and a relatively high carboxylic acid group mass fraction of aMA OM with an average of 15% (Table 1.1).

The aMA OM concentrations were not statistically different between seasons ($p \gg 0.01$, Table 1.10), but the maximum value was observed in Winter (0.30 ± 0.22 μg m^{-3}, n = 8) and the minimum in Early Spring (0.1 μg m^{-3}, n=1) (Table 1.1). Hydroxyl group concentrations were strongly correlated (r = 0.9) with Na concentrations obtained from thermal desorption chemical ionization mass spectrometry (TDCIMS) (Lawler et al., 2020; Saliba et al., 2020). This finding supports the interpretation that the hydroxyl group is from a marine source (Bahadur et al., 2010; Frossard et al., 2014; Lynn M. Russell, Bahadur, & Ziemann, 2011; L. M. Russell et al., 2010). Furthermore, hydroxyl group OM for all four campaigns did not correlate with BC (Saliba et al., 2020, Figure S4), providing additional evidence that the hydroxyl group is a primary marine compound rather than a combustion or secondary product. High wind speeds and consistent polar air masses during the Winter campaign likely resulted in the stronger marine signature, which was dominated by hydroxyl group contributions (L. M. Russell et al., 2010) and less continental mixing compared to others seasons.

There were no statistical differences in the OM mass concentrations between the different seasons, though Winter did have the strongest marine signal with the highest hydroxyl group concentration. Overall, these results show that aMA filters are a complex mixture of marine and continental components, with the marine components comprising the majority of the signal.

1.3.2 aPMA Composition and Seasonal Differences

The aPMA category is likely most representative of ocean sea spray sources. aPMA had a broad range of OM concentrations (0.07 to 0.83 μg m^{-3}), even though condensation nuclei (CN) number concentrations were consistently below 500 cm^{-3} for 96% of the sampling time. The average aPMA OM concentrations for Winter, Late Spring, and Autumn were not statistically different from each other ($p>0.01$, two-sample student's t-test (Walpole, Myers, Myers, & Ye, 2012), Table 1.10), with the Late Spring only nominally different from Autumn ($p = 0.0103$) and the other seasons indistinguishable (Winter versus Late Spring $p = 0.66$, Winter versus Autumn $p = 0.21$, Table 1.10). Late Spring had the highest average aPMA OM concentration at 0.37 ± 0.08 μg m^{-3}, Winter had an average aPMA OM concentration of 0.3 ± 0.22 μg m^{-3}, and Early Spring had the lowest aPMA OM concentration of 0.12 ± 0.04 μg m^{-3} (Table 1.1).

Three cruises had half or more of the aMA samples classified as aPMA because of their similar composition, with an average of 78 (±6) % hydroxyl, 10 (±4) % alkane, 6 (±2) % amine, and 7 (±5) % carboxylic acid organic functional groups (OFG) (Table 1.1). Campaign mass averages for OFG of aPMA were within one standard deviation of each other, but we note here that the acid group standard deviation was high relative to the average (Winter: 1±4%, Late Spring: 8±7%, and Autumn: 10±17%). The aPMA and aMA filters have high acid group mass concentration in Late Spring and Autumn, whereas Winter and Early Spring (aMA only) showed little to no acid group mass concentration (Table 1.1). Since the Early Spring aMA category

included only one sample, this result is not assumed to be representative of the entire season. The aPMA composition is generally comparable to measurements from prior North Atlantic and Arctic sampling (L. M. Russell et al., 2010), with the hydroxyl group mass ranging from 70% to 85% followed by alkane group masses ranging from roughly 5% to 10%, and amine groups ranging from 5% to 8% (Table 1.1). More specifically, the NAAMES aPMA filters were slightly more enriched in hydroxyl groups and slightly more depleted in alkane groups in comparison to values reported for ocean cruises in Frossard et al. (2014) (Western Atlantic in 2012, North Atlantic and Arctic in 2008, and the Eastern Pacific in 2010 and 2011), which had an average hydroxyl mass of 65% ± 12% and alkane mass of 21% ± 9%.

The spectral averages of aPMA for each NAAMES cruise are similar to each other with cosine similarity values ranging from 0.89 to 0.94 (Table 1.7). Winter had consistent spectra with the highest cosine similarities and low standard deviation (0.97 ± 0.02), whereas Autumn was more similar to other seasons (0.9 ± 0.08) than to itself (0.82 ± 0.1, Table 1.7). These high cosine similarities result from the spectral characteristics of the <1 μm filters, which were similar for all seasons. The NAAMES aPMA seasonal averages show a persistent maximum hydroxyl peak at 3380 cm^{-1} (Figure 1.2), which is consistent with the aPMA hydroxyl peak location identified previously (Frossard et al., 2014). C-H alkane absorption was present for all seasons, with the 2925 cm^{-1} peak consistently being the sharpest peak throughout the alkane region (Figure 1.2). As expected given the aPMA selection criteria, the aPMA spectra had a cosine similarity >0.9 for <1 μm filters (thus OFG mass fractions from different seasons were within one standard deviation of each other) (Table 1.7). This result is somewhat surprising given that the biological conditions corresponding to the aPMA filters were highly variable between seasons and that

chlorophyll concentrations ranged from 0.2 in Autumn to 5.3 mg C m^{-3} in Late Spring (Behrenfeld et al., 2019; Fox et al., 2020).

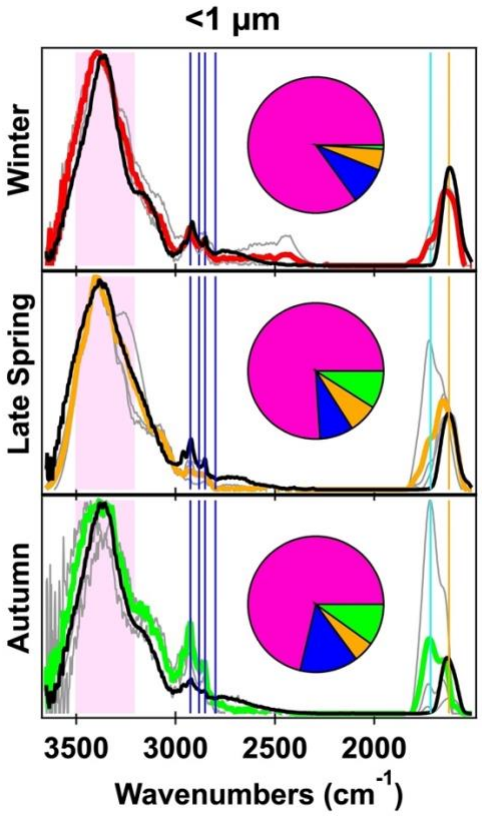

Figure 1.2: FTIR spectra normalized to the alcohol group peak of the <1 µm aPMA seasonal averages (winter in red, late spring in orange, and autumn in green) and gPMA (black) averages with the individual aPMA spectra shown in grey. The pie charts show the average OFG composition with hydroxyl (pink), alkane (blue), amine (orange), and acid (green) groups. The spectral peak locations for the OFG are indicated with the hydroxyl region in the shaded pink area, 4 alkane peaks (vertical blue lines), carbonyl (both acidic and non-acidic, vertical teal line), and amine (vertical orange line).

The relative invariability between seasons of aPMA composition (Figure 1.2) is consistent with the hypothesis that the organic fraction of aPMA is influenced more by dissolved organic carbon (DOC) than particulate organic carbon (POC) (Bates et al., 2020; Kieber et al., 2016; Patricia K. Quinn et al., 2014), as DOC is a larger and less variable fraction of ocean carbon than is POC (Hansell, Carlson, Repeta, & Schlitzer, 2009).

1.3.3 gPMA Composition and Seasonal Differences

Average <1 μm OM concentrations of gPMA normalized to Na showed a maximum during Autumn (0.93 ± 0.3) and a minimum in Late Spring (0.47 ± 0.16) (Table 1.6). gPMA composition was relatively constant, with the hydroxyl group having the largest amount of OM relative to the quantified OM for all four seasons. Autumn had the highest average gPMA hydroxyl organic functional group mass (87 ± 5%) and Early Spring had the lowest (61 ± 22%) (Table 1.6). The average gPMA alkane group mass varied from 8% to 27% of the quantified OM, with a maximum in Early Spring. Average amine group mass varied from 5% to 12% for gPMA. The <1 μm and <1.1 μm gPMA had the highest hydroxyl contribution to masses in Autumn (87 and 86%, respectively) and the highest alkane group contributions to masses in Early Spring (27 and 22%, respectively). The <0.18 μm filters also had the highest OM contribution during Autumn (0.85 ± 0.71). The highest hydroxyl group concentration for <0.18 μm gPMA filters (83 ± 5%) was observed during Early Spring (Table 1.6).

Campaign average values of OM/Na for <1.1 μm gPMA (Table 1.6) showed that Autumn was statistically different from the other seasons ($p<0.01$, Table 1.10). <0.18 μm gPMA filters had no seasons that were statistically different and only Late Spring compared to Autumn was statistically different for <1 μm gPMA filters ($p<0.01$, Table 1.10). While these differences were

statistically significant, within-campaign standard deviations for each size class were greater than observed between-campaign (i.e., seasonal) differences. Additionally, gPMA number size distributions and cloud condensation nuclei (CCN) activity exhibited campaign averages varied less between seasons than within seasons (Bates et al., 2020). However, the low number of samples with OFG above detection during each season (Table 1.6) means that such averages may not be statistically representative of each season.

The gPMA samples had a large range of average OFG fractions and OM/Na values and, statistically, the 1.1 μm Autumn OM/Na was significantly different than the other campaigns ($p<0.01$). However, the variations within each campaign were larger, on average, than the differences between seasons for all sizes.

1.4 Discussion

Here we discuss the seasonal carboxylic acid group contribution in aMA and aPMA filters and their possible sources, compare the composition of different sized aPMA samples, and investigate the effect of latitude on organic functional group composition. Finally, we compare and contrast gPMA and aPMA composition to identify the extent to which gPMA accounts for the composition of aPMA.

1.4.1 aPMA and aMA Carboxylic Acid Group Contribution

Carboxylic acid groups were only present in 1 of 8 aMA filters in Winter and 0 of 1 in Early Spring, but they were present in 5 of 5 aMA filters in Late Spring and 2 of 5 in Autumn. This difference between seasons was also present in the aPMA filters, where only 1 of 8 filters in Winter contained acid groups, whereas 3 of 3 in Late Spring and 1 of 3 in Autumn had detectable acid group mass. The average aPMA acid group concentration for Winter (0.002 μg m^{-3}) was an order of magnitude less than the Late Spring average (0.027 μg m^{-3}), and the average acid group

mass concentration in Autumn was 0.014 μg m^{-3}. There is a large standard deviation in the average acid group mass fraction for the <1 μm aPMA and aMA filters in Late spring and Autumn (Table 1.1). While some carboxylic acids are measured in seawater (Gagosian & Stuermer, 1977), seawater concentrations (relative to Na) that have been reported are much lower than what could be measured by FTIR for either ambient or Sea Sweep. This finding suggests that the measured acid groups have an atmospheric source. The lack of carboxylic acid groups in gPMA and presence of a substantial acid group fraction in aMA and aPMA for Late Spring and Autumn both support a secondary source. A strong correlation with the carboxylic acid group fraction of OM and photosynthetically active radiation (PAR) above 100 Wm^{-2} was found in a previous study, indicating recent formation of secondary organic aerosol (SOA) (Frossard et al., 2014). The carboxylic acid group concentration for aMA from NAAMES had a weak (r=0.26) correlation with PAR above 100 W m^{-2} (Figure S1). This weak correlation to sunlight may have been caused by conditions during NAAMES being less homogeneous regionally than during previously reported studies (Frossard et al. 2014). In addition, there could have been a longer or variable time lag between photooxidation and acid group mass concentrations that would have prevented a correlation (Gantt et al., 2011). NAAMES also had a large range of locations, sea surface temperature, biological activity, and other variables that could have confounded an acid-group-to-PAR relationship.

Black carbon (BC) can be a useful anthropogenic tracer since it is a combustion product that has no natural ocean source. The range of correlations between BC and carboxylic acid group mass concentration varies from no correlation (r = -0.01) in Early Spring to moderate correlation (r = 0.58) in Late Spring (Figure S4). The inconsistency of this correlation could indicate that the acid group is associated with local ship emissions in Late Spring but not in Early

Spring or Autumn, or it could suggest a greater contribution from transported continental emissions. Marine and mixed filters had high correlations of acid group mass concentration with nitrate mass concentration (marine filters r = 0.80, mixed filters r = 0.71), but continental filters had only weak correlations (r = 0.20) (Figure S8). The clean marine atmosphere has few sources of nitrate (Jickells et al., 2003; Prospero, Savoie, Arimoto, Olafsson, & Hjartarson, 1995), making it likely that the nitrates are from continental sources or ship emissions. Gaseous nitrate radicals could be contributing to the acid group concentrations present in the aPMA filters by oxidizing larger unsaturated hydrocarbons or fatty acids (Kawamura & Gagosian, 1987; Monks, 2005). It is interesting that the acid group is negligible in the continental air masses in both Winter and Early Spring, but the acid group fraction is present in all filter categories (aPMA, aMA, mixed, and continental) for both the Late Spring and Autumn (Table 1.1). The acid group mass concentration weakly correlates with PAR and strongly correlates with nitrate concentration (Figures S1 and S8). Since nitrate likely has continental sources that are co-located with continental VOCs, this correlation is consistent with SOA with some contribution from continental sources. Together, these results show that the carboxylic acid group is likely SOA resulting from continental VOCs reacting in the marine atmosphere during sunny seasons.

1.4.2 aPMA and gPMA Size Differences

Three different sizes of ambient aerosol particles (<0.18, <0.5, and <1 μm) were collected simultaneously and analyzed during the NAAMES campaigns. The aPMA subset was classified based on back-trajectory restrictions and high spectral similarity with the Frossard et al. (2014) aPMA cluster of <1 μm filters. The <0.18 and <0.5 μm samples were identified as aPMA if they were concurrent with <1 μm aPMA filters, where we defined concurrent as start

and stop times within 2 hours. There were 8 aPMA filters in Winter for <1 µm, but only two of those had times in which all sizes were sampled. The other seasons had the same number of <1 µm and smaller size aPMA samples. All three size filters generally have the same four OFG: hydroxyl, alkane, amine, and acid groups, but in varying relative amounts. For paired sets of samples, the <0.18 and <0.5 µm filters often have sharp double-peaked alkane group absorbances, but the hydroxyl group absorbance was frequently below detection for the <0.18 µm filters.

The <1 µm filters have higher cosine similarity values within each season (0.82, 0.94, 0.97 from Table 1.9) and lower standard deviations (<0.1) than do the filters in the smaller sizes, which had lower cosine similarity values for Late Spring and Autumn (<0.8, Table 1.9). Not surprisingly, cosine similarity values were below 0.9 for six of the seven comparisons between different size cuts (Figure 1.3, Table 1.9). There is a lot of variability within the individual seasons of <0.18 and <0.5 µm spectra with lower cosine similarity values and higher standard deviations (Table 1.9). The smaller size cut filters were more similar with higher cosine similarities (>0.9) during Late Spring. The low cosine similarity values of the smaller samples indicates that the OFG composition is more varied filter-to-filter than the <1 µm filters, which is likely due to a more dynamic mixture of sources including sea spray, long-range transport, and local ship emissions.

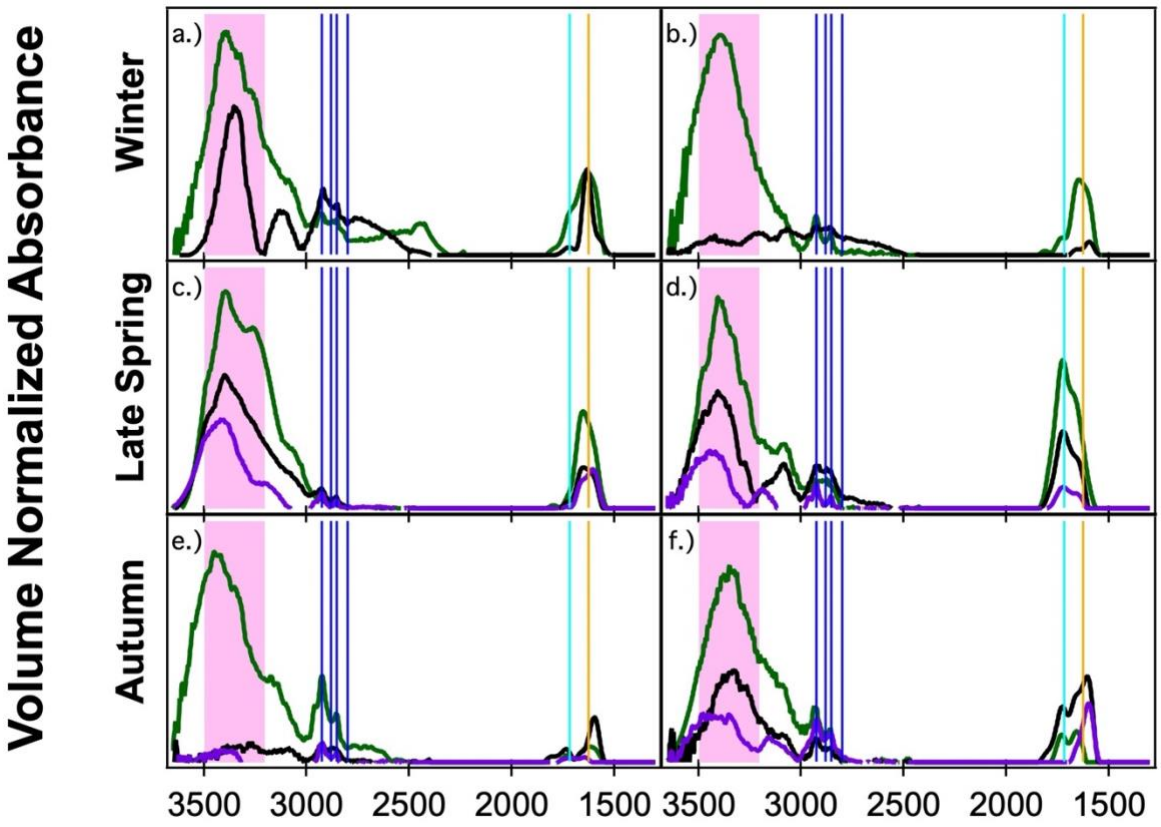

Figure 1.3: FTIR spectra normalized by volume of concurrently sampled filters in three size ranges: <1 µm (green), <0.5 µm (black), and <0.18 µm (purple) during clean marine periods. The spectral peak locations for the OFG are indicated with the hydroxyl region in the shaded pink area, 4 alkane peaks (vertical blue lines), carbonyl (both acidic and non-acidic, vertical teal line), and amine (vertical orange line). The times of sampling are as follows: a.) 11/12/15 10:00 - 11/13/15 8:00, b.) 11/24/15 22:00 – 11/25/15 8:00, c.) 5/15/16 10:00-5/17/16 8:00, d.) 6/1/16 10:50 – 6/2/16 9:00, e.) 9/9/17 8:00 – 9/10/17 7:00, and f.) 9/17/17 8:00 – 9/18/17 7:00.

Ocean biogenic sources from a variety of campaigns included high relative amounts of oxidized functional groups, with hydroxyl being the largest functional group by relative mass (typically >50% of quantified OM being hydroxyl group mass) (Lynn M. Russell et al., 2011). The similarity in composition among the gPMA filters in which the OFG fraction averages are within one standard deviation of each other, regardless of size (except for the <0.18 μm Winter filter, Table 1.6), suggests that there is not a clear size-related difference in gPMA composition when the particles are initially emitted, although the OM/Na ratio is generally lower for <0.18 μm relative to <1 μm and <1.1 μm size cuts.

Differences in composition between the simultaneously collected filters at different sizes may be due to sizes smaller than 1 μm being disproportionately affected by sources other than sea spray. Higher variability in cosine similarity values for the <0.5 and <0.18 μm aPMA filters indicates that the smaller particles may be more influenced by a mix of sea spray, long-range transport, and regional ship emissions than by more homogeneous ocean sea spray sources.

1.4.3 Latitudinal Dependence

To investigate whether regional effects, such as weather and phytoplankton bloom dynamics, could be influencing composition, samples from individual days were binned by low and high latitude with a cutoff of 47°N latitude (Bolaños et al., 2020; Fox et al., 2020). The 47°N latitude cutoff was chosen because it was close to the average latitude (47.5 °N) of the Winter, Late Spring, and Autumn cruises (Early Spring was excluded from this average since it started at a much lower average latitude). The median <1 μm gPMA OM/Na above 47°N showed a maximum during Autumn and a minimum during Winter (Figure 1.4).

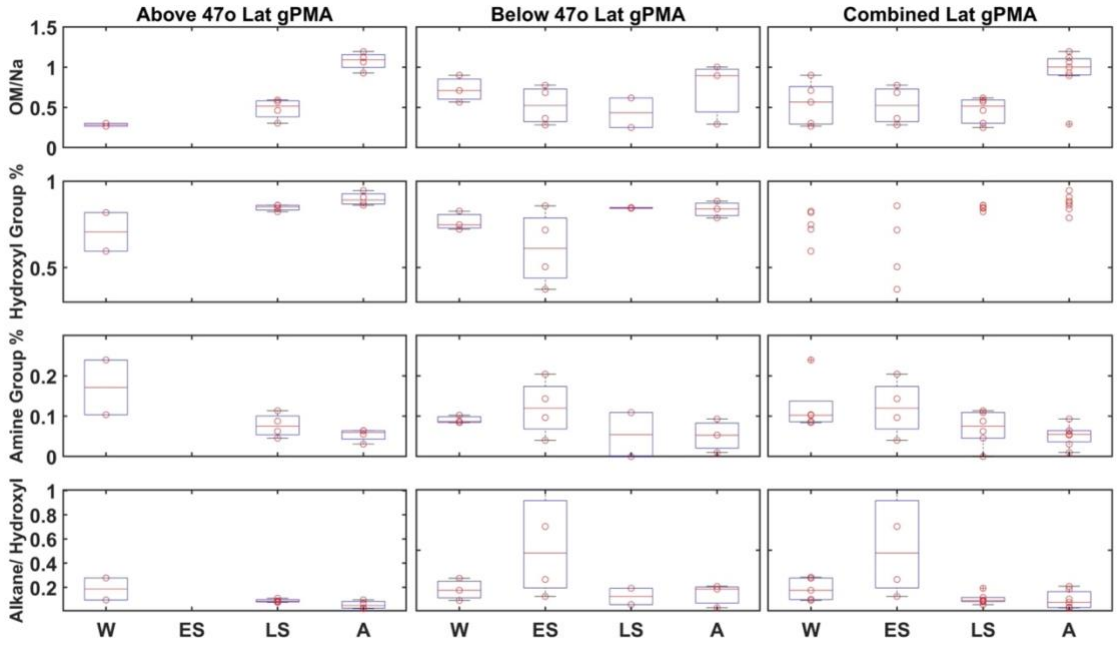

Figure 1.4: <1 µm gPMA OM, normalized by Na, hydroxyl group percentage, amine group percentage, and alkane group percentage divided by hydroxyl group percentage (top to bottom) from each campaign (W = Winter, ES = Early Spring, LS = Late Spring, and A = Autumn): above 47°N, 47°N or below, and with no latitudinal separation (left to right). There were no filters above 47°N for Early Spring. The data are presented as box-whisker plots. The solid red line is the median and boxes cover the 25 – 75% percentile in the data. Red circle datapoints (individual measurements) are shown on top of box plots.

However, the low latitude gPMA showed little to no change between seasons, with less variability within each campaign (Figure 1.4). The median value of OM/Na in Autumn is higher than the standard deviation of the other seasons for high latitudes, but this difference is not seen in the low or combined latitudes. The higher variability and fewer seasonal differences at low latitudes means that the differences at high latitudes are dampened in the combined average. Additionally, there are more samples below 47°N than above, which also weights the combined average toward the low latitude results of no seasonal differences. In addition to OM/Na, three other variables were separated by latitude to investigate seasonal differences: hydroxyl group

mass (%), amine group mass (%), and the ratio of alkane group mass to hydroxyl group mass. Unlike OM/Na, there is no seasonal difference in these other variables at the high latitudes, as all medians fall within the standard deviations of the other seasons (Figure 1.4). Some minor differences with latitude are evident, although the variability within the campaigns may be masked by the project averages. The differences in OM/Na medians between high and low latitudes persist when the campaigns are separated by project median latitude rather than 47°N, indicating that the lack of seasonality in the combined average is not a result of the higher number of low-latitude samples (Figure 1.3).

The aPMA and aMA OM seasonal medians were all within their standard deviations when separated by latitude (Table 1.7 and Table 1.8). The lack of difference in ambient samples could reflect the more direct relationship between seawater properties and aerosol composition in gPMA, whereas aPMA and aMA filters are not produced where sampling occurs, leading to a less direct relationship to seawater properties. Differences between gPMA results at low and high latitudes suggests that the ocean properties at these different latitudes (SST, phytoplankton composition, etc.) could drive some differences in sea spray composition, but more localized sampling for longer time periods would be needed to substantiate those trends.

1.4.4 gPMA and aPMA Comparison

The <1 μm NAAMES gPMA and aPMA filters have cosine similarity >0.85 within each cruise (Table 1.8). The similarity of gPMA and aPMA to each other supports the idea that aPMA mass is largely sea spray aerosol during these seasons. The <1 μm gPMA and aPMA have similar spectral shapes, with a prominent hydroxyl peak at 3380 cm^{-1} (Figure 1.2) and most of the quantified organic mass being attributed to the hydroxyl group (72 to 87%, Table 1.1 and Table 1.6). The <0.18 μm gPMA filters also have the largest mass contribution from the

hydroxyl group (60 to 83%, Table 1.6). The alkane group peaks in the <0.18 μm gPMA filters are visually sharper than in the <1 μm gPMA filters, but in both cases the alkane group mass contributions are substantially smaller than the hydroxyl group mass when the former is above the detection limit. There are only three <0.18 μm aPMA filters that are above the OM detection limit and those three filters have hydroxyl groups as the largest OFG by mass as well (Figure 1.5). The <0.18 μm gPMA and aPMA have high cosine similarity during Late Spring (>0.8), but lower values during Autumn (<0.7) (Table 1.8). This is reflected in the <1 μm gPMA and aPMA comparison as well, although the Autumn difference is not as pronounced.

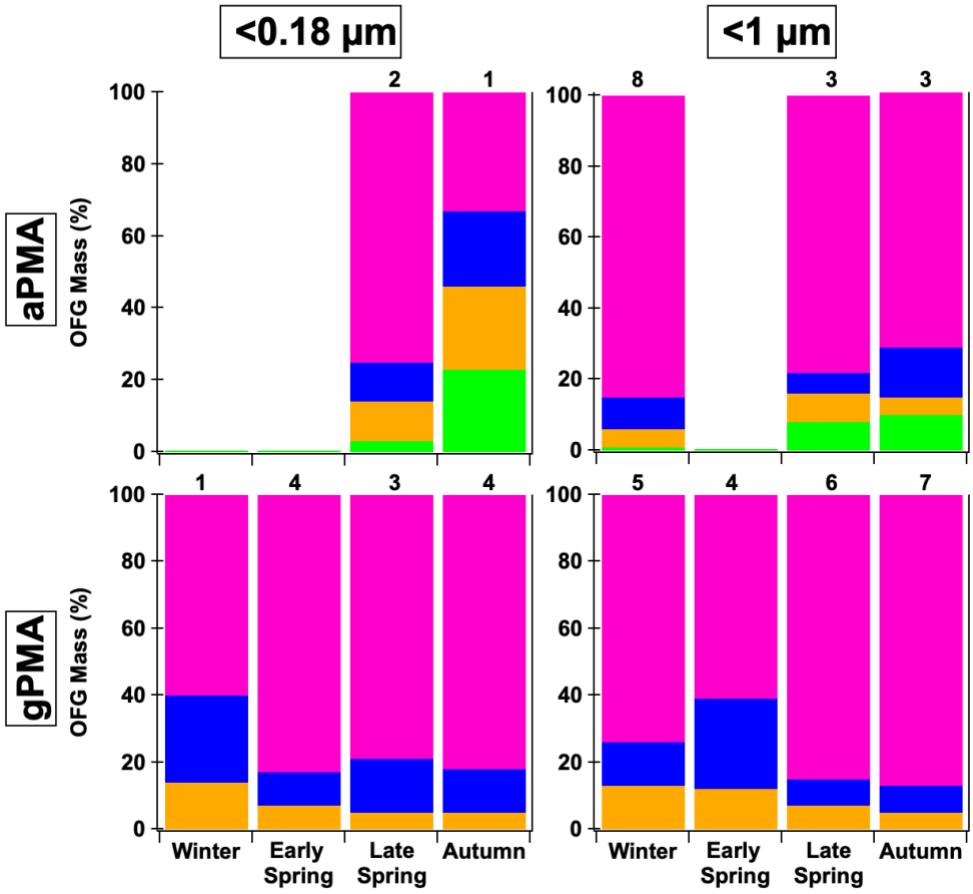

Figure 1.5: Comparison of two sizes, <0.18 µm and <1 µm, and two different sampling methods – ambient (aPMA) and generated (gPMA) throughout the four seasons. The average composition percentage is shown with the following functional groups: hydroxyl (pink), alkane (blue), amine (orange), and acid (green) groups. <0.18 µm aPMA filters have a larger alkane group fraction than the gPMA filters whereas <1 µm filters have similar alkane group fractions in both aPMA and gPMA. Numbers above each bar indicate the number of samples available for each average. <0.5 µm aPMA filters are not included because there are no complementary <0.5 µm gPMA.

When comparing gPMA and aPMA, the gPMA for sizes <0.18 and <1 μm shows a more consistent composition of three functional groups (hydroxyl, alkane, and amine groups), with hydroxyl group mass comprising over 75% of the quantified OM for the majority of samples (Figure 1.5). There were more samples in the gPMA category than the aPMA category due to the limited sampling of clean air masses. The aPMA subset showed more variability in composition than the gPMA filters, including the consistent presence of four functional groups (hydroxyl, alkane, amine, and acid groups), with hydroxyl groups ranging from 30% to 85% of the quantified mass for the <0.18 μm samples (Figure 1.5). The <1 μm aPMA and gPMA hydroxyl group mass fraction throughout the seasons are within 10% of each other, whereas the average hydroxyl group mass fractions are 20% different between the <0.18 μm gPMA and aPMA (81% and 61%, Figure 5). The similarity in composition between the <1 μm aPMA and gPMA samples indicates the aPMA is often representative of freshly emitted sea spray. The <0.18 μm aPMA and gPMA were similar, but not as consistent as the <1 μm pairing, further supporting the interpretation that <0.18 μm aPMA variability reflects a mixture of sea spray and transported continental components.

1.5 Conclusions

Three seasons of <1 μm atmospheric primary marine aerosol (aPMA) OM in the North Atlantic had similar composition: the hydroxyl group was consistently the largest by mass at 78 (±6) % of the quantified organic mass, followed by 10 (±4) % for the alkane group, 6 (±2) % for the amine group, and 7(±5) % for the carboxylic acid group. The aPMA OFG mass fractions were within the standard deviation of each other for all seasons, as expected given the selection criteria. OM concentrations of aMA and aPMA were not significantly different from each other ($p>0.01$), suggesting that there are not strong seasonal differences in the organic mass

contribution to aPMA in the North Atlantic. The aMA filters showed a wider range of OFG composition than aPMA, reflecting contributions from more non-marine sources.

The different sizes for the aPMA filters (<0.18, <0.5, and <1 μm) yielded samples with similar composition, where the majority of organic mass consisted of hydroxyl groups, followed by alkane, amine, and carboxylic acid groups. The <0.18 and <0.5 μm filters showed more variability within the filters in those size cuts than between different sizes. The variability in spectra during marine periods for <0.18 and <0.5 μm filters was larger than for the <1 μm filters, suggesting that these two smaller size cuts were likely a mixture of combustion and marine sources. This is consistent with the fact that the <0.18 and <0.5 μm particles are smaller and have longer lifetimes, making them more likely to have contributions from a variety of sources. Characterizing seasonal changes in organic composition for different sizes in the remote marine environment would require additional observations to quantify how the composition of the smaller sizes of aPMA and gPMA differ from that of the <1 μm size fraction.

Average generated primary marine aerosol (gPMA) composition was consistent across the four seasons when all latitudes were included, however there was a large range of OM/Na concentrations during each season. When the gPMA samples were separated by latitude, low latitudes (<47°N) showed negligible differences in OM/Na between seasons, but high latitudes (>47°N) showed a maximum in Autumn, with a median value that exceeded the medians of the other seasons by more than one standard deviation. The lack of change at lower latitudes in the North Atlantic is consistent with the smaller seasonal changes in sea surface temperatures and Chl *a* at these latitudes. The seasonal difference for high latitudes provides some caution against combining both high and low latitude regions, as this may hide the more northerly seasonal

dependence. Regardless, a longer latitude-constrained time series would be needed to unravel such process-based regional differences in this dynamic area of the North Atlantic Ocean.

1.6 Appendix

1.6.1 Aerosol Sampling Blanks

Blank 37 mm Teflon filters (Pall Inc., 1 μm pore size) were collected for approximately 20% of the samples during each campaign. The blank filter is directly downflow of the sample and processed in the same way as samples i.e. collected for 12-23 hours, unloaded into petri dishes, and frozen for offline analysis at Scripps Institution of Oceanography. The blanks serve as both a handling blank and a background measurement for each quantified functional group.

1.6.2 Alkane Group Detection Limit

The previously published minimum observable peak (MOP) for the alkane functional group was 0.09 bond detection limit (μmol) [*Russell et al.*, 2009] and the MOP used in this work is 0.015 bond detection limit (μmol). When the original MOP detection limit was used in this dataset, only 19% of the alkane groups were above detection limit (ADL), but most of the spectra clearly showed distinct alkane groups. This is likely due to the low particle loads on the filters during the NAAMES campaigns. The alkane detection limit is affected by two variables: the standard deviation of the functional group, which is derived from the uncertainty of the blank, and the alkane peak area being larger than the MOP. The blank used in the uncertainty calculation was an average of all blank samples taken during the 4 campaigns. The MOP was determined to be 0.015 by: 1.) evaluating every spectrum individually and flagging filters that alkane peaks were clearly visible 2.) iterating through various MOP values to see which would eliminate the filters with indistinguishable alkane peaks while retaining the lower alkane peaks that were visible. Using this method, the MOP of 0.015 bond detection limit (μmol) was found to be optimal with 85% of alkane groups being above detection limit when just using the MOP and 83% of alkane groups being ADL when both the standard deviation and MOP were used. While

this lower cutoff provides higher uncertainty in the alkane group concentration, the revised criteria were needed to prevent excluding a majority of the samples.

1.6.3 Cosine Similarity Calculations

The cosine similarity calculations in tables 1.7, 1.8, and 1.9 were calculated by taking the cosine similarity of all spectra above the spectral detection limit, and then averaging the values within the relevant categories i.e. all Winter <1 µm.

1.6.4 Two-Sample T-Tests of OFG

Two sample t-tests were performed on all filter categories (type, season, and size) where the category had 3 or more filters within it. There were only several times in which the p-value was <0.01, indicating a statistical difference. In the atmospheric samples, there were only two examples: <1 µm aPMA Winter (8 samples) x Autumn (3 samples) Alkane/Hydroxyl ($p = 0.01$) and <0.5 µm aMA Winter (4) x Late Spring (9) Acid ($p = 0.005$).In the generated samples, there were 6 instances of low p-values: <1 µm gPMA Late Spring (6 samples) x Autumn (7 samples) hydroxyl ($p = 0.007$), <1 µm Late Spring (6) x Early Spring (4) alkane ($p = 4.7*10^{-4}$), <1.1 µm gPMA Late Spring (12) x Autumn (12) hydroxyl ($p = 2.4*10^{-7}$), alkane ($p = 0.001$), amine ($7.8*10^{-4}$), and <1.1 µm gPMA Autumn (12) x Early Spring (12) hydroxyl ($p = 1.3*10^{-6}$). All other tests had p values above 0.01.

Table 1.2: Campaign comparisons of marine and continental air masses as percentage of time and percentage of filters

	Marine (time)	**Continental (time)**	**Marine (filters)**	**Continental (filters)**	**Mixed (filters)**
Winter	63 %	37 %	47 %	44 %	9 %
Early Spring	31 %	69 %	12 %	65 %	23 %
Late Spring	62 %	38 %	40 %	35 %	25 %
Autumn	42 %	58 %	30 %	44 %	26 %

Table 1.3: Campaign averages of wind speed and chlorophyll

	Wind Speed (m/s)		**Chlorophyll**	
	Marine	Continental	Marine	Continental
Winter	9.8 $\pm$ 3.9	10.4 $\pm$ 4.1	0.3 $\pm$ 0.16	0.3 $\pm$ 0.4
Late Spring	7.0 + 4.0	6.1 + 2.6	1.6 $\pm$ 1.2	1.5 $\pm$ 1.3
Autumn	8.4 + 3.0	6.2 + 2.5	0.4 $\pm$ 0.2	0.2 $\pm$ 0.2
Early Spring	9.2 + 3.2	11.8 + 4.1	0.6 $\pm$ 0.3	0.6 $\pm$ 0.4

Table 1.4: The percentage of filters that sampled when BC < 0.05 µg m^{-3} for 90, 80, and 70% of the sampling time.

	90%	**80%**	**70%**
Marine	47%	62%	71%
Mixed	0%	18%	36%
Continental	14%	22%	22%

Table 1.5: aPMA Alkane/Alcohol average ratios of 3 different sizes

	1 µm	**0.5 µm**	**0.18 µm**
NA1	0.11	0.51	
NA2	0.09	0.80	0.29
NA3	0.19	0.37	0.57

Table 1.6: Campaign OM and mass fraction averages of generated primary marine aerosol in 3 different sizes

	Winter	**Late Spring**	**Autumn**	**Early Spring**
gPMA <1.1 µm OM/Na	0.29 ± 0.13 (2)	0.68 ± 0.36 (12)	1.63 ± 0.28 (12)	0.84 ± 0.28 (7)
Hydroxyl Group (%)	66 ± 6	85 ± 9	86 ± 3	69 ± 26
Alkane (%)	19 ± 10	8 ± 6	7 ± 3	22 ± 20
Amine (%)	15 ± 4	7 ± 5	7 ± 2	9 ± 6
Alkane/Alcohol	0.29 ± 0.18	0.11 ± 0.09	0.08 ± 0.03	0.62 ± 1.06
gPMA <1 µm OM/Na	0.55 ± 0.27 (5)	0.47 ± 0.16 (6)	0.93 ± 0.3(7)	0.53 ± 0.24 (4)
Hydroxyl Group (%)	75 ± 9	85 ± 1	87 ± 5	61 ± 22
Alkane (%)	13 ± 5	8 ± 4	8 ± 6	27 ± 15
Amine (%)	12 ± 7	7 ± 4	5 ± 3	12 ± 7
Alkane/Alcohol	0.18 ± 0.09	0.1 ± 0.05	0.09 ± 0.07	0.55 ± 0.46
gPMA <0.18 µm OM/Na	0.44 (1)	0.11 ± 0.03 (3)	0.85 ± 0.64(4)	0.39 ± 0.3 (4)
Hydroxyl Group (%)	60	79 ± 6	82 ± 8	83 ± 5
Alkane (%)	26	16 ± 3	13 ± 9	10 ± 7
Amine (%)	14	5 ± 7	5 ± 3	7 ± 6
Alkane/Alcohol	0.44	0.2 ± 0.04	0.16 ± 0.12	0.12 ± 0.09

Table 1.7: Cosine similarity values of <1 µm aPMA to compare different seasons

<1 µm aPMA	**Winter (8)**	**Late Spring (3)**	**Autumn (3)**
Winter (8)	0.97 ± 0.02	-	-
Late Spring (3)	0.94 ± 0.04	0.94 ± 0.03	-
Autumn (3)	0.9 ± 0.08	0.89 ± 0.05	0.82 ± 0.10

Table 1.8: Cosine similarity values of both < 1 and <0.18 µm aPMA and gPMA samples to compare how different sampling methods compare during the different campaigns

<1 µm	**Winter gPMA (7)**	**Late Spring gPMA (18)**	**Autumn gPMA (15)**	<0.18 µm	**Winter gPMA (2)**	**Late Spring gPMA (5)**	**Autumn gPMA (8)**
Winter aPMA (8)	0.93 ± 0.07	0.94 ± 0.06	0.95 ± 0.04	**Winter aPMA (0)**	NA	NA	NA
Late Spring aPMA (3)	0.92 ± 0.06	0.93 ± 0.04	0.93 ± 0.04	**Late Spring aPMA (3)**	0.95 ± 0.02	0.82 ± 0.14	0.92 ± 0.05
Autumn aPMA (3)	0.86 ± 0.09	0.87 ± 0.09	0.89 ± 0.08	**Autumn aPMA (3)**	0.67 ± 0.11	0.66 ± 0.14	0.63 ± 0.11

Table 1.9: Cosine similarity values of concurrently sampled aPMA filters of three sizes (<0.18, <0.5, and <1 µm) during different seasons. The first 3 columns are the average cosine similarity values of individual filters when comparing one size with another. The last 3 columns are the average cosine similarity values of individual filters when compared with other filters of the same size.

aPMA	**<0.18 and <0.5**	**<0.18 and <1**	**<0.5 and <1**	**<0.18**	**<0.5**	**<1**
Winter	-	-	0.73 ± 0.13	-	0.84	0.97
Late Spring	0.89 ± 0.06	0.93 ± 0.04	0.89 ± 0.09	0.94 ± 0.01	0.87 ± 0.07	0.94 ± 0.03
Autumn	0.7 ± 0.08	0.66 ± 0.09	0.74 ± 0.18	0.62 ± 0.08	0.71 ± 0.17	0.82 ± 0.1

Table 1.10: P values from two-sample t-test of aMA, aPMA, and gPMA filters. Categories were omitted with sample populations less than 3. This included all <0.18 µm aPMA samples, Winter and Autumn <0.5 µm aPMA samples, all Early Spring aMA samples, and Winter <0.18 µm aMA. P values in bold were less than 0.05.

	Winter x L. Spring	Winter x Autumn	Winter x E. Spring	L.Spring x Autumn	L.Spring x E. Spring	Autumn x E. Spring
<1 µm aPMA OM	0.6587	0.2096	NA	**0.0103**	NA	NA
<1 µm aPMA Alk/Alc	0.5119	**0.0095**	NA	0.0826	NA	NA
<1 µm aMA OM	0.9025	0.4496	NA	0.5801	NA	NA
<1 µm aMA Alk/Alc	**0.0295**	0.0585	NA	0.8904	NA	NA
<0.5 µm aMA OM	0.6019	0.8292	NA	0.9096	NA	NA
<0.5 µm aMA Alk/Alc	0.3305	0.1585	NA	0.6698	NA	NA
<0.18 µm aMA OM	NA	NA	NA	0.4072	NA	NA
<0.18 µm aMA Alk/Alc	NA	NA	NA	0.7592	NA	NA
<1 µm gPMA OM	0.963	**0.0412**	0.2602	**0.0013**	0.0871	0.0969
<1 µm gPMA Alk/Alc	0.0917	0.0903	0.1141	0.7988	**0.0379**	**0.0236**
<1.1 µm gPMA OM	0.1243	**0.0019**	**0.0338**	**$4.476e^{-6}$**	0.2955	**0.0019**
<1.1 µm gPMA Alk/Alc	**0.0374**	**0.0011**	0.6848	0.4232	0.1067	0.0916
<0.18 µm gPMA OM	0.2485	0.4281	0.7456	0.1047	0.0982	0.2391
<0.18 µm gPMA Alk/Alc	**0.0370**	0.1448	0.0549	0.6714	0.2375	0.5935

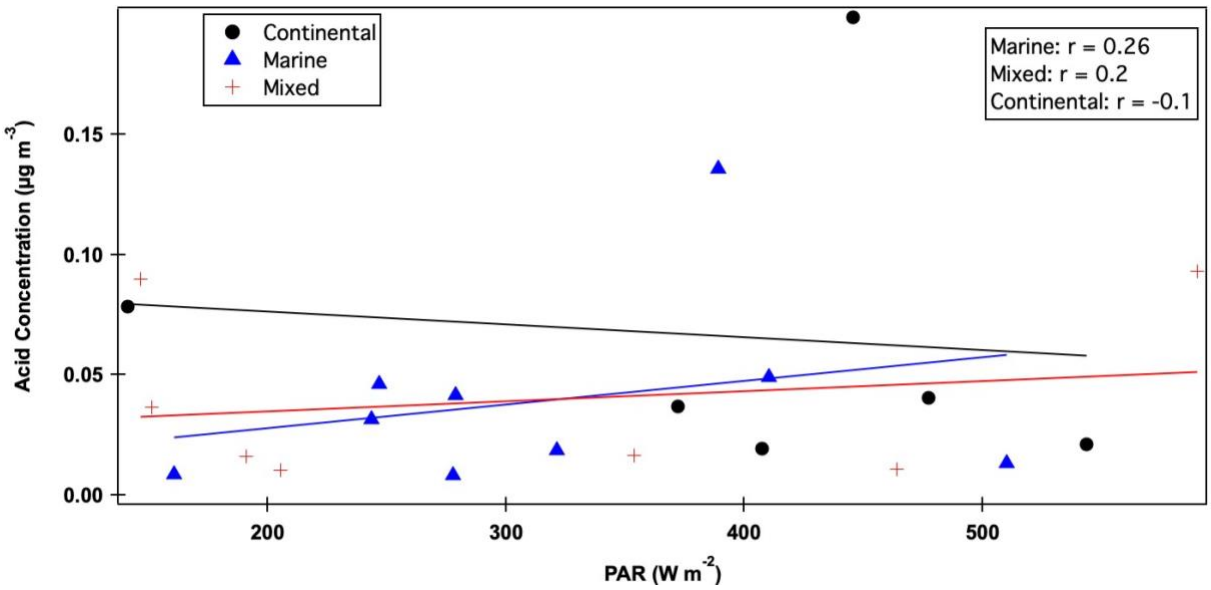

Figure 1.6: Non-zero acid concentrations from <1 µm filters when PAR values are over 100 W m^{-2}. Little to no relationship was found between any of the filter categories, but the marine category had the strongest.

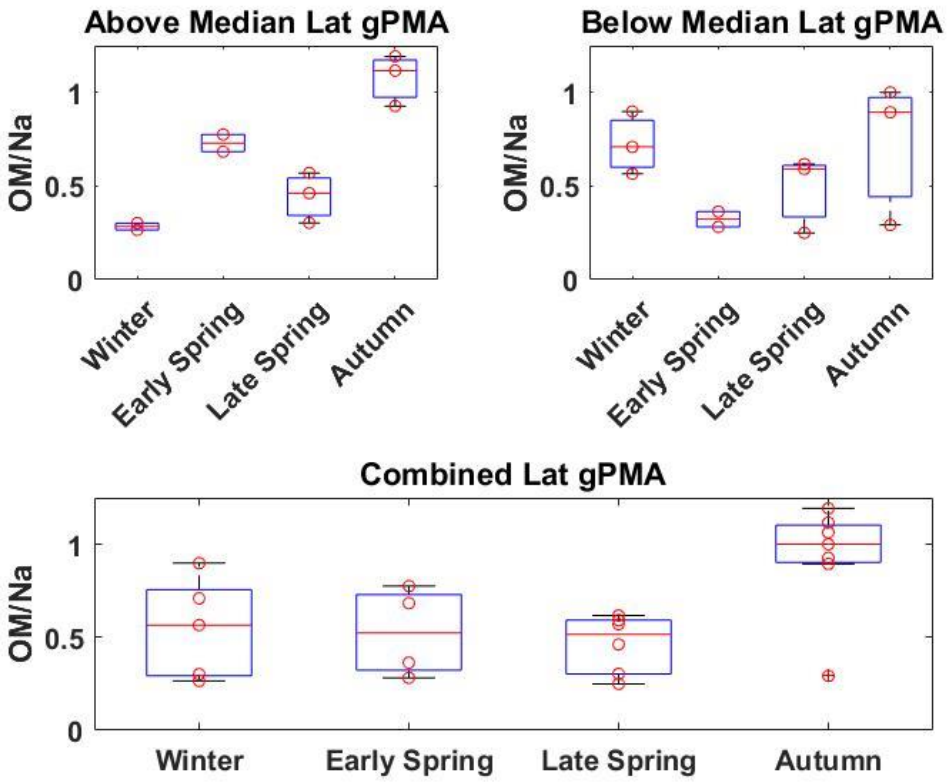

Figure 1.7: <1 µm gPMA OM, normalized by Na, separated by the median latitude of each campaign with filters a.) above the median, b.) below the median, and c.) with no latitudinal separation. The median latitudes for Winter, Late Spring, Autumn, and Early Spring were 46.2° N, 47.7 ° N, 48.6 ° N, and 39.4 ° N.

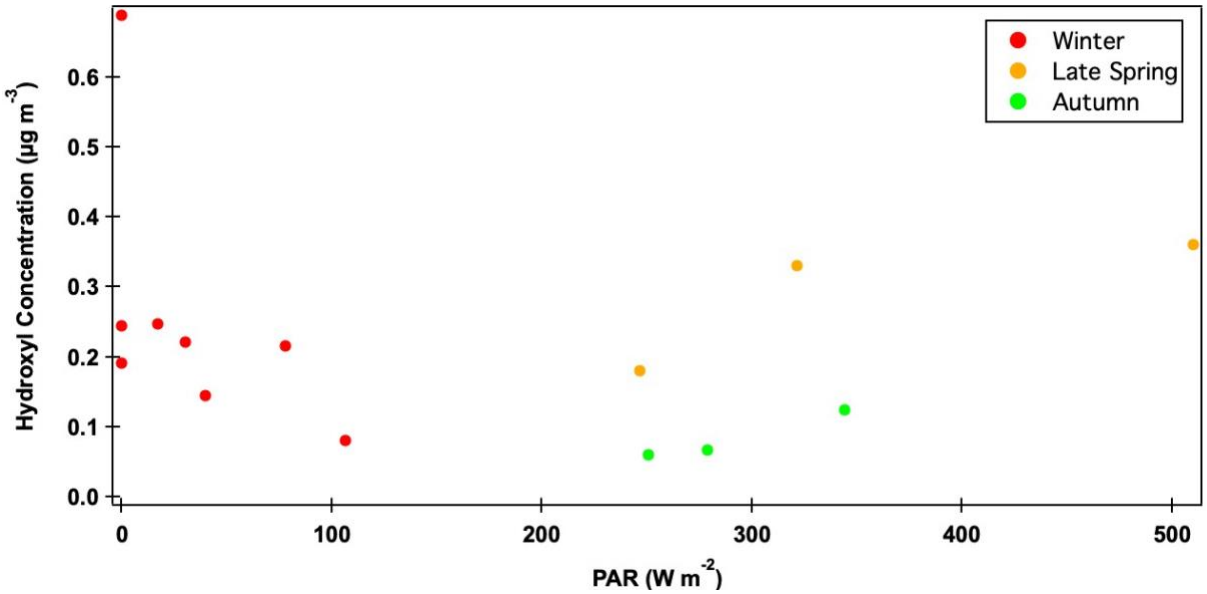

Figure 1.8: Hydroxyl concentrations from <1 µm aPMA filters from all three campaigns: Winter, Late Spring, and Autumn. No relationship was found when the campaigns were combined (r = -0.14) and there were too few points for a correlation to be used for Late Spring and Autumn campaigns.

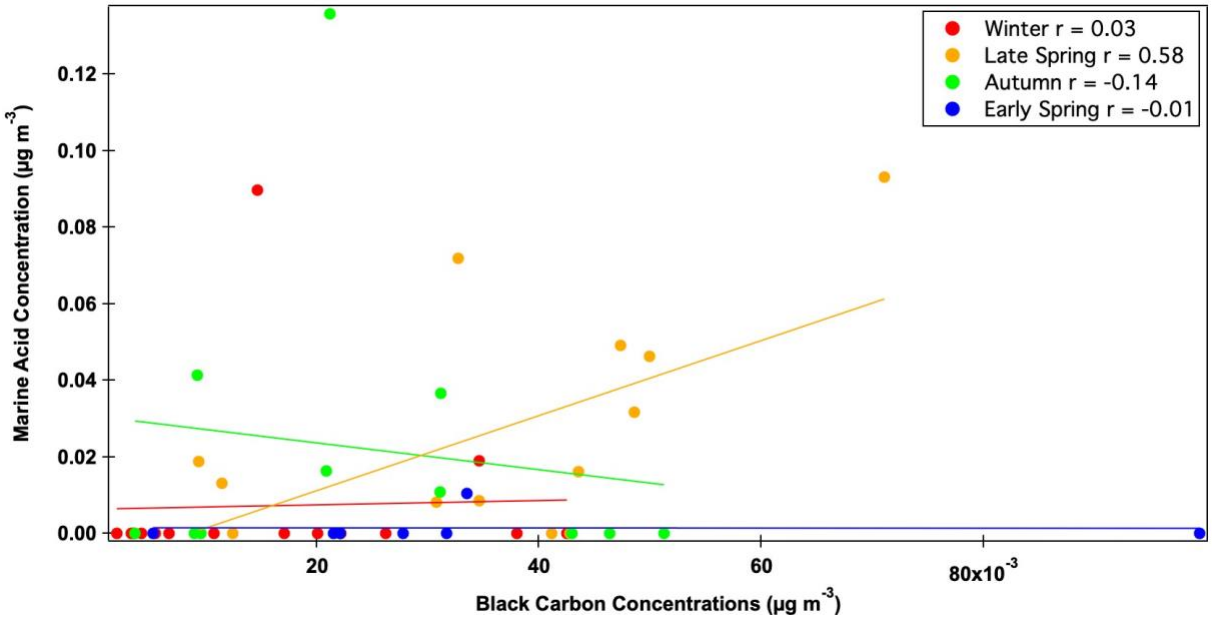

Figure 1.9: Scatter plot of carboxylic acid concentrations from <1 µm marine filters and BC concentrations. Most campaigns showed no relationship, but the late spring acid had a moderate correlation (r = 0.58).

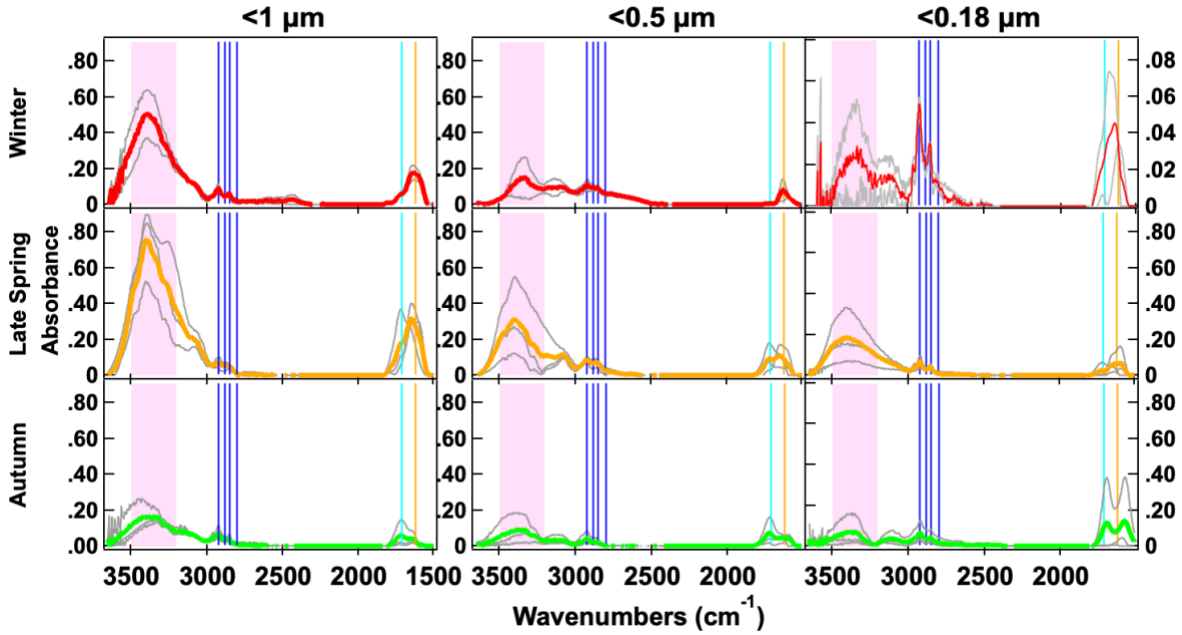

Figure 1.10: Normalized FTIR spectra of the 3 sizes of aPMA (<1 µm, <0.5 µm, <0.18 µm) seasonal averages (Winter in red, Late Spring in orange, and Autumn in green) with individual spectra shown in grey. The spectral peak locations for the OFG are indicated with the hydroxyl region in the shaded pink region, 4 alkane peaks (blue), carbonyl (both acidic and non-acidic, teal), and amine (orange).

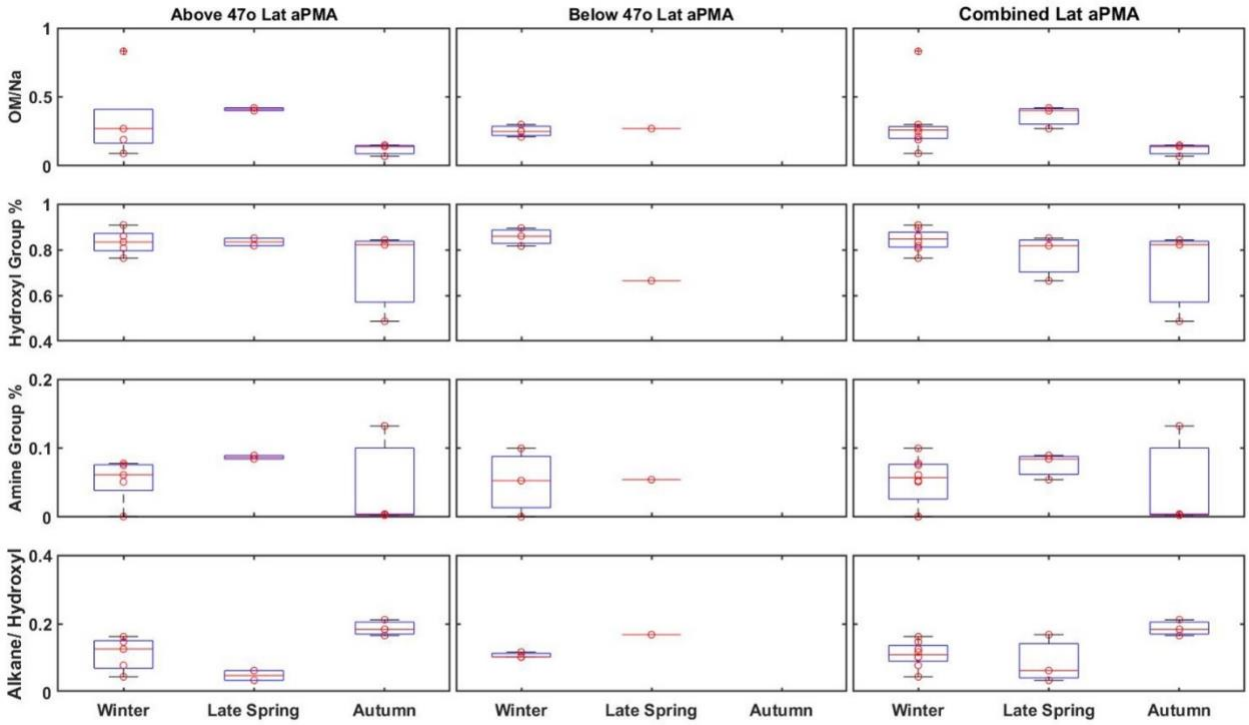

Figure 1.11: <1 µm aPMA OM, normalized by Na, hydroxyl group fraction of the quantified OM, amine group fraction, and alkane group mass divided by hydroxyl group mass from each campaign (top to bottom): above 47°, 47° or below, and with no latitudinal separation (left to right). Horizontal red lines indicate the median value, red circles are individual values, the top and bottom of the boxes indicate the 25th and 75th percentile, and the whiskers extend to the most extreme data points that are not considered outliers, which are shown with a plus symbol. There were no filters above 47° for the Early Spring campaign.

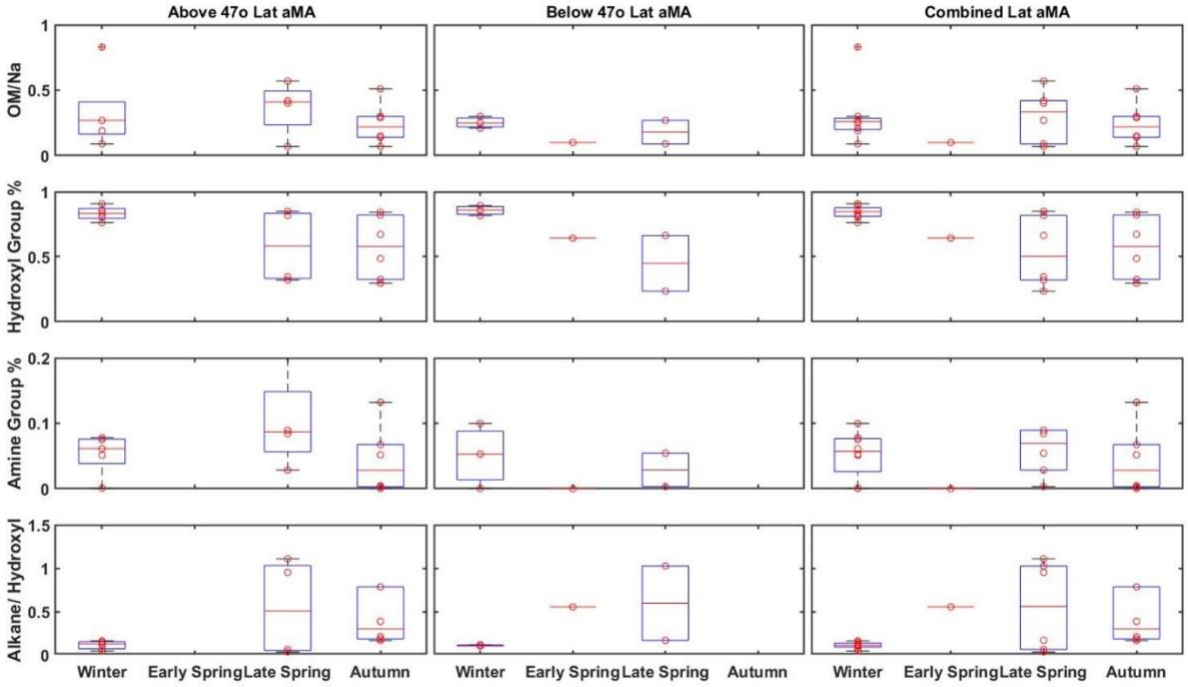

Figure 1.12: <1 µm aMA OM, normalized by Na, hydroxyl group fraction of the quantified OM, amine group fraction, and alkane group mass divided by hydroxyl group mass from each campaign (top to bottom): above 47°, 47° or below, and with no latitudinal separation (left to right). There were no filters above 47° for the Early Spring campaign.

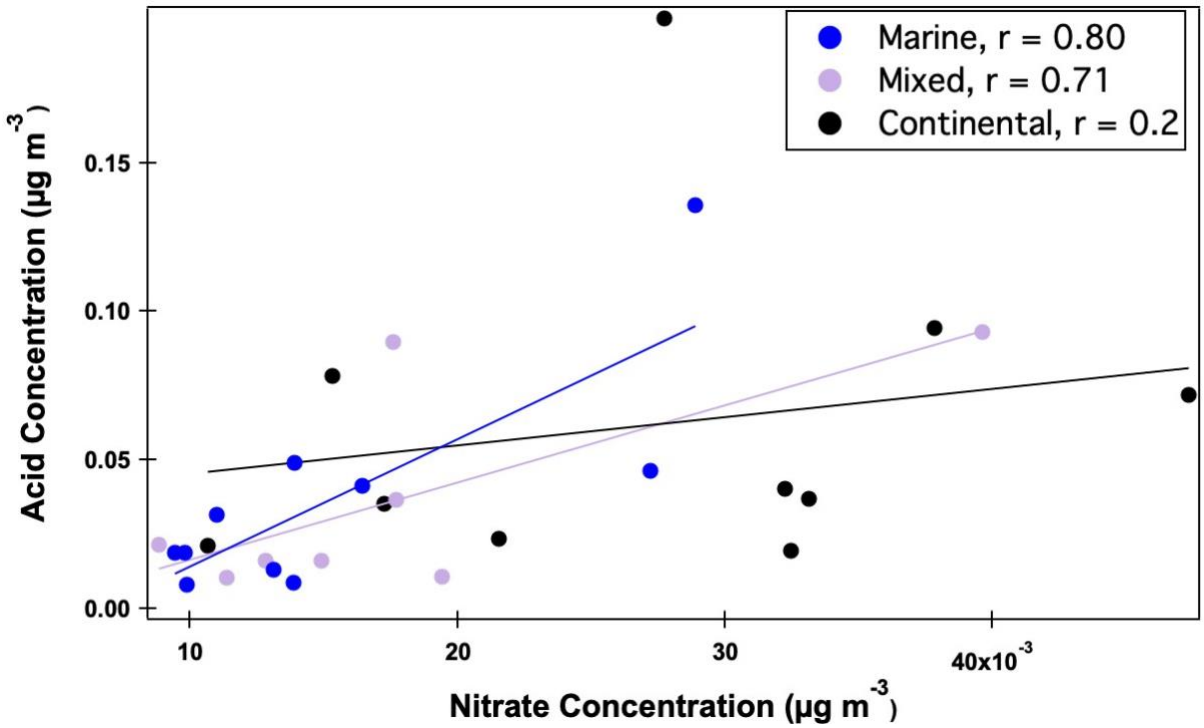

Figure 1.13: Scatter plot of carboxylic acid group concentration versus nitrate concentrations during marine, mixed, and continental periods. The datapoints are colored by air mass category. The best fit lines, colored by air mass category, are obtained using an ordinary least squares regression.

1.7 Acknowledgements

The authors would like to thank the dedicated officers and crew of the R/V *Atlantis*. The authors would also like to acknowledge Laura Ravelin, Chia-Li Chen, Raghu Betha, Derek Price, Maryam Askari Lamjiri, Derek Coffman, and Lucia Upchurch for their contributions to collecting and reducing data. This work was funded by NASA NAAMES grant NNX15AE66G, and Savannah Lewis was supported by the National Science Foundation Graduate Research Fellowship. This is PMEL contribution number 5258.

Chapter 1, in full, is a reprint of the material as it appears in *Frontiers of Marine Science*. Lewis, S. L., Saliba, G., Russell, L. M., Quinn, P. K., Bates, T. S., & Behrenfeld, M. J. (2021).

"Seasonal Differences in Submicron Marine Aerosol Particle Organic Composition in the North Atlantic". The dissertation author was the primary investigator and author of this paper.

References

Aller, J. Y., Radway, J. C., Kilthau, W. P., Bothe, D. W., Wilson, T. W., Vaillancourt, R. D., . . . Knopf, D. A. (2017). Size-resolved characterization of the polysaccharidic and proteinaceous components of sea spray aerosol. *Atmospheric Environment, 154*, 331-347. doi:https://doi.org/10.1016/j.atmosenv.2017.01.053

Bahadur, R., Uplinger, T., Russell, L. M., Sive, B. C., Cliff, S. S., Millet, D. B., . . . Bates, T. S. (2010). Phenol Groups in Northeastern U.S. Submicrometer Aerosol Particles Produced from Seawater Sources. *Environmental Science & Technology, 44*(7), 2542-2548. doi:10.1021/es9032277

Bates, T. S., Quinn, P. K., Coffman, D. J., Johnson, J. E., Upchurch, L., Saliba, G., . . . Behrenfeld, M. J. (2020). Variability in Marine Plankton Ecosystems Are Not Observed in Freshly Emitted Sea Spray Aerosol Over the North Atlantic Ocean. *Geophysical Research Letters, 47*(1), e2019GL085938. doi:10.1029/2019GL085938

Bates, T. S., Quinn, P. K., Frossard, A. A., Russell, L. M., Hakala, J., Petaja, T., . . . Keene, W. C. (2012). Measurements of ocean derived aerosol off the coast of California. *Journal of Geophysical Research-Atmospheres, 117*. doi:10.1029/2012jd017588

Behrenfeld, M. J., Moore, R. H., Hostetler, C. A., Graff, J., Gaube, P., Russell, L. M., . . . Ziemba, L. (2019). The North Atlantic Aerosol and Marine Ecosystem Study (NAAMES): Science Motive and Mission Overview. *Frontiers in Marine Science, 6*(122). doi:10.3389/fmars.2019.00122

Blanchard, D. C. (1964). Sea-to-Air Transport of Surface Active Material. *Science, 146*(3642), 396. doi:10.1126/science.146.3642.396

Bolaños, L. M., Karp-Boss, L., Choi, C. J., Worden, A. Z., Graff, J. R., Haëntjens, N., . . . Giovannoni, S. J. (2020). Small phytoplankton dominate western North Atlantic biomass. *The ISME Journal, 14*(7), 1663-1674. doi:10.1038/s41396-020-0636-0

Carlson, C. A., Ducklow, H. W., & Michaels, A. F. (1994). Annual flux of dissolved organic carbon from the euphotic zone in the northwestern Sargasso Sea. *Nature, 371*(6496), 405-408. doi:10.1038/371405a0

Collins, D. B., Ault, A. P., Moffet, R. C., Ruppel, M. J., Cuadra-Rodriguez, L. A., Guasco, T. L., . . . Prather, K. A. (2013). Impact of marine biogeochemistry on the chemical mixing state and cloud forming ability of nascent sea spray aerosol. *Journal of Geophysical Research: Atmospheres, 118*(15), 8553-8565. doi:https://doi.org/10.1002/jgrd.50598

Draxler, R. R., & Hess, G. (1998). An overview of the HYSPLIT_4 modelling system for trajectories. *Australian meteorological magazine, 47*(4), 295-308.

Facchini, M. C., Rinaldi, M., Decesari, S., Carbone, C., Finessi, E., Mircea, M., . . . O'Dowd, C. D. (2008). Primary submicron marine aerosol dominated by insoluble organic colloids and aggregates. *Geophysical Research Letters, 35*(17). doi:https://doi.org/10.1029/2008GL034210

Fox, J., Behrenfeld, M. J., Haëntjens, N., Chase, A., Kramer, S. J., Boss, E., . . . Halsey, K. H. (2020). Phytoplankton Growth and Productivity in the Western North Atlantic: Observations of Regional Variability From the NAAMES Field Campaigns. *Frontiers in Marine Science, 7*(24). doi:10.3389/fmars.2020.00024

Frossard, A. A., & Russell, L. M. (2012). Removal of Sea Salt Hydrate Water from Seawater-Derived Samples by Dehydration. *Environmental Science & Technology, 46*(24), 13326-13333. doi:10.1021/es3032083

Frossard, A. A., Russell, L. M., Burrows, S. M., Elliott, S. M., Bates, T. S., & Quinn, P. K. (2014). Sources and composition of submicron organic mass in marine aerosol particles. *Journal of Geophysical Research: Atmospheres, 119*(22), 12,977-913,003. doi:10.1002/2014JD021913

Gagosian, R. B., & Stuermer, D. H. (1977). The cycling of biogenic compounds and their diagenetically transformed products in seawater. *Marine Chemistry, 5*(4), 605-632. doi:https://doi.org/10.1016/0304-4203(77)90045-7

Gantt, B., Meskhidze, N., Facchini, M. C., Rinaldi, M., Ceburnis, D., & O'Dowd, C. D. (2011). Wind speed dependent size-resolved parameterization for the organic mass fraction of sea spray aerosol. *Atmos. Chem. Phys., 11*(16), 8777-8790. doi:10.5194/acp-11-8777-2011

Gaston, C. J., Furutani, H., Guazzotti, S. A., Coffee, K. R., Bates, T. S., Quinn, P. K., . . . Prather, K. A. (2011). Unique ocean-derived particles serve as a proxy for changes in ocean chemistry. *Journal of Geophysical Research: Atmospheres, 116*(D18). doi:https://doi.org/10.1029/2010JD015289

Hansell, D. A., Carlson, C. A., Repeta, D. J., & Schlitzer, R. (2009). Dissolved Organic Matter in the Ocean: A Controversy Stimulates New Insights. *Oceanography, 22*(4), 202-211.

Hoppel, W. A., Fitzgerald, J. W., Frick, G. M., Larson, R. E., & Mack, E. J. (1990). Aerosol size distributions and optical properties found in the marine boundary layer over the Atlantic Ocean. *Journal of Geophysical Research: Atmospheres, 95*(D4), 3659-3686. doi:https://doi.org/10.1029/JD095iD04p03659

Jickells, T. D., Kelly, S. D., Baker, A. R., Biswas, K., Dennis, P. F., Spokes, L. J., . . . Yeatman, S. G. (2003). Isotopic evidence for a marine ammonia source. *Geophysical Research Letters, 30*(7). doi:10.1029/2002GL016728

Kawamura, K., & Gagosian, R. B. (1987). Implications of ω-oxocarboxylic acids in the remote marine atmosphere for photo-oxidation of unsaturated fatty acids. *Nature, 325*(6102), 330-332. doi:10.1038/325330a0

Keene, W. C., Maring, H., Maben, J. R., Kieber, D. J., Pszenny, A. A. P., Dahl, E. E., . . . Sander, R. (2007). Chemical and physical characteristics of nascent aerosols produced by bursting bubbles at a model air-sea interface. *Journal of Geophysical Research: Atmospheres, 112*(D21). doi:10.1029/2007JD008464

Kieber, D. J., Keene, W. C., Frossard, A. A., Long, M. S., Maben, J. R., Russell, L. M., . . . Bates, T. S. (2016). Coupled ocean-atmosphere loss of marine refractory dissolved organic carbon. *Geophysical Research Letters, 43*(6), 2765-2772. doi:10.1002/2016gl068273

Lawler, M., Lewis, S., Russell, L., Quinn, P., Bates, T., Coffman, D., . . . Saltzman, E. (2020). *North Atlantic marine organic aerosol characterized by novel offline thermal desorption mass spectrometry approach: polysaccharides, recalcitrant material, secondary organics*.

Leck, C., Gao, Q., Mashayekhy Rad, F., & Nilsson, U. (2013). Size-resolved atmospheric particulate polysaccharides in the high summer Arctic. *Atmos. Chem. Phys., 13*(24), 12573-12588. doi:10.5194/acp-13-12573-2013

Liu, J., Russell, L. M., Lee, A. K. Y., McKinney, K. A., Surratt, J. D., & Ziemann, P. J. (2017). Observational evidence for pollution-influenced selective uptake contributing to biogenic secondary organic aerosols in the southeastern U.S. *Geophysical Research Letters, 44*(15), 8056-8064. doi:https://doi.org/10.1002/2017GL074665

Liu, S., Liu, C.-C., Froyd, K. D., Schill, G. P., Murphy, D. M., Bui, T. P., . . . Gao, R.-S. (2021). Sea spray aerosol concentration modulated by sea surface temperature. *Proceedings of the National Academy of Sciences, 118*(9), e2020583118. doi:10.1073/pnas.2020583118

Mansour, K., Decesari, S., Facchini, M. C., Belosi, F., Paglione, M., Sandrini, S., . . . Rinaldi, M. (2020). Linking Marine Biological Activity to Aerosol Chemical Composition and Cloud-Relevant Properties Over the North Atlantic Ocean. *Journal of Geophysical Research: Atmospheres, 125*(13), e2019JD032246. doi:https://doi.org/10.1029/2019JD032246

Maria, S. F., Russell, L. M., Turpin, B. J., & Porcja, R. J. (2002). FTIR measurements of functional groups and organic mass in aerosol samples over the Caribbean. *Atmospheric Environment, 36*(33), 5185-5196. doi:10.1016/s1352-2310(02)00654-4

Meskhidze, N., Petters, M. D., Tsigaridis, K., Bates, T., O'Dowd, C., Reid, J., . . . Zorn, S. R. (2013). Production mechanisms, number concentration, size distribution, chemical composition, and optical properties of sea spray aerosols. *Atmospheric Science Letters, 14*(4), 207-213. doi:https://doi.org/10.1002/asl2.441

Monks, P. S. (2005). Gas-phase radical chemistry in the troposphere. *Chem Soc Rev, 34*(5), 376-395. doi:10.1039/b307982c

O'Dowd, C. D., Facchini, M. C., Cavalli, F., Ceburnis, D., Mircea, M., Decesari, S., . . . Putaud, J.-P. (2004). Biogenically driven organic contribution to marine aerosol. *Nature, 431*(7009), 676-680. doi:10.1038/nature02959

Ovadnevaite, J., Ceburnis, D., Leinert, S., Dall'Osto, M., Canagaratna, M., O'Doherty, S., . . . O'Dowd, C. (2014). Submicron NE Atlantic marine aerosol chemical composition and abundance: Seasonal trends and air mass categorization. *Journal of Geophysical Research: Atmospheres, 119*(20), 11,850-811,863. doi:10.1002/2013jd021330

Prather, K. A., Bertram, T. H., Grassian, V. H., Deane, G. B., Stokes, M. D., DeMott, P. J., . . . Zhao, D. (2013). Bringing the ocean into the laboratory to probe the chemical complexity of sea spray aerosol. *Proceedings of the National Academy of Sciences of the United States of America, 110*(19), 7550-7555. doi:10.1073/pnas.1300262110

Prospero, J. M., Savoie, D. L., Arimoto, R., Olafsson, H., & Hjartarson, H. (1995). Sources of aerosol nitrate and non-sea-salt sulfate in the Iceland region. *Science of The Total Environment, 160-161*, 181-191. doi:https://doi.org/10.1016/0048-9697(95)04355-5

Quinn, P. K., Bates, T. S., Coffman, D. J., Upchurch, L., Johnson, J. E., Moore, R., . . . Behrenfeld, M. J. (2019). Seasonal Variations in Western North Atlantic Remote Marine Aerosol Properties. *Journal of Geophysical Research: Atmospheres, 124*(24), 14240-14261. doi:https://doi.org/10.1029/2019JD031740

Quinn, P. K., Bates, T. S., Schulz, K. S., Coffman, D. J., Frossard, A. A., Russell, L. M., . . . Kieber, D. J. (2014). Contribution of sea surface carbon pool to organic matter enrichment in sea spray aerosol. *Nature Geoscience, 7*(3), 228-232. doi:10.1038/ngeo2092

Randles, C., Russell, L., & Ramaswamy, V. (2004). Hygroscopic and optical properties organic sea salt aerosol and consequences for climate forcing. *Geophys. Res. Lett, 31*. doi:10.1029/2004GL020628

Rinaldi, M., Fuzzi, S., Decesari, S., Marullo, S., Santoleri, R., Provenzale, A., . . . Facchini, M. C. (2013). Is chlorophyll-a the best surrogate for organic matter enrichment in submicron primary marine aerosol? *Journal of Geophysical Research: Atmospheres, 118*(10), 4964-4973. doi:https://doi.org/10.1002/jgrd.50417

Russell, L. M. (2003). Aerosol Organic-Mass-to-Organic-Carbon Ratio Measurements. *Environmental Science & Technology, 37*(13), 2982-2987. doi:10.1021/es026123w

Russell, L. M., Bahadur, R., Hawkins, L. N., Allan, J., Baumgardner, D., Quinn, P. K., & Bates, T. S. (2009). Organic aerosol characterization by complementary measurements of chemical bonds and molecular fragments. *Atmospheric Environment, 43*(38), 6100-6105. doi:10.1016/j.atmosenv.2009.09.036

Russell, L. M., Bahadur, R., & Ziemann, P. J. (2011). Identifying organic aerosol sources by comparing functional group composition in chamber and atmospheric particles.

Proceedings of the National Academy of Sciences, 108(9), 3516. doi:10.1073/pnas.1006461108

Russell, L. M., Hawkins, L. N., Frossard, A. A., Quinn, P. K., & Bates, T. S. (2010). Carbohydrate-like composition of submicron atmospheric particles and their production from ocean bubble bursting. *Proceedings of the National Academy of Sciences of the United States of America, 107*(15), 6652-6657. doi:10.1073/pnas.0908905107

Russell, L. M., Huebert, B. J., Flagan, R. C., & Seinfeld, J. H. (1996). Characterization of submicron aerosol size distributions from time-resolved measurements in the Atlantic Stratocumulus Transition Experiment/Marine Aerosol and Gas Exchange. *Journal of Geophysical Research: Atmospheres, 101*(D2), 4469-4478. doi:https://doi.org/10.1029/95JD01372

Russell, L. M., Takahama, S., Liu, S., Hawkins, L. N., Covert, D. S., Quinn, P. K., & Bates, T. S. (2009). Oxygenated fraction and mass of organic aerosol from direct emission and atmospheric processing measured on the R/V Ronald Brown during TEXAQS/GoMACCS 2006. *Journal of Geophysical Research: Atmospheres, 114*(D7). doi:10.1029/2008jd011275

Saliba, G., Chen, C.-L., Lewis, S., Russell, L. M., Quinn, P. K., Bates, T. S., . . . Behrenfeld, M. J. (2020). Seasonal Differences and Variability of Concentrations, Chemical Composition, and Cloud Condensation Nuclei of Marine Aerosol Over the North Atlantic. *Journal of Geophysical Research: Atmospheres, 125*(19), e2020JD033145. doi:10.1029/2020JD033145

Sciare, J., Favez, O., Sarda-Estève, R., Oikonomou, K., Cachier, H., & Kazan, V. (2009). Long-term observations of carbonaceous aerosols in the Austral Ocean atmosphere: Evidence of a biogenic marine organic source. *Journal of Geophysical Research: Atmospheres, 114*(D15). doi:https://doi.org/10.1029/2009JD011998

Stein, S. E., & Scott, D. R. (1994). Optimization and testing of mass spectral library search algorithms for compound identification. *Journal of the American Society for Mass Spectrometry, 5*(9), 859-866. doi:10.1016/1044-0305(94)87009-8

Takahama, S., Johnson, A., & Russell, L. M. (2013). Quantification of Carboxylic and Carbonyl Functional Groups in Organic Aerosol Infrared Absorbance Spectra. *Aerosol Science and Technology, 47*(3), 310-325. doi:10.1080/02786826.2012.752065

Tsigaridis, K., Koch, D., & Menon, S. (2013). Uncertainties and importance of sea spray composition on aerosol direct and indirect effects. *Journal of Geophysical Research: Atmospheres, 118*(1), 220-235. doi:https://doi.org/10.1029/2012JD018165

Walpole, R. E., Myers, R. H., Myers, S. L., & Ye, K. (2012). *Probability & statistics for engineers & scientists*. Boston: Prentice Hall.

Wan, K. X., Vidavsky, I., & Gross, M. L. (2002). Comparing similar spectra: From similarity index to spectral contrast angle. *Journal of the American Society for Mass Spectrometry, 13*(1), 85-88. doi:10.1016/S1044-0305(01)00327-0

Wang, X., Sultana, C. M., Trueblood, J., Hill, T. C. J., Malfatti, F., Lee, C., . . . Prather, K. A. (2015). Microbial Control of Sea Spray Aerosol Composition: A Tale of Two Blooms. *ACS Central Science, 1*(3), 124-131. doi:10.1021/acscentsci.5b00148

Yoon, Y. J., Ceburnis, D., Cavalli, F., Jourdan, O., Putaud, J. P., Facchini, M. C., . . . O'Dowd, C. D. (2007). Seasonal characteristics of the physicochemical properties of North Atlantic marine atmospheric aerosols. *Journal of Geophysical Research: Atmospheres, 112*(D4). doi:10.1029/2005JD007044

Chapter 2 Characterization of Sea Surface Microlayer and Marine Aerosol Organic Composition using STXM-NEXAFS and FTIR Spectroscopy

Atmospheric submicron particles, generated primary marine aerosol (gPMA), seawater (depth 5 m), and sea surface microlayer (depth ~0.001 m) samples were collected during the North Atlantic Aerosol and Marine Ecosystem Study (NAAMES) on the R/V *Atlantis* in September 2017 and March 2018 and analyzed by Scanning Transmission X-ray Microscopy with Near Edge X-Ray Absorption Fine Structure (STXM NEXAFS) and Fourier Transform Infrared spectroscopy (FTIR). Three organic functional groups (hydroxyl, alkane, and amine) were in all sample types, with the hydroxyl group typically being 50-90% of the quantified organic mass concentration. Microlayer and atmospheric particle samples both had a larger range of hydroxyl group to alkane group mass ratios than either seawater or gPMA. These measurements suggest that the sea surface microlayer organic composition contributes to the range of submicron atmospheric aerosol organic functional group composition. Atmospheric and microlayer sample alkane/hydroxyl group ratio variations were also associated with tracers of seawater biological activity, including chlorophyll and net primary production. Seawater and gPMA samples had relatively constant organic functional group composition for all of the sampled locations and varying phytoplankton activity conditions, suggesting they are associated with the more consistent nature of dissolved organic carbon fraction that is ubiquitous in seawater. Eight k-means clusters of STXM-NEXAFS particles were identified from the spectra

for all four sample types (atmospheric aerosol particles, gPMA, seawater, and microlayer), which showed that all four sample types had particles in four of the clusters and seven of the eight clusters included a mixture of sample types. These STXM-NEXAFS results support the FTIR measurements by showing consistent organic particle clusters across the four sample types as well as heterogeneity within each type.

2.1 Introduction

The microlayer has been proposed to be a significant source of organic material to the marine atmosphere because it is the interface between the atmosphere and ocean (Michael Cunliffe et al., 2013; Anja Engel et al., 2017), but there are few observations supporting this connection. The sea surface microlayer (SML) is operationally defined as the uppermost 1 – 1000 μm of the ocean (Hunter & Liss, 1977; Liss, 1997). The SML is characterized by its enrichment of organic and inorganic components, including amino acids, proteins, and lipids, compared to sub-surface seawater. This enrichment is attributed to bubbles rising through the water column and scavenging organics that subsequently accumulate in the SML (Aller et al., 2017; Anja Engel et al., 2017; Tseng, Viechnicki, Skop, & Brown, 1992).

The SML plays a role in the enrichment of organic components of primary marine aerosol through the mechanism of bubbles bursting at the ocean surface. When the entrained bubbles reach the surface, seawater drains from the bubble film, leaving an organic rich film that, when it bursts, ejects small particles into the atmosphere (Blanchard, 1964; Facchini et al., 2008). The SML has a heterogeneous composition which can be comprised of organic carbon, amino acids, carbohydrates, and Transparent Exopolymer Particles (TEP) (A. Engel & Galgani, 2016; Wurl & Holmes, 2008). The chemical properties of the SML, including concentrations of TEP, free amino acids, and phosphate, have been shown to be variable, with the standard deviation of some variables being greater than the average of measured values (Reinthaler, Sintes, & Herndl, 2008; Zäncker, Bracher, Röttgers, & Engel, 2017).

For comparison, marine aerosol particles have been shown to be both homogeneous in terms of submicron organic functional group composition (Frossard et al., 2014; L. M. Russell, Hawkins, Frossard, Quinn, & Bates, 2010) and heterogeneous in terms of variety of micron-sized

particle types (Hawkins & Russell, 2010; G. Saliba et al., 2021). The consistency in organic composition and CCN activity of marine aerosol, defined as the aerosol present during clean marine conditions, has been shown across several open ocean regions of the Pacific and Atlantic Oceans (Bates et al., 2020; Frossard et al., 2014; Quinn et al., 2014; L. M. Russell et al., 2010). Aerosol particles collected from Sea Sweep, a device that generates primary aerosol by bubbling seawater from 1 m below the sea surface, have shown that gPMA results in relatively consistent CCN activity and size-resolved mass fractions (Bates et al., 2020; Bates et al., 2012). From these studies, it has been hypothesized that dissolved organic carbon (DOC) is the pool of carbon that has a greater influence on gPMA composition than particulate organic carbon (POC), since dissolved organic matter is the largest ocean reservoir of reduced carbon (Beaupré et al., 2019; C. A. Carlson & Hansell, 2015; Hansell, Carlson, Repeta, & Schlitzer, 2009; Lewis et al., 2021). This hypothesis is consistent with the fact that DOC has a relatively consistent fraction in comparison to particulate organic carbon (POC) and is present in both the SML and sub-surface water (C. A. Carlson & Hansell, 2015; Gasparovic, Plavšić, Ćosović, & Reigstad, 2005; van Pinxteren et al., 2017). However, the few available measurements of organic composition for individual particles sampled from within the SML span a diverse range of types that might indicate a role for POC and the SML in influencing sea spray formation.

To understand what role the SML plays in the composition of submicron atmospheric aerosol, we collected and analyzed samples of the SML, atmospheric aerosol particles, subsurface seawater, and gPMA that were collected within four hours of each other. There are very few studies in which SML, seawater, and atmospheric aerosol particles have been sampled simultaneously to allow assessment of how SML composition transfers to atmospheric aerosol (van Pinxteren et al., 2017). SML samples (depth ~0.001 m), sub-surface seawater samples

(depth 5 m), gPMA from Sea Sweep (Bates et al., 2012) (depth of ~1 m), and atmospheric aerosol particles (height 18 m) collected in September 2017 and March 2018 during the North Atlantic Aerosol and Marine Ecosystem Study (NAAMES) (Behrenfeld et al., 2019) were analyzed using both single particle microscopy from Scanning Transmission X-Ray Microscopy with Near Edge X-Ray Absorption Fine Structure (STXM-NEXAFS) and FTIR. This study investigates this unique dataset to assess the degree to which SML and seawater have similar organic composition to gPMA and atmospheric aerosol particles.

2.2 Methods

2.2.1 NAAMES

NAAMES was an interdisciplinary investigation conducted to improve understanding of Earth's ocean-aerosol-cloud system (Behrenfeld et al., 2019). The campaign consisted of four cruises on the R/V *Atlantis* in the North Atlantic that each included 26 days at sea in November 2015 (NAAMES 1, Winter), May-June 2016 (NAAMES 2, Late Spring), September 2017 (NAAMES 3, Autumn), and March-April 2018 (NAAMES 4, Early Spring). The ship traveled to and from Woods Hole, MA, to ~ 55°N for the first three cruises. For NAAMES 4, the ship departed from San Juan, Puerto Rico, to ~44.5°N and returned to Woods Hole, MA. During each cruise, the ship occupied five to seven multi-day sampling stations to conduct biological and oceanographic experiments. SML samples were only collected on NAAMES 3 and NAAMES 4, so those are the only data used in this study.

2.2.2 Sea Sweep

The Sea Sweep is a primary marine aerosol particle generator that has been used to provide a surrogate for particles formed from bubble bursting at the ocean surface to investigate the properties of primary marine aerosol (Bates et al., 2012). Sea Sweep consists of a stainless-

steel frame attached to two inflatable pontoon floats and was deployed off the port bow of the R/V *Atlantis*. The sea surface inside the sampling hood is contained to capture aerosols produced from the microlayer, but splashing in high-wave conditions may modify the microlayer. The stainless-steel hood on top of the frame maintains a laminar flow air curtain of particle-free air (charcoal and HEPA filtered) at the bow and stern ends of the frame (Bates et al., 2012). Stainless steel frits, 200 μm in size, were positioned below the sea surface at approximately 0.75 m. The resulting particles were then transported to the instruments for analysis. Because the particles are transported directly to sampling instrumentation without time for atmospheric processes, they provide a convenient proxy for the "primary" component of sea spray aerosol.

2.2.3 Atmospheric Particle and gPMA Filter Collection

Atmospheric and gPMA particles were collected through a temperature-and humidity-controlled inlet during NAAMES. Atmospheric and generated primary marine aerosol (gPMA) particles were dried using diffusion driers filled with silica gel and collected on 37 mm Teflon filters (Pall Inc., 1 μm pore size) for FTIR spectroscopy analyses. < 1 μm filters for atmospheric and gPMA were sampled at 8.3 L min^{-1} after a <1 μm cyclone (SCC 2.229) at a flow rate of 16.7 L min^{-1}. Filters for <0.18 and <0.5 μm atmospheric and <1.1 μm gPMA particles were sampled at 10 L min^{-1} after Berner impactors sampling at 30 L min^{-1}. Filters were collected for 12-23 hours for atmospheric particle samples (<0.18, <0.5, and <1 μm) and two hours for Sea Sweep samples (<0.18, <1, and <1.1 μm), resulting in filtered air volumes of 1-13.8 m^{-3}. After collection, the filters were immediately unloaded, stored in petri dishes, and frozen at 0°C for later analysis at Scripps Institution of Oceanography.

2.2.4 Seawater and Microlayer Collection

Seawater and sea surface microlayer (SML) samples were collected during the NAAMES 3 (September 2017) and NAAMES 4 (March-April 2018) cruises when on station, which is described in Behrenfeld et al. (2019). Six SML samples were chosen for further investigation: four from NAAMES 3 (09/10/17, 09/12/17, 09/15/17, and 09/16/17) and two from NAAMES 4 (03/27/18 and 04/03/18) (Table 1). These six SML samples were chosen because they had a start times within four hours of gPMA and atmospheric particle filter start times. The SML samples were collected via a Garrett screen (Garrett, 1967) (57.5 cm^2), which was attached to a nylon rope and lowered over the starboard side of the ship until it touched the surface of the ocean while horizontal and then pulled back up to the deck. The screen was then held at an angle to allow the SML sample to drain off the screen for approximately 1 minute, through an acid-cleaned glass funnel, and into an acid-cleaned polycarbonate bottle following the procedures used in prior studies (M. Cunliffe & Wurl, 2014). This process was repeated until approximately 1.5 L was collected. Nitrile gloves were used whenever the Garrett screen was handled before and during sampling. The screen was rinsed with seawater between samples. The seawater samples were collected the same hour as the SML samples either using the ship in-line near-surface sampling system (NAAMES 3) or from 5-m CTD mounted Niskin bottles (NAAMES 4). The Imaging FlowCytobot (IFCB) cell biovolume was measured for the SML samples as well as for the in-line and Niskin seawater samples (Chase et al., 2020; Moberg & Sosik, 2012). After SML collection, ~60 mL of seawater and SML samples were poured into amber storage bottles and immediately frozen at -20^o C to be later processed and analyzed for FTIR and STXM-NEXAFS analysis at Scripps Institution of Oceanography.

2.2.5 FTIR Spectroscopy and Algorithm

Samples on Teflon filters were analyzed using FTIR spectroscopy (Bruker Tensor 27 spectrometer with a deuterated triglycine sulfate, DTGS, detector) to measure the infrared transmission using 2 cm^{-1} resolution (Takahama, Johnson, & Russell, 2013). The FTIR was located in a temperature and humidity-controlled cleanroom, and the sample was purged with pure nitrogen at approximately 3 LPM for 3 min prior to the collection of each spectrum. FTIR spectra were checked for hydrate absorption, and no samples had an identifiable amount so dehydration was not required (Frossard & Russell, 2012). The FTIR spectrum for each filter was analyzed using an automated fitting algorithm (Maria, Russell, Turpin, & Porcja, 2002; L. M. Russell et al., 2009; Takahama et al., 2013). When the baselining procedure resulted in degenerate spectra, defined as spectra that have no discernable peaks and low signal to noise, they were excluded from further analysis. In this dataset, no filters had degenerate spectra. The FTIR spectrum for each filter was analyzed using an automated fitting algorithm (Maria et al., 2002; L. M. Russell et al., 2009; Takahama et al., 2013). Five organic functional groups were quantified from these mixtures (alkane, hydroxyl, amine, carboxylic acid, and non-acidic carbonyl) and summed together to quantify the organic mass (OM) concentration, with alkene, aromatic, organosulfate, and organonitrate groups excluded because they were below detection.

OM group concentrations were considered above detection if they met three criteria: 1) the fitted peak area for the individual functional group exceeded the minimum observable peak area (defined below), 2) the fitted peak area for the individual functional group exceeded twice the standard deviation of the pre-scan background area, and 3) the alkane functional group was one of the groups that met the first two criteria (Lewis et al., 2021). OM from this technique has an uncertainty of ± 20% due to functional groups that overlapped the Teflon absorption,

unquantified functional groups, and semi-volatile properties (Maria et al., 2002; Lynn M. Russell, 2003; Lynn M. Russell et al., 2009; L. M. Russell et al., 2009; Takahama et al., 2013). Cosine similarity (dot-product cosine on normalized spectra) was used to quantify spectral similarity because it has been shown to be sensitive to small spectral differences in FTIR and similar chemical spectra (Frossard et al., 2014; Liu et al., 2017; Stein & Scott, 1994; Wan, Vidavsky, & Gross, 2002).

2.2.6 Net Primary Production and Chlorophyll Measurements

Net Primary Production (NPP) (μmol C L^{-1} d^{-1}) was estimated using the Photoacclimation Productivity Model from Fox et al. (2020), which showed strong agreement with available measurements from 24 hour ^{14}C sodium bicarbonate uptake incubations. Shipboard chlorophyll concentrations were analyzed by a Wetlabs ACS which measured hyperspectral particulate attenuation and absorption, which are optical measurements commonly used to estimate chlorophyll concentration, calibrated to the NAAMES campaign (Boss, Twardowski, & Herring, 2001; Cetinić et al., 2012). NPP was normalized to the integrated depth of the euphotic zone for each station to obtain a consistent metric for the maximum column productivity. The column maximum was used since the bubble entrainment depth is not known and the mixing layer depth was variable (6-231 m during the NAAMES campaigns).

2.2.7 Sample Preparation

Frozen seawater and SML samples were brought to room temperature, atomized with a constant output atomizer (TSI Model 3076), dried using diffusion driers filled with silica gel, and collected on silicon nitride windows (Si_3N_4; Silson Ltd.) mounted on a rotating impactor (Streaker; PIXE International, Inc.) at 1 LPM. The sampling times ranged from 3 to 5 minutes for STXM-NEXAFS. Teflon filters for FTIR were also atomized and dried using diffusion driers

filled with silica gel at 1 LPM using the same sampling system after the collection on the silicon nitride windows for STXM-NEXAFS. The sampling times ranged from 2 to 6 hours for FTIR filters. The atomizer and impactor were cleaned with isopropanol between seawater and SML samples and DI water was atomized for a minimum of 2 hours between samples. Windows and filters were frozen directly after collection and stayed frozen until time of analysis (samples were analyzed between September 2019 and June 2021). The size distribution was not measured during this process, but the particles collected after drying are expected to be smaller than 1 μm based on the design.

Atmospheric particles and gPMA were collected on Teflon filters that were used directly for nondestructive FTIR spectroscopy. After FTIR was completed, the particles on each filter were extracted and dried on silicon nitride windows in order to compare the composition by STXM-NEXAFS (Crilley, Ayoko, & Morawska, 2013). To extract the particles from the filters, the filters were placed in a fume hood on isopropanol cleaned aluminum foil and 200 μL of HPLC-grade DI water (Sigma Aldrich) was aliquoted onto the center of the filter and agitated for 2 min. 20 μL from the filter were transferred to the silicon nitride windows and left to dry overnight. The samples were frozen at 0˚C until analysis. The particles that formed after the extracts collected on these samples dried ranged from 0.2 to 7.5 μm diameter.

2.2.8 Organic Functional Group Composition by STXM-NEXAFS

In all, 34 samples of extracted atmospheric particles, atomized SML, extracted gPMA, and atomized seawater from NAAMES 3 (September 2017) and NAAMES 4 (March 2018) were analyzed at the Advanced Light Source at Lawrence Berkeley National Laboratories Beamline 5.3.2.2 in a He-filled chamber using scanning transmission X-ray microscopy (STXM) with near edge X-ray absorption fine structure (NEXAFS) following established protocols (Maria Steven,

Russell Lynn, Gilles Mary, & Myneni Satish, 2004; Lynn M. Russell, Maria, & Myneni, 2002). These 34 samples resulted in 219 stacks of spectra from particles that ranged in size from 0.2 to 7.5 μm, where these sizes reflect the extracted or atomized sizes rather than their innate characteristics (and hence are not discussed here). These spectra were analyzed by an automated-shape recognition algorithm, which identified areas of high pre-edge density (non-carbon components) and high carbon density (post-edge minus pre-edge) (Takahama, Liu, & Russell, 2010). Of these 219 particles stacks, 122 (56%) particles passed the quality control checks, including having carbon absorbance sufficiently above the noise. The 122 particles were then clustered into eight categories using the MATLAB k-means clustering algorithm.

2.3 Results

In this section, we report the differences in functional group composition for the different sample types (seawater, gPMA, SML, and atmospheric particle) and describe individual days on which multiple sample types were collected within four hours of each other. The morphology of the extracted (atmospheric particles and gPMA) or atomized (SML and seawater) STXM-NEXAFS particles are included (Table S1) as they contribute to chemical identification even though they are not representative of airborne samples.

2.3.1 Comparison of Different Sample Types

The four sample types (seawater, SML, gPMA, and atmospheric particle) show generally similar functional group composition by FTIR and STXM-NEXAFS, although indicators of small differences in molecular structures are present (Figures 2.1 and 2.2, respectively).

FTIR (Figure 1) and STXM-NEXAFS (Figure 2.2) spectra for seawater were similar during the three days that were sampled and above detection limit.

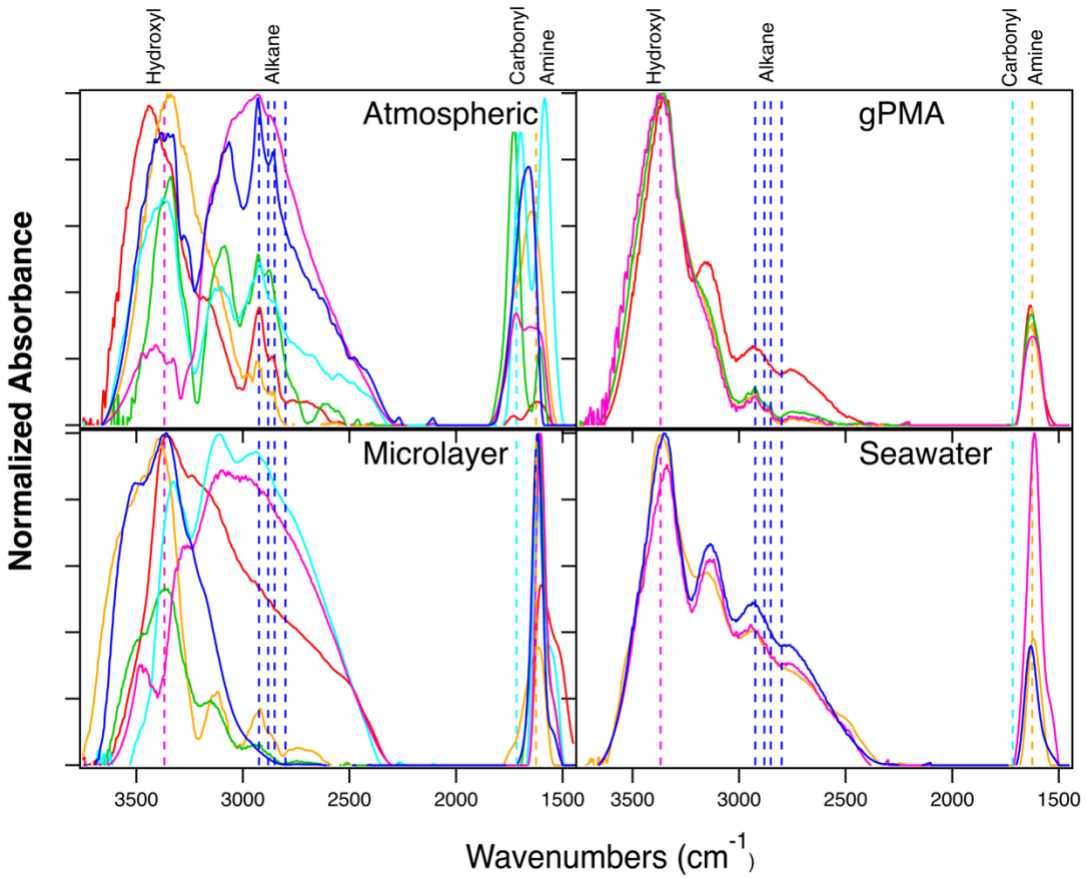

Figure 2.1 Normalized FTIR spectra from 4 sample types (Atmospheric, gPMA, Microlayer, and Seawater) collected on 6 different days: 09/10/17 (red), 09/12/17 (orange), 09/15/17 (green), 09/16/17 (teal), 03/27/18 (blue), and 04/03/18 (pink). The dashed vertical lines indicate the hydroxyl group peak location at 3369 cm^{-1} (pink), alkane group peak locations at 2800, 2852, 2882, and 2925 cm^{-1} (blue lines), carbonyl group peak location at 1717 cm^{-1} (teal), and amine group peak location at 1625 cm^{-1} (orange).

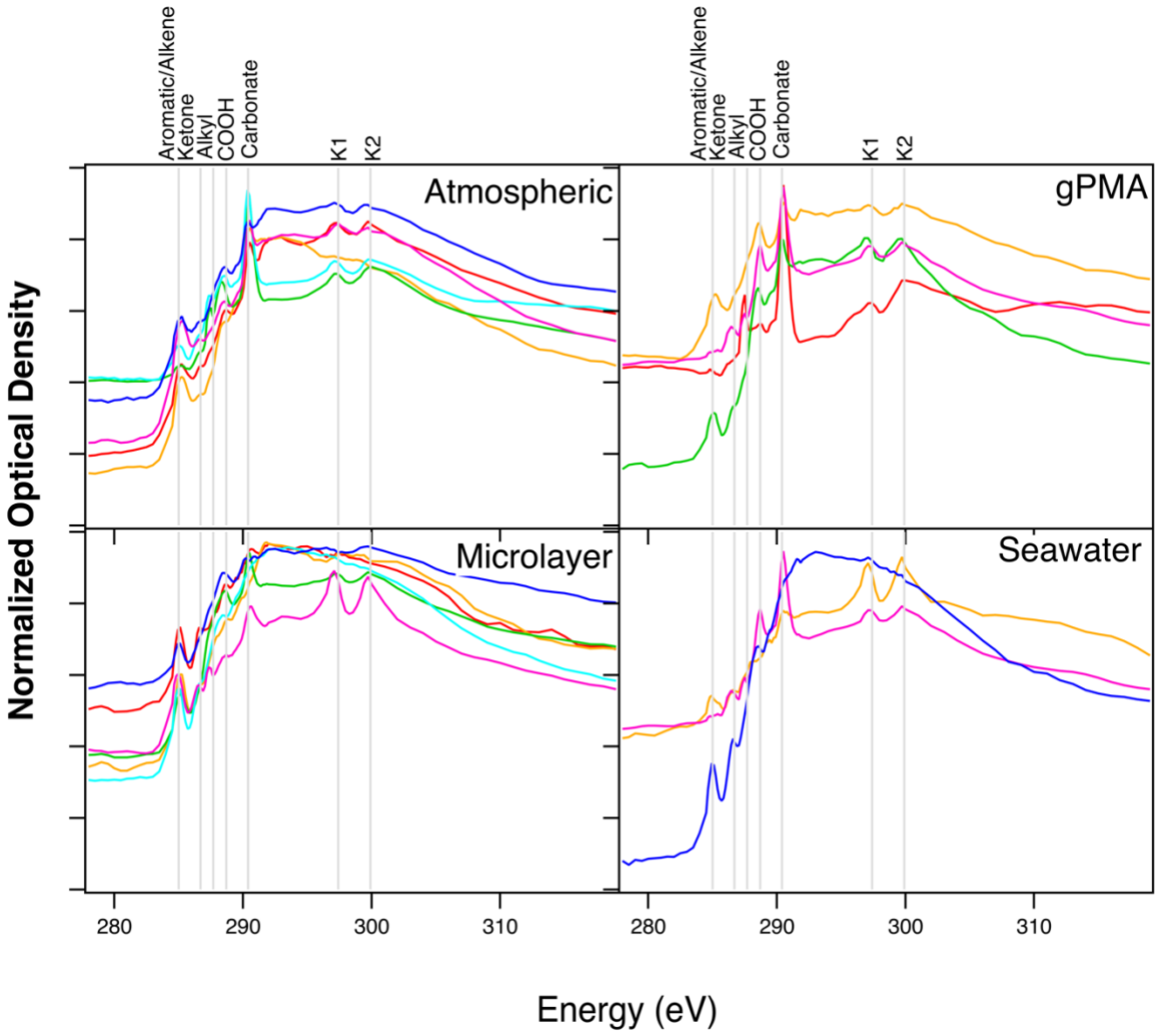

Figure 2.2: Normalized STXM-NEXAFS centroids from 4 sample types (Atmospheric, gPMA, Microlayer, and Seawater) collected on 6 different days: 09/10/17 (red), 09/12/17 (orange), 09/15/17 (green), 09/16/17 (teal), 03/27/18 (blue), and 04/03/18 (pink). Vertical grey lines in each panel indicate peak locations for the selected functional groups, from left to right, are aromatic (285 eV), ketone (286.7 eV), alkyl (287.7 eV), carboxylic acid (288.7 eV), carbonate (290.4 eV), and two potassium peaks (297.4 and 299.9 eV).

All samples had high cosine similarity values with low standard deviations of 0.98 ± 0.02 (N=3) for FTIR and 0.97 ± 0.02 (N=7) for STXM-NEXAFS (Table 2). Seawater typically had an FTIR spectra with two hydroxyl group peaks, a broad alkane group peak at 2927 cm^{-1}, and a narrow amine group peak at 1615 cm^{-1} (Figure 2.1). The hydroxyl group fraction was 65-75% of the OM, followed by alkane group (15-25%) and amine group (<10%). The STXM-NEXAFS spectra show an aromatic/alkene carbon peak, alkyl carbon peak, and a small carboxylic acid carbon peak, with about one in three also having potassium peaks. The carboxylic acid group was below detection limit for FTIR, as is expected for seawater (Frossard et al., 2014), but STXM-NEXAFS is a more sensitive instrument and carboxylic acids are a trace component of seawater composition (Gagosian & Stuermer, 1977; Hertkorn et al., 2006). STXM-NEXAFS shows four different k-means clusters of spectra for the seawater sample type.

Similar to previous studies (Bates et al., 2012; Frossard et al., 2014), gPMA FTIR spectra showed a high cosine similarity value with a low standard deviation (0.94 ± 0.06, N=4) between different days and two seasons, with hydroxyl groups having the highest group mass concentration, followed by alkane and amine functional groups (Figure 2.1). The STXM-NEXAFS spectra show carboxylic acid carbon, carbonate, and potassium peaks in four out of six of the samples and aromatic/alkene carbon peaks in half of the samples (Figure 2.2). The STXM-NEXAFS spectra were also similar to each other with a cosine similarity value of 0.97 ± 0.02 (N=19). There were six different k-means clusters of spectra for the gPMA sample type, showing a variety of individual particle compositions.

The SML FTIR spectra show the most variability, as demonstrated by the lowest cosine similarity value and highest standard deviation of the different sample types (0.72 ± 0.18, N=6). The different peak shapes and locations in the FTIR spectra vary from sample to sample (Figure

2.1, top right panel). However, FTIR-based organic functional group composition showed that the OM in the SML samples predominately consisted of the hydroxyl group (50 – 80%), followed by smaller mass contributions of alkane and amine functional groups (5 – 35%) (Figure 2.3). STXM-NEXAFS had a cosine similarity of 0.98 ± 0.02 (N=38). STXM-NEXAFS shows six different k-means clusters of spectra for the SML sample type, illustrating that the individual particle components are variable.

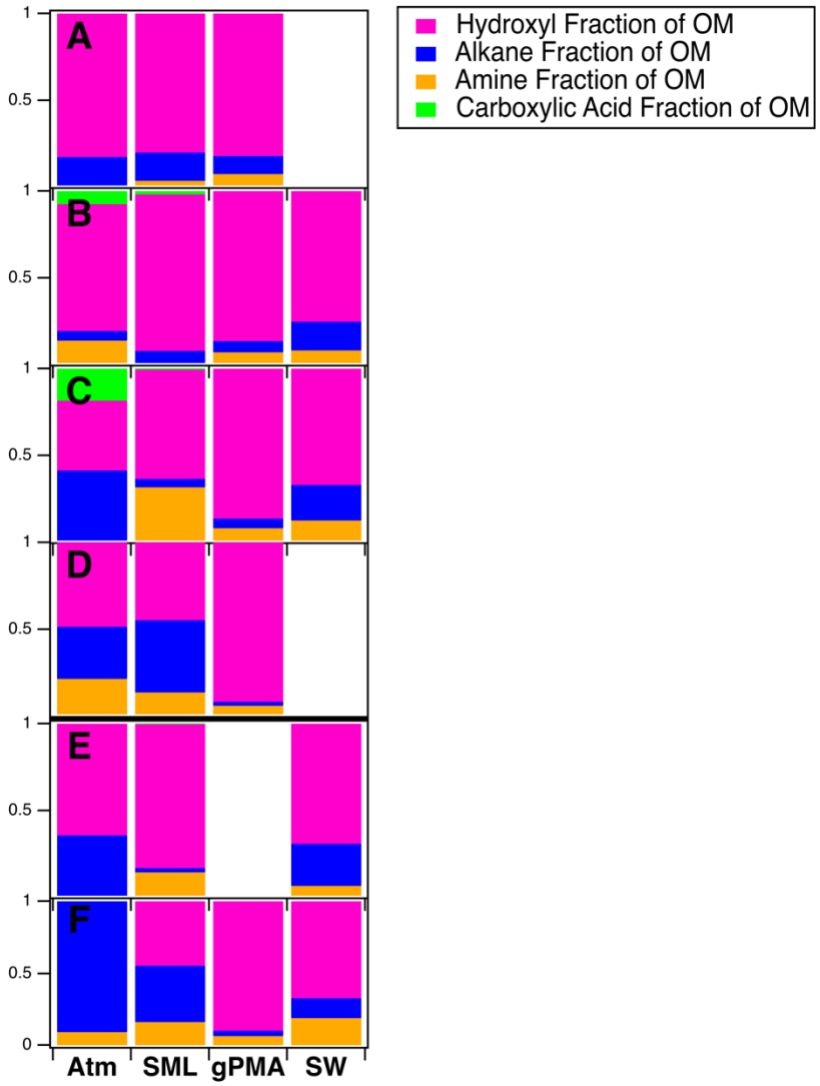

Figure 2.3: The organic functional group fraction from FTIR spectra with hydroxyl groups (pink), alkane groups (blue), amine groups (orange), and acid groups (green). The four sample types are atmospheric particles (Atm), sea surface microlayer (SML), gPMA, and seawater (SW). The panels show the dates sampled: (A) 09/10/17, (B) 09/12/17, (C) 09/15/17, (D) 09/16/17, (E) 03/27/18, and (F) 04/03/18. The seasonal change occurs between panels D and E and is denoted with a thick black bar. The NPP values for each panel, as described in Table 1, are: (A) 0.19 µmol C $l^{-1}d^{-1}$, (B) 0.42 µmol C $l^{-1}d^{-1}$, (C) 0.59 µmol C $l^{-1}d^{-1}$, (D) 0.72 µmol C $l^{-1}d^{-1}$, (E) 0.6 µmol C $l^{-1}d^{-1}$, and (F) 1.31 µmol C $l^{-1}d^{-1}$.

Two of six atmospheric particle FTIR spectra and all six STXM-NEXAFS spectra had carboxylic acid groups that were likely from secondary photo-oxidative processing. The presence of carboxylic acid groups is consistent with previous observations of ambient marine aerosol samples in clean conditions (Frossard et al., 2014; L. M. Russell et al., 2010; Georges Saliba et al., 2020). While the FTIR hydroxyl group fraction varied from 50 to 90% of the measured OM, there was no statistical difference ($p>0.05$) when the fractions of hydroxyl, alkane, and amine groups from the different sources were compared. Atmospheric particle samples had the second lowest FTIR cosine similarity value (0.75 ± 0.15, N=6) and the lowest STXM-NEXAFS cosine similarity value (0.95 ± 0.1, N=58). All six centroids of STXM-NEXAFS spectra had an aromatic/alkene carbon peak, a carboxylic acid carbon peak, and a carbonate peak. Four of the six STXM-NEXAFS spectra also had an alkyl carbon peak and potassium peaks. All eight of the k-means clusters were found in the atmospheric particle sample type, making it the only sample type that contains every cluster.

2.3.2 Comparison of Sampled Days

Six sets of samples that were each collected on the same day were used to investigate connections between the four sample types (subsurface seawater, SML, gPMA, atmospheric aerosol) (Figure 2.4). This comparison was investigated to identify if there was a chemical signature that linked subsurface seawater and SML as sources for the gPMA or atmospheric particles.

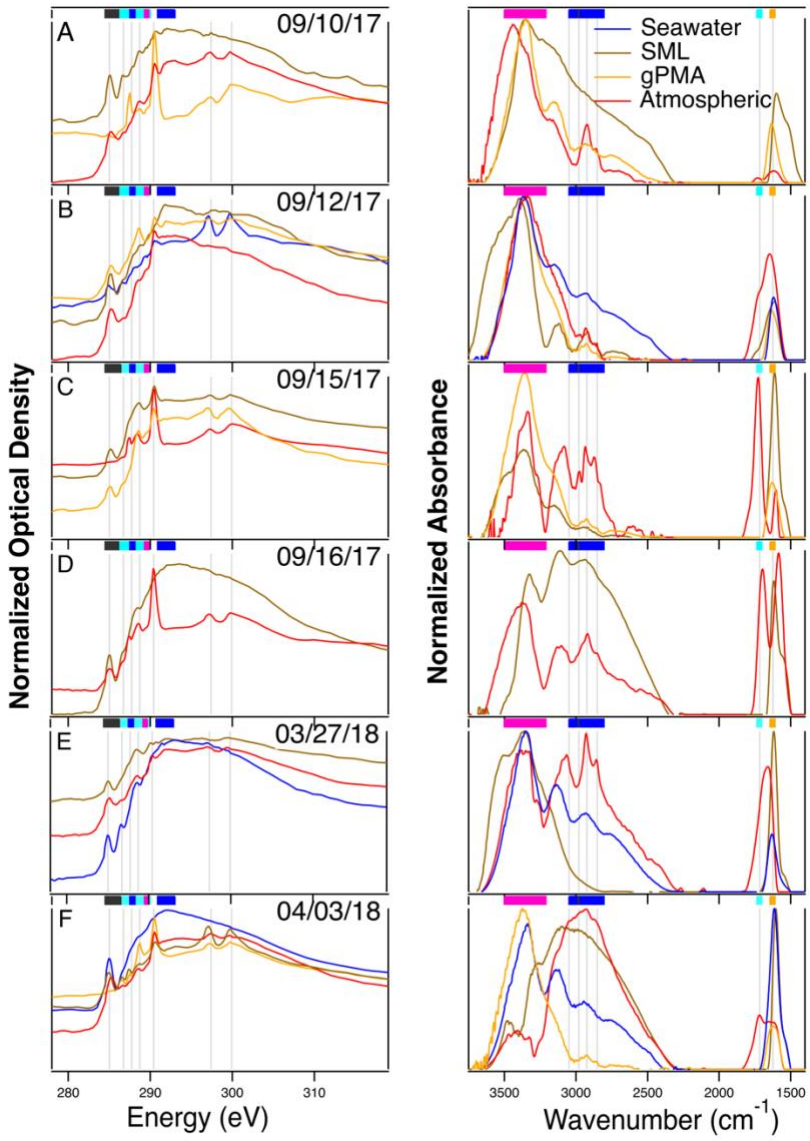

Figure 2.4**:** Centroids of normalized STXM-NEXAFS spectra from 6 separate days (left column) and normalized FTIR spectra (right column). Spectra were normalized to the highest absorbance peak before averaging. The rows show the dates sampled (with the number of particles within each STXM-NEXAFS spectra in parentheses): [A] 09/10/17 (Atmospheric: 8, gPMA: 2, SML: 3), [B] 09/12/17 (Atmospheric: 3, gPMA: 4, Seawater: 3, SML: 3), [C] 09/15/17 (Atmospheric: 8, gPMA: 5, SML: 9), [D] 09/16/17 (Atmospheric: 7, SML: 5), [E] 03/27/18 (Atmospheric: 7, Seawater: 2, SML: 9), and [F] 04/03/18 (Atmospheric: 8, gPMA: 3, Seawater: 2, SML: 4). The colored bars on top indicate shared functional group peak locations with aromatic/alkene absorption in black, hydroxyl in pink, alkane in blue, carbonyl in teal, and amine in orange. The STXM-NEXAFS functional groups identified by the grey lines, from left to right, are aromatic (285 eV), ketone (286.7 eV), alkyl (287.7 eV), carboxylic acid (288.7 eV), carbonate (290.4 eV), and two potassium peaks (297.4 and 299.9 eV). Table 1 contains the number of particles within each STXM-NEXAFS sample for each source for each day.

The first set of samples analyzed from NAAMES 3 was on 10 September 2017 (Figure 2.4, row A), when there were three sample types: SML, gPMA, and atmospheric particles. The STXM-NEXAFS atmospheric particles and SML spectra both had an aromatic/alkene carbon peak, carboxylic acid carbon peak, and carbonate peaks. The gPMA spectrum also had a sharp alkyl carbon peak and carbonate peak.

Sampling on 12 September 2017 (Figure 2.4, row B) included all four sample types. STXM-NEXAFS showed that all four types have an aromatic/alkene carbon peak, and the gPMA, atmospheric particle, and sea water samples had a carbonate carbon peak. The FTIR showed the hydroxyl group peaks having nearly identical peak locations between 3338 and 3395 cm^{-1}. All four FTIR spectra had hydroxyl, alkane, and amine group peaks.

On 15 September 2017 (Figure 2.4, row C), three sample types were collected and analyzed (SML, gPMA and atmospheric particle), with each corresponding STXM-NEXAFS spectrum showing a carboxylic acid carbon peak, carbonate carbon peak, and potassium peaks. The atmospheric particle sample did not have an aromatic/alkene carbon peak, which was different than on 10 and 12 September 2017. The FTIR spectra from the three sample types were noticeably different from each other, with the atmospheric aerosol particle spectrum having an alkane group fraction that was twice as high as in the SML and seawater samples, as well as a large carboxylic acid group peak. The gPMA FTIR spectrum was similar to those from 10 and 12 September 2017. The SML FTIR spectrum had a similar hydroxyl group peak shape, but a larger amine group contribution than on 10 and 12 September 2017.

On 16 September 2017 (Figure 2.4, row D), the ship continued sampling at the same location as on 15 September 2017 and there were two types collected and analyzed: SML and atmospheric particle. The atmospheric particle sample had a STXM-NEXAFS spectrum with

alkyl carbon peak, carboxylic acid carbon peak, and carbonate peaks, as well as an aromatic/alkene carbon peak. The FTIR spectrum showed a broader hydroxyl group peak and larger alkane group peaks in the atmospheric particle sample than in the SML sample. Compared to 15 September 2017, the SML FTIR spectrum had a larger alkane group contribution and smaller hydroxyl group contribution.

The first set of samples analyzed from NAAMES 4 was 27 March 2018 (Figure 2.4, row E), when there were three sample types: SML, seawater, and atmospheric particle. STXM-NEXAFS spectra showed that all three types have aromatic/alkene and carboxylic acid carbon peaks. The FTIR spectra showed that the three samples have similar hydroxyl group peak locations, with overlapping primary peaks between 3350 and 3370 cm^{-1}. The SML sample has a partial peak at 3510 cm^{-1} that is in three of the six SML samples in Figure 2.4. The atmospheric particle FTIR spectrum had sharp alkane group peaks, while the seawater had broad alkane group peaks and the SML had very little alkane group absorption.

On 3 April 2018 (Figure 2.4, row F), all four sample types were collected and analyzed. STXM NEXAFS spectra show a varied functional group composition, in which the seawater only had an aromatic/alkene carbon peak. The SML sample STXM-NEXAFS spectrum had an aromatic/alkene carbon peak, alkyl carbon peak, carboxylic acid carbon peak, carbonate peak, and potassium peaks. The gPMA sample has a carboxylic acid carbon peak, carbonate peak, and potassium peaks. The atmospheric aerosol particles STXM-NEXAFS spectrum had aromatic/alkene carbon, carboxylic acid carbon, and carbonate peaks. The FTIR spectra displayed two main composition types, where SML and atmospheric particle types had narrower hydroxyl group peaks that are smaller than the broad alkane group peak. gPMA and seawater spectra showed a broad hydroxyl group peak with smaller and narrower alkane group peaks.

Seawater and gPMA (<1 and <1.1 μm) samples (blue and orange in Figure 2.4) show FTIR spectra that do not show much variation in composition (cosine similarity of 0.94 ± 0.06 and 0.98 ± 0.02) throughout the six days of sampling, with two hydroxyl group peaks comprising most of the OM, followed by broad alkane group absorption and an amine group absorption. STXM-NEXAFS spectra consistently (five of six) had aromatic/alkene and alkyl carbon peaks and occasionally (three of six) had carbonate and potassium absorption peaks. Atmospheric and SML samples (red and brown in Figure 2.4) showed far more variability in their FTIR spectra throughout the six days, as demonstrated by the high standard deviation in cosine similarity (0.75 ± 0.15 and 0.72 ± 0.18). The FTIR spectra showed more variation than STXM-NEXAFS spectra, as indicated by cosine similarity values lower than 0.8 (Table 2.2). STXM-NEXAFS showed that the majority (11 of 12) of atmospheric particle and SML spectra had an aromatic/alkene carbon peak and carboxylic acid carbon peak. All six atmospheric particle filters also had carbonate peaks, whereas only two of six SML samples had carbonate. The atmospheric particle filters were the most dissimilar of the four sample types using STXM-NEXAFS (0.95 ± 0.1).

FTIR spectra had lower cosine similarity values than NEXAFS spectra (Table 2), with hydroxyl, alkane, and amine groups being present in all samples and hydroxyl group accounting for 50 – 90% of the quantified OM. Seawater and gPMA samples had similar composition with hydroxyl groups comprising 70-90% of the quantified OM, with the remainder from alkane groups (5-20%) and amine groups (2-20%), throughout the sampling days which span two different seasons. The SML and atmospheric particle samples had FTIR spectra that were more variable, but still included the same three organic functional groups (hydroxyl, alkane, and amine), and the hydroxyl group accounted for 40 - 80% of quantified OM.

The variability in the SML and atmospheric particle spectra were compared using the alkane-to-hydroxyl functional group ratio and several biological proxies, including in-line chlorophyll and net primary production (NPP) (Figure 2.5 and Figure 2.9). The alkane-to-hydroxyl group ratios had small ranges of alkane-to-hydroxyl group ratio, as evidenced by small standard deviations, for both seawater (0.08 ± 0.04) and gPMA (0.26 ± 0.08). SML and atmospheric particle alkane-to-hydroxyl group ratios showed more variability, with 0.37 ± 0.42 for SML and 0.5 ± 0.37 for atmospheric particles. Here, we found weak and moderate correlations between the alkane-to-hydroxyl group ratio and both in-line chlorophyll (Figure 2.9) and NPP (Figure 2.5) for both atmospheric particle (with no significance, $p = 0.24$) and SML samples (with no significance, $p = 0.12$) over a range of alkane to hydroxyl group ratios from 0 to 1 (0.5 ± 0.4 and 0.4 ± 0.4, respectively). For seawater, there was no correlation, and the range of alkane to hydroxyl group ratios were 0.2 ± 0.1. For gPMA, there was a strong negative correlation (with no significance, $p = 0.14$), but again low values and little variation in alkane to hydroxyl group ratio 0.1 ± 0.01. While the sample size is too small to establish statistical significance of the correlations, the difference in the ranges of values is noteworthy with atmospheric particle and SML ranges 2-10 times greater than seawater and gPMA ranges. The in-line chlorophyll had similar correlations to that of NPP for atmospheric particle and SML alkane to hydroxyl group ratios.

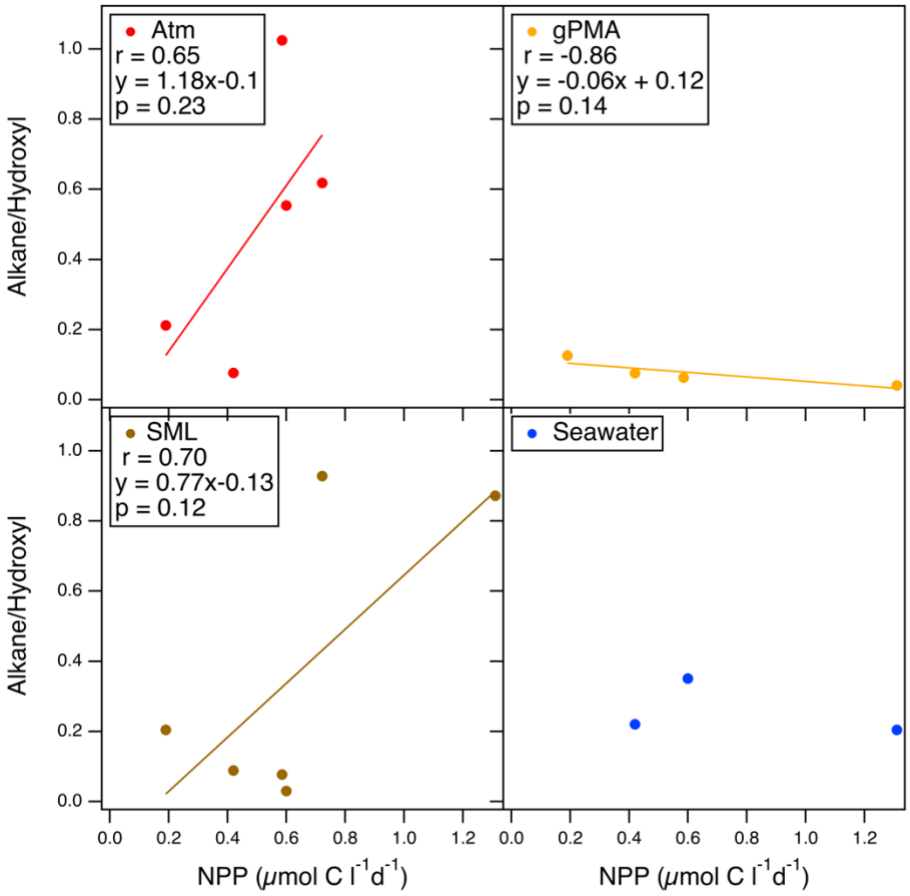

Figure 2.5: The alkane to hydroxyl ratio of atmospheric particle (top left), SML (bottom left), gPMA (top right), and seawater (bottom right) samples compared to NPP. NPP was integrated and normalized to the depth of the euphotic zone and obtained from (Baetge et al., 2021). Linear fit lines are shown for r>0.3. The points include measurements above detection for sample types collected on 09/10/17, 09/12/17, 09/15/17, 09/16/17, 03/27/18, and 04/03/18.

2.3.3 Clusters of STXM-NEXAFS Spectra for Sampled Particles

The average spectra of 122 particles were clustered into eight spectra categories (Figures 2.6 and 2.7). Five of the spectra categories are similar enough to previously reported categories presented by Takahama *et al.*,(2007) that they are considered to be the same category (Figure 2.6 and Table 2.3). These five categories represented particles that were previously named d, g, j, l, and m and associated with combustion (g,m), freshly emitted black carbon (d), humic-like biogenic sources (g,j,m), and unidentified (l). Two other categories, Macid and Mcarb, were similar to particles identified as derived from ocean sea spray sources over the Southern Ocean, reported in Saliba et al (2021).

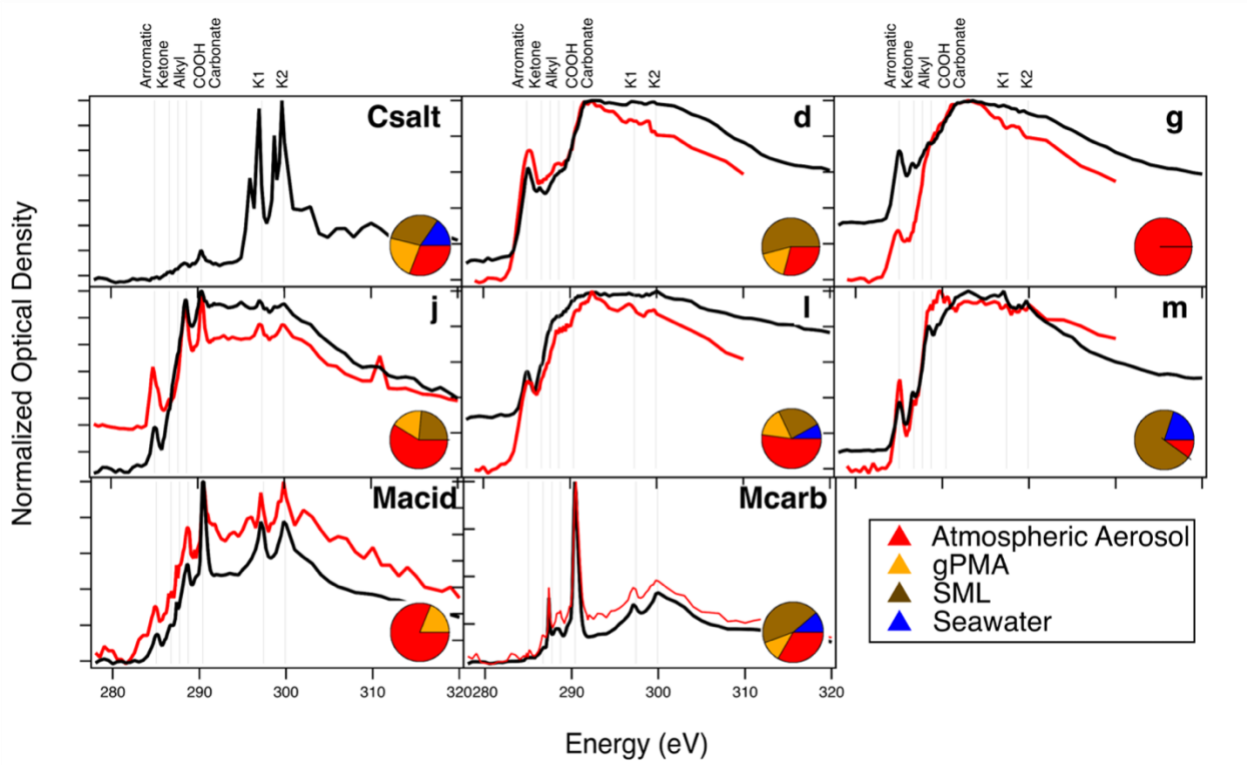

Figure 2.6: Normalized k-means STXM-NEXAFS clusters from the NAAMES campaign (black) compared to reference STXM-NEXAFS spectra (red). The reference spectra in m, j, d, l, and g are from Takahama et al. (2007) and the reference spectra from Macid and Mcarb are from Saliba et al. (2021). Vertical grey lines in each panel indicate peak locations for the selected functional groups, from left to right, are aromatic (285 eV), ketone (286.7 eV), alkyl (287.7 eV), carboxylic acid (288.7 eV), carbonate (290.4 eV), and two potassium peaks (297.4 and 299.9 eV). The pie chart indicates the number of particles from each sample type with seawater in blue, SML in brown, gPMA in orange, and atmospheric particle in red with the number of particles within each source for each category described in Table 3.

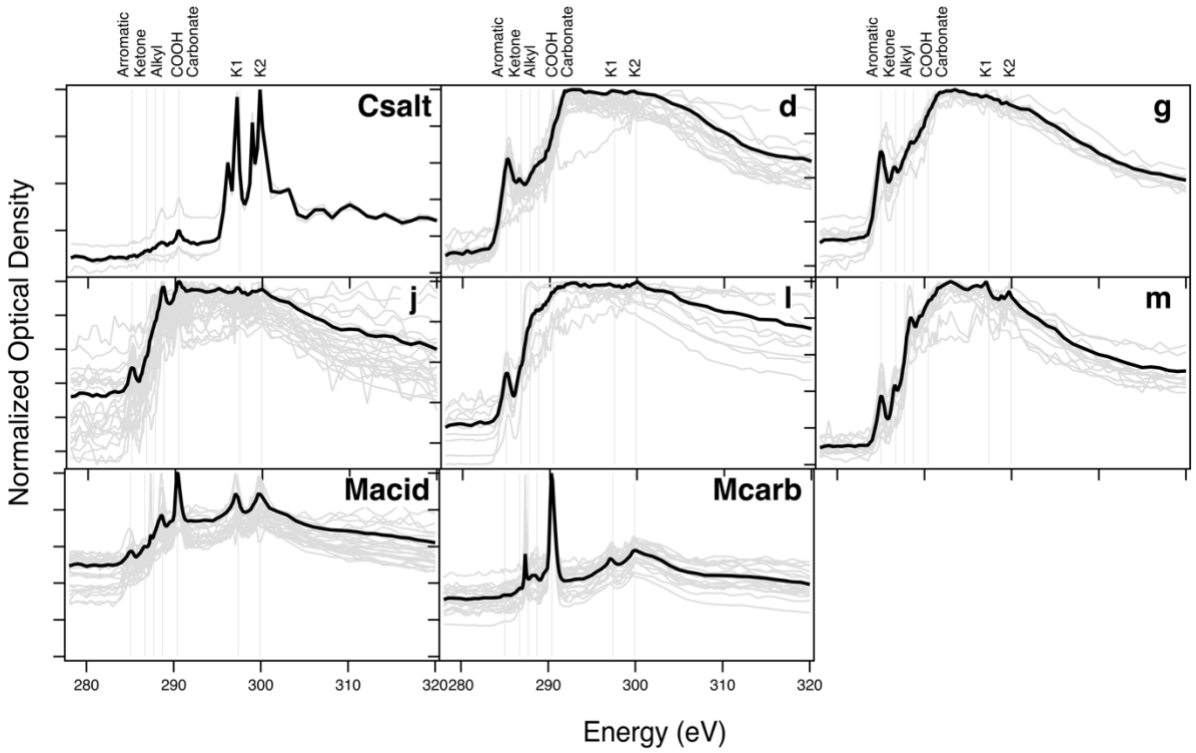

Figure 2.7: Normalized k-means cluster centroids of STXM-NEXAFS spectra from NAAMES campaign (black) and the individual particle-averaged STXM-NEXAFS spectra that comprise each cluster (grey). Reference spectra labeling is the same as Figure 2.6. Vertical grey lines in each panel indicate peak locations for the selected functional groups, from left to right, are aromatic (285 eV), ketone (286.7 eV), alkyl (287.7 eV), carboxylic acid (288.7 eV), carbonate (290.4 eV), and two potassium peaks (297.4 and 299.9 eV).

Particle spectra in cluster m had absorption in the aromatic/alkene, ketonic carbonyl, and alkyl carbon regions, similar to cluster m particles from Takahama et al., (2007) (cosine similarity = 0.99, two common peaks, Table 3). This cluster has particles from all four sample types (seawater, SML, gPMA, and atmospheric particle). The majority of SML particles (13 of 34) were in this cluster, which could mean that aromatic or alkene-containing substances such as phenols or humic materials are the source of the aromatic/alkene carbon peak (D. J. Carlson & Mayer, 1980; Knulst, Boerschke, & Loemo, 1998). It is also possible the aromatic/alkene carbon signal is from black carbon that had been deposited onto the sea surface or dissolved into the water column (Bao, Niggemann, Luo, Dittmar, & Kao, 2017). The particles had a high carbon

content and were mostly spherical, although it is prudent to recall that particle shape for atmospheric particle and gPMA filters represents the morphology of the dried extract rather than airborne particle morphology.

Particle spectra in cluster j had absorption in the aromatic/alkene carbon, carboxylic carbonyl carbon, carbonate, and potassium regions. This cluster was similar to Type j particles identified by *Takahama et al., (2007)* with a cosine similarity value of 0.94 and four common peaks (Table 3). This cluster had the second highest number of spectra with 24 out of 122 particles, including 13 SML, four gPMA, and seven atmospheric particles. Cluster j had the highest amount of SML particles. The morphology was a mixture of inorganic cores with organic coatings and clumps of organic-containing particles, indicating a likely marine biogenic source. Prior association of this type with humic and fulvic acids, soil substances, and biomass combustion by *Takahama et al., (2007)* suggests complex organic substances that may be surface active (Hayase & Tsubota, 1983) and have been measured previously in the SML (Drozdowska et al., 2017).

Particle spectra in cluster d (cosine similarity 0.99, one common peak) have absorbance in the aromatic/alkene carbon region and small absorbance in the ketonic carbonyl carbon region. This cluster was present during both NAAMES 3 and NAAMES 4. This cluster had 17 out of 122 particles, including four SML, three gPMA, and 10 atmospheric particle samples. The lack of peaks in this cluster other than the aromatic/alkene carbon absorption indicates it is likely fresh black carbon (Takahama et al., 2007)

Particle spectra in cluster Macid (cosine similarity 0.99, four common peaks, Table 3) were identified over the Eastern Pacific and over the Southern Ocean (Laskin et al., 2012; G. Saliba et al., 2021). This cluster is in NAAMES 3 and NAAMES 4 as well, along with

carboxylic carbonyl carbon, carbonate carbon, and potassium peaks. This cluster had the highest number of spectra with 25 particles from all four of the sample types. The morphology of atomized and extracted particles typically included low organic cuboidal shapes coated by organics, which likely represents a salt core with an organic coating (L. M. Russell et al., 2010). The acidic groups in the atmospheric particle samples may indicate that secondary photochemical processes have occurred.

Particles in cluster l had a clear absorption in the aromatic/alkene carbon region and a broader absorption in the ketonic carbonyl carbon region. These particles were similar to type l identified by Takahama et al., (2007) (cosine similarity = 0.99, two common peaks, Table 3), which was classified as not having an identified source because of the limited number of particles found and the limited availability of tracers for some types of sources. This cluster may be indicative of biological remnants such as cell fragments and lipid-like materials (sometimes identified as TEP) that have been measured previously in both SML and nascent sea spray aerosol (Aller et al., 2017; Wurl and Holmes, 2008). This particle cluster had several different morphologies that included cuboidal, amorphous, and spherical shapes after atomization, making it different from previously-reported BC morphology (Takahama et al., 2007). This cluster was present during both NAAMES 3 and NAAMES 4. This cluster had 10 out of 122 particles, including seven SML, one atmospheric, and two seawater particles.

Particles in cluster Mcarb accounted for 21 out of 122 particles and mostly consisted of extracted atmospheric particle particles, which are 17 out of the 21 particles. This cluster was present during both NAAMES 3 and NAAMES 4. This cluster was first observed in Saliba et al., (2021). The cluster spectra include three peaks, namely alkyl carbon, carbonate, and potassium, and the spectra in the cluster have a cosine similarity of 0.98. This cluster is also similar to the

calcareous phytoplankton cluster found in Hawkins and Russell, (2010). However, the morphology of the particles from this campaign often had salt cores and diverse morphologies, whereas the calcareous phytoplankton type had structures that resembled cell or shell parts without salt cores. This particle type was likely sea spray particles, but it included only particles that were extracted from filters (atmospheric particle and gPMA) for which the extracted morphology may be different from their airborne state.

Particles in cluster g included all four sample types and contained nine out of 122 particles from both campaigns. This particle type was previously identified (Takahama et al., 2007) (cosine similarity = 0.96, two shared peaks, Table 3), and the particle cluster was identified as combustion-related due to the prominent aromatic/alkene carbon peak and amorphous carboxylic carbonyl carbon absorption. The high carbon content and lack of potassium or alkyl groups in this cluster makes it likely that the cluster g particles in NAAMES 3 and NAAMES 4 are from combustion sources.

Particle spectra in cluster Csalt (crystallized salt) only accounted for three out of 122 particles and were from a single extracted atmospheric particle sample from NAAMES 3. This cluster is distinguished by the peak splitting at the two potassium peaks (297.4 and 299.9 eV). This may be due to the extracted particles crystalizing onto the silicon nitride windows, which has been shown to cause ligand field splitting (Vedrinskii et al., 1982).

2.4 Discussion

Prior work has indicated the SML to be enriched in amino acids, lipids, and organics in comparison to subsurface seawater (Aller, Kuznetsova, Jahns, & Kemp, 2005; Anja Engel et al., 2017; Obernosterer et al., 2008), suggesting that there would be a distinct difference in organic

composition between the SML and the other sample types (seawater, gPMA, and atmospheric particles). SML and atmospheric particle samples are different from the seawater and gPMA samples as shown by their lower cosine similarity values for FTIR and higher standard deviations between cosine similarity values of individual FTIR spectra within the same sample type (Table 2.2, Figures 2.1 and 2.2). However, we see many similarities in composition between the four types of samples with both FTIR and STXM-NEXAFS. All have three organic functional groups (hydroxyl, alkane, and amine) with hydroxyl consistently being the largest fraction (Figures 2.1 and 2.3). Most particles sampled have an aromatic/alkene carbon peak in STXM-NEXAFS spectra, regardless of sample source (Figure 2.2). Both FTIR and STXM-NEXAFS show hydroxyl groups and alkane groups; alkene groups are present in the STXM-NEXAFS spectra for the four sample types, although alkene groups are below the detection limit for FTIR quantification (Figure 2.4). Seawater and gPMA samples had very consistent FTIR spectra across the sampled days with high cosine similarity values for spectra from the same sample type (Table 2.2). When the STXM-NEXAFS particles were separated into categories by k-means clustering, the only cluster that had particles from a single sample type was Csalt, which had only three atmospheric aerosol particles. Other than this new category (which may be associated with a salt artifact), there were no unique particle clusters that were from only one sample source, rather the particle clusters had particles from most of the sample sources.

While the FTIR organic functional group composition was similar on average for the four sample types, the FTIR spectra showed peaks at different locations and with different shapes, particularly in the alkane region, for SML and atmospheric particle samples. The variability of the FTIR composition of both atmospheric particle and SML samples is evident in the low cosine similarity values (<0.8) and high standard deviations among samples within the same type (Table

2). In contrast, seawater and gPMA samples had much more consistent FTIR spectra, shown by the high cosine similarity values (>0.93) and low standard deviations (Table 2). This range of different organic composition of SML and atmospheric aerosol samples are consistent with prior measurements showing the presence of varying amounts of polymers, proteinaceous matter, and TEP in both SML and marine aerosol (Aller et al., 2017; Hendrickson et al., 2021; Kuznetsova, Lee, & Aller, 2005). Longer chain saccharides have been observed to be enriched in atmospheric aerosol particles and SML that are present, but not enriched, in seawater (Hasenecz, Kaluarachchi, Lee, Tivanski, & Stone, 2019). The SML has been shown to have a highly heterogeneous and variable composition (Chance et al., 2018; A. Engel & Galgani, 2016; Zäncker et al., 2017), whereas seawater often has less variability (Chance et al., 2018). The IFCB cell biovolume was also more concentrated and more variable in the SML compared to the inline seawater measurements ($p<0.05$) (Figures S2 and S3). The individual particles measured by STXM-NEXAFS are also consistent with the heterogeneity of SML with particles having a range of structures from salt cores with organic coatings to solid organic to mixtures of the two.

In Figure 2.3, Panels C, D, and F show sampling times that have higher NPP than in Panels A, B, E (Table 2.1). When NPP was higher, both SML and atmospheric aerosol particle samples had higher alkane/hydroxyl group ratios with high standard deviations (0.37±0.42 and 0.49±0.37, respectively), whereas seawater and gPMA samples were nearly identical with low standard deviations (0.25±0.08 and 0.08±0.04, respectively) despite the observed differences in NPP and Chl. The correlations of the four-sample alkane/hydroxyl group ratio to both chlorophyll (Figures 2.9 and 2.12) and NPP (Figure 2.5) indicate a possible role for the SML in contributing to the variability in atmospheric aerosol particle composition, perhaps driving the atmospheric particle correlation to biological tracers, as illustrated in Figure 2.8.

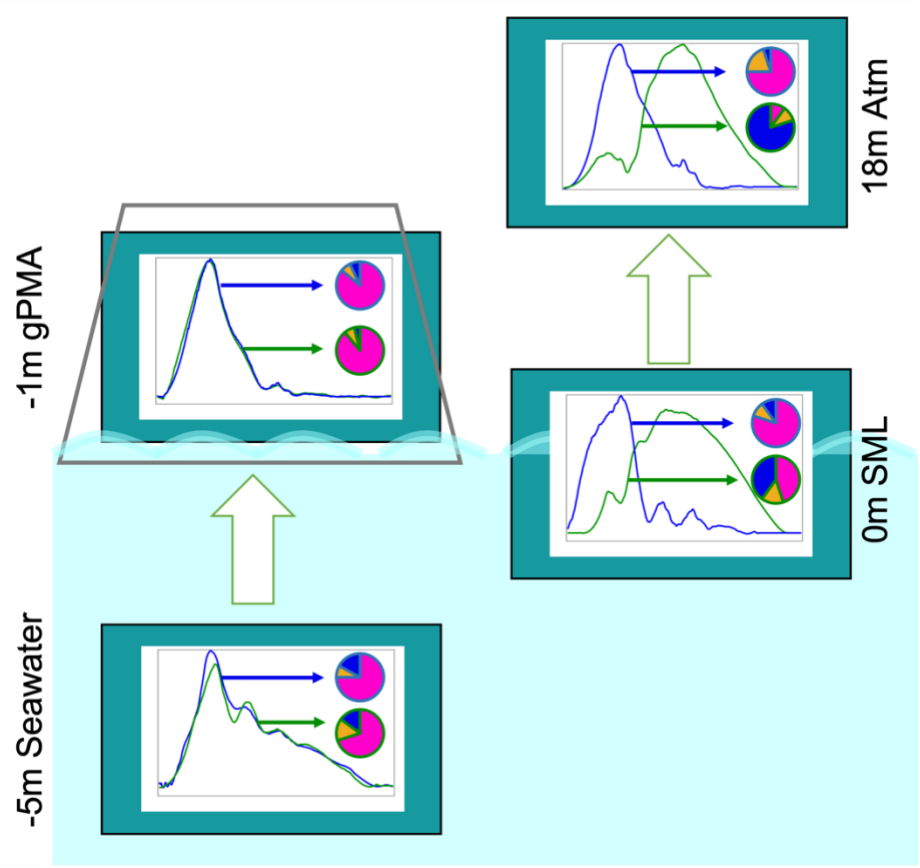

Figure 2.8: Diagram illustrating the influence of seawater (bottom left) on gPMA (top left with a trapezoid representing Sea Sweep) aerosol particle composition and the influence of SML (bottom right) on atmospheric particle composition (top right). The arrows are based on the similarity of composition shown in the pie charts and the spectra and do not indicate that they are the only source as seawater and SML components can be mixed. The individual FTIR spectra shown are during a lower chlorophyll period (blue, 12 September 2017) and higher chlorophyll period (green, 3 April 2018). The pie graphs, outlined in corresponding color for low vs. high chlorophyll demonstrate the organic functional group FTIR composition with hydroxyl groups (pink), alkane groups (blue), and amine groups (orange).

The gPMA and seawater alkane-to-hydroxyl group ratio are consistently unrelated to NPP, showing almost no change for the 6 days that were sampled (0.1±0.01 (gPMA) and 0.2±0.1 (seawater) alkane/hydroxyl group ratio). This could be due to gPMA and seawater organic composition being largely influenced by DOC, which has a relatively consistent fraction in

comparison to POC (Beaupré et al., 2019; Frossard et al., 2014; Quinn et al., 2014). This smaller seawater range may contribute to the similarly small range in gPMA, suggesting that for the NAAMES open ocean conditions gPMA particles may have more contributions from seawater (and less from SML) than do the atmospheric particles. In contrast, atmospheric particles and SML samples show much wider variability, both spanning the range of 0.1 to 1 for alkane/hydroxyl group ratio and showing weak positive correlations with both chlorophyll and NPP. STXM-NEXAFS showed multiple particle clusters for all sample types, however the low number of particles sampled with STXM-NEXAFS means that we cannot rule out more similarity in seawater and gPMA than in SML and atmospheric aerosol particles.

Phytoplankton blooms are associated with an increase in surface active compounds, particularly lipids, with increasing POC concentrations (Kharbush et al., 2020). Recent contributions from recently produced DOC (Baetge et al., 2021) may explain the changing composition of the SML during these times. Atmospheric aerosol particles could also be influenced by secondary atmospheric processes of organic components, but there is no evidence of such processes changing the alkane and hydroxyl group fractions (Frossard et al., 2014). The lack of expected changes to the alkane/hydroxyl group ratio from photochemical processes means that the ratio could serve as an approximately-conserved tracer for composition between these reservoirs. If this ratio is conserved on transfer between the ocean and the atmosphere, then the 0.1-1 range of alkane/hydroxyl group ratio in the atmospheric particles and the SML would not be explained by the seawater source range of 0-0.3.

Similar positive correlations of alkane and hydroxyl group contributions to biological activity have also been found in gPMA aerosol particles in more productive waters, where gPMA samples had higher alkane group fractions (and lower hydroxyl group fractions) than non-

productive waters during the Western Atlantic Climate Study (WACS) and California Nexus (CalNex) projects (Frossard et al., 2014). This difference from our results could be explained by the larger range of chlorophyll concentrations or the lower range of wind speeds (4 ± 2 m s^{-1} for WACS and 5 ± 2 m s^{-1} for CalNex)) in the WACS/CalNEX datasets than in NAAMES 3 and NAAMES 4. In fact, the WACS/CalNEX measurements of hydroxyl and alkane groups also did not have a clear trend for chlorophyll <1 (which is the range of all the NAAMES3 and NAAMES4 measurements), it was only at larger concentrations that the gPMA composition showed a moderate correlation to biological proxies. The contributions of SML and seawater to gPMA aerosol particles may vary with ocean conditions such as wind speed (Obernosterer et al., 2008; Rahlff et al., 2017), since very little is known about the prevalence and variability of the SML or its effects on gPMA sampling.

2.5 Conclusion

Our results show the organic functional groups in atmospheric particles have chemical similarities to seawater, gPMA, and SML in the North Atlantic. The four sample types were analyzed using single particle microscopy by STXM-NEXAFS and FTIR spectroscopy. Both measurements showed the presence of hydroxyl, alkyl, and alkene functional groups, and FTIR hydroxyl groups were consistently 50 - 90% of the quantified OM.

The larger range of alkane/hydroxyl group ratios, the greater FTIR spectral differences (low cosine similarity values and high standard deviations of cosine similarity values for individual spectra within the same sample type), and the weak correlations to tracers of biological activity for both atmospheric particle and SML samples suggest a biologically-influenced source contributing to a wider range of composition for SML and atmospheric particles than was found for seawater or gPMA. Both atmospheric particle and SML samples

showed an increased alkane/hydroxyl group ratio (associated with decreases in hydroxyl group fraction and increases in alkane group fraction) during periods of higher biological activity tracers, which suggests that the SML was an important contributor to the organic composition of atmospheric aerosol particles. Seawater and gPMA samples had more consistent composition, showing little variation for the range of biological activity that was observed and supporting previous findings that seawater contributes a relatively consistent organic functional group composition to atmospheric aerosol particles.

Of the eight STXM-NEXAFS clusters that were identified, there were no clusters that only contained SML particle types and only one small cluster, Csalt, that was only found in a single atmospheric particle sample. This variety of particle compositions is consistent with other observations in open-ocean conditions around the world (Hawkins & Russell, 2010; L. M. Russell et al., 2010; G. Saliba et al., 2021), illustrating the heterogeneity of components within the SML.

The SML showed more variability in FTIR spectra among the six case-study days than either seawater or gPMA, with a FTIR cosine similarity value of 0.72 ± 0.18 for SML compared to FTIR cosine similarity values of 0.98 ± 0.02 for seawater and 0.94 ± 0.06 for gPMA. This heterogeneity of composition could explain why some reports show a robust link between marine aerosol composition and SML and others do not (Michael Cunliffe et al., 2013; Anja Engel et al., 2017; Gasparovic et al., 2005; Reinthaler et al., 2008; van Pinxteren et al., 2017), particularly given the limited sample number of the few available studies of microlayer and aerosol composition.

The variability of the SML during sampled days displays the need for a longer time-series in which day-to-day variability can be teased apart from various environmental factors including

wind speed and biological activity. Sampling the atmospheric particle and gPMA samples directly onto substrates for STXM-NEXAFS analysis would have allowed for characterization of airborne-relevant particle morphology and diameter, and additional sampling would have provided a more robust data set for understanding seasonal and regional differences.

2.6 Appendix

2.6.1 Sharp carbonate peak in many extracted samples

Mcarb and Macid particle types had carbonate absorptions and contained a large fraction of extracted particles (21 out of 21 and 17 out of 25, respectively). The extraction method used water, so it is possible that the fairly water insoluble carbonate (K_{sp} = 3.36 x 10^{-9} at 25^{o} C) precipitated out and had an enhanced signal. Crilley et al., (2013) used a 45 minute water sonication extraction method on Teflon filters and ran the solution through an Aerodyne Mass Spectrometer (AMS). When these results were compared with real-time AMS spectrums from 5 sites, excellent agreement was found between the extracted organic mass and the real-time AMS organics with r^2 values ranging from 0.89 and 0.98, supporting the fidelity of the extraction method for representing the ambient particle population.

The carbonate could be enhanced in particles by the drying process, but prior observation of this same category of particles suggest that it is not an artifact of the extraction method (Saliba et al., 2021). However, the widespread presence of carbonate in all Mcarb and most Macid particles needs verification with directly-collected single particle samples.

2.6.2 Persistent NEXAFS aromatic/alkene peak in all sample types

All sample types had the aromatic/alkene NEXAFS peak: three of three seawater samples, six of six SML samples, two of four Sea Sweep samples, and five of six ambient samples. Six of the eight clusters (d, g, j, l, m, and Macid) contain this aromatic/alkene peak. The 285 eV NEXAFS peak in aerosol samples has been associated with alkenes and aromatics (Shakya et al., 2013). This peak has also been frequently attributed to soot (Knopf et al., 2014; Moffet, Henn, Laskin, & Gilles, 2010; Takahama, Gilardoni, Russell, & Kilcoyne, 2007), due to the known C 1s $\rightarrow \pi^*_{C=C}$ transition in elemental carbon. Ault et al., (2013) found that the

aromatic peak (285.4 eV) was not in a wave-flume experiment initially, but was present after the addition of bacteria, phytoplankton, and growth media (Figure 2.10). This absorption was attributed to chlorophyll, which has both aromatic and alkene bonds. Chlorophyll was present at all sampling locations in average concentrations ranging from 0.11 – 68 mg C m^{-3} (Table 1). Polycylic aromatic hydrocarbons (PAH) are another possible source of the absorption at 285 eV which can come from biomass burning that can be transferred to seawater and sediments (Rogge, Hildemann, Mazurek, Cass, & Simoneit, 1998; Samburova et al., 2016; Zhang et al., 2016). Lastly, nanoplastics are an option with poly(ethylene terephthalate) (PET) displaying clear peaks at both 284.4 and 285.1 eV (Yang, Luo, & Nowack, 2021) and many other common nanoplastic polymers showing aromatic/alkene absorptions at 285 eV (Foetisch, Filella, Watts, Vinot, & Bigalke, 2021).

Table 2.1: Detailed information about every particle that was above the detection limit for STXM-NEXAFS

SampleID	Sample Type	Cluster Type	Morphology	Air Mass Category	Alkene/ Aromatic	Ketonic Carbonyl	Alkyl	COOH Carbonyl	Carbonate	Potassium
532_190909129	SML	1	spherical	-	1	1	0	1	1	1
532_190912111	Ambient	1	oblong	Mixed	1	1	0	1	0	0
532_190913010	Ambient	1	multi-clump	Mixed	1	0	0	1	0	0
532_190913036	SeaSweep	1	multi-clump	-	1	1	0	1	0	0
532_190913052	SeaSweep	1	multi-clump	-	0	0	0	1	0	1
532_190913052	SeaSweep	1	multi-clump	-	0	0	0	0	0	0
532_200930123	SML	1	oblong	-	1	1	1	0	0	0
532_201001050	SML	1	oblong	-	1	1	1	0	0	1
532_201001093	SML	1	spherical	-	1	1	0	1	0	0
532_201002186	Seawater	1	oblong	-	1	1	0	0	0	0
532_201002190	Seawater	1	spherical	-	1	1	0	1	0	0
532_210628040	Ambient	1	oblong	Marine	1	1	0	1	1	0
532_210629116	Ambient	1	oblong	Marine	1	1	0	1	0	1

Table 2.1 (Continued): Detailed information about every particle that was above the detection limit for STXM-NEXAFS

SampleID	Sample Type	Cluster Type	Morphology	Air Mass Category	Alkene/ Aromatic	Ketonic Carbonyl	Alkyl	COOH Carbonyl	Carbonate	Potassium
532_210629116	Ambient	1	oblong	Marine	1	1	0	1	0	1
532_190909089	SML	2	irregular	-	0	0	0	0	0	0
532_190909158	SML	2	multi-clump	-	1	0	0	0	0	0
532_190909213	SML	2	coated-cubic	-	1	0	0	0	0	0
532_190911021	SML	2	coated-cubic	-	0	0	0	0	0	0
532_190911028	SML	2	multi-clump	-	1	1	0	1	1	0
532_190912126	Ambient	2	multi-clump	Mixed	0	0	0	1	1	1
532_190912126	Ambient	2	multi-clump	Mixed	0	0	0	1	1	1
532_200927144	SeaSweep	2	irregular	-	0	1	0	1	1	1
532_200927180	SeaSweep	2	multi-clump	-	0	1	0	1	1	1
532_200928028	SeaSweep	2	multi-clump	-	1	0	1	1	1	0
532_200928030	SeaSweep	2	coated-cubic	-	1	0	0	1	0	0
532_200930083	SML	2	irregular	-	1	0	0	0	0	0
532_201001081	SML	2	spherical	-	1	1	0	0	0	0
532_201001123	Ambient	2	spherical	Mixed	0	0	0	1	1	1
532_201002045	Ambient	2	coated-cubic	Mixed	1	0	0	0	0	0
532_210629081	Ambient	2	multi-clump	Marine	0	0	0	1	1	1
532_210629125	Ambient	2	multi-clump	Marine	1	0	0	1	0	0
532_210629136	Ambient	2	spherical	Marine	0	0	0	1	1	1
532_210629181	SML	2	spherical	-	0	0	0	0	0	0
532_210629185	SML	2	coated-cubic	-	1	0	0	1	0	0
532_210629195	SML	2	spherical	-	1	0	0	1	0	0
532_210629222	SML	2	spherical	-	1	0	0	1	1	0
532_210630000	SML	2	irregular	-	0	0	0	0	0	0
532_210630010	SML	2	spherical	-	0	0	0	0	0	0
532_190911080	Ambient	3	film	Mixed	0	0	0	1	1	1
532_190911086	Ambient	3	oblong	Mixed	0	0	0	0	1	1
532_190911088	Ambient	3	irregular	Mixed	0	0	0	0	1	1

Table 2.1 (Continued): Detailed information about every particle that was above the detection limit for STXM-NEXAFS

SampleID	Sample Type	Cluster Type	Morphology	Air Mass Category	Alkene/ Aromatic	Ketonic Carbonyl	Alkyl	COOH Carbonyl	Carbonate	Potassium
532_190909223	SML	4	oblong	-	1	1	0	1	1	0
532_190912199	Ambient	4	multi-clump	Mixed	1	1	0	0	0	0
532_190913042	SeaSweep	4	spherical	-	1	1	0	0	0	0
532_200925008	Ambient	4	irregular	Marine	0	0	0	0	1	0
532_200925021	Ambient	4	halo	Marine	0	0	0	0	0	0
532_200925039	Ambient	4	multi-clump	Marine	1	0	0	0	0	0
532_200927040	Ambient	4	spherical	Continental	1	0	0	0	0	0
532_200927087	Ambient	4	spherical	Continental	1	1	0	1	1	1
532_200928048	SeaSweep	4	spherical	-	1	0	0	0	0	0
532_200930038	SML	4	oblong	-	1	1	0	0	0	0
532_201001045	SML	4	coated-cubic	-	1	0	0	0	0	1
532_201001097	SML	4	spherical	-	1	1	0	0	0	0
532_201002109	Seasweep	4	irregular	-	1	1	0	0	0	0
532_201003059	Ambient	4	spherical	Continental	1	0	0	0	0	0
532_210628052	Ambient	4	irregular	Marine	1	0	0	0	0	1
532_210629106	Ambient	4	oblong	Marine	1	0	0	1	0	0
532_210629162	Ambient	4	irregular	Marine	1	0	0	0	0	0
532_190909085	SML	5	multi-clump	-	0	0	0	1	1	1
532_190909102	SML	5	halo	-	1	0	0	1	1	1
532_190909117	SML	5	spherical	-	0	0	0	1	1	1
532_190911071	Ambient	5	irregular	Mixed	1	1	1	0	1	1
532_190912036	Ambient	5	irregular	Mixed	0	0	1	1	1	1
532_190912045	Ambient	5	halo	Mixed	0	0	1	1	1	1
532_190912055	Ambient	5	halo	Mixed	0	0	0	0	1	1
532_190912058	Ambient	5	multi-clump	Mixed	0	0	0	0	1	1
532_190912062	Ambient	5	halo	Mixed	0	0	0	0	1	1
532_190912075	Ambient	5	irregular	Mixed	0	0	0	0	1	1
532_190912169	Ambient	5	multi-clump	Mixed	0	1	1	1	1	1
532_200925058	Ambient	5	spherical	Marine	1	1	0	0	1	1

Table 2.1 (Continued): Detailed information about every particle that was above the detection limit for STXM-NEXAFS

SampleID	Sample Type	Cluster Type	Morphology	Air Mass Category	Alkene/ Aromatic	Ketonic Carbonyl	Alkyl	COOH Carbonyl	Carbonate	Potassium
532_200926033	SeaSweep	5	spherical	-	0	0	0	1	1	1
532_200927054	Ambient	5	coated-cubic	Continental	1	0	0	0	1	1
532_200928039	SeaSweep	5	coated-cubic	-	0	0	0	1	1	1
532_200930006	SML	5	spherical	-	1	0	0	0	0	1
532_200930010	SML	5	coated-cubic	-	0	0	1	0	1	1
532_200930032	SML	5	spherical	-	1	0	0	0	0	1
532_201002027	Ambient	5	coated-cubic	Mixed	0	0	0	1	1	1
532_201002088	Seasweep	5	coated-cubic	-	0	1	1	1	1	1
532_201002118	Seasweep	5	spherical	-	0	0	0	0	1	0
532_210628011	Ambient	5	coated-cubic	Marine	0	1	0	1	1	0
532_210629087	Ambient	5	irregular	Marine	1	0	0	0	1	0
532_210630061	Seawater	5	irregular	-	1	0	0	0	1	1
532_210630109	Seawater	5	halo	-	1	0	0	0	1	1
532_190909122	SML	6	oblong	-	1	0	1	0	0	0
532_190909137	SML	6	film	-	1	0	1	0	0	0
532_190910039	SML	6	coated-cubic	-	1	1	0	1	0	1
532_200930087	SML	6	irregular	-	1	0	0	0	0	0
532_201001034	SML	6	irregular	-	1	1	0	1	0	0
532_201002010	Ambient	6	spherical	Mixed	1	1	0	1	0	0
532_210629189	SML	6	oblong	-	1	0	0	1	1	0
532_210630014	SML	6	spherical	-	0	0	0	0	0	0
532_210630073	Seawater	6	spherical	-	0	0	0	0	0	0
532_210630162	Seawater	6	multi-clump	-	1	0	0	1	0	0
532_190911097	Ambient	7	spherical	Mixed	0	0	1	0	1	1
532_190912003	Ambient	7	spherical	Mixed	0	0	1	0	1	1
532_190912031	Ambient	7	multi-clump	Mixed	0	0	1	0	1	1
532_190912041	Ambient	7	coated-cubic	Mixed	0	0	1	1	1	1

Table 2.1 (Continued): Detailed information about every particle that was above the detection limit for STXM-NEXAFS

SampleID	Sample Type	Cluster Type	Morphology	Air Mass Category	Alkene/ Aromatic	Ketonic Carbonyl	Alkyl	COOH Carbonyl	Carbonate	Potassium
532_190912121	Ambient	7	multi-clump	Mixed	0	0	1	0	1	0
532_190912131	Ambient	7	spherical	Mixed	0	0	1	0	1	1
532_190912162	Ambient	7	multi-clump	Mixed	0	0	1	0	1	0
532_190912179	Ambient	7	halo	Mixed	0	0	1	0	1	0
532_190912189	Ambient	7	multi-clump	Mixed	0	0	0	0	1	0
532_190913049	SeaSweep	7	multi-clump	-	0	0	0	0	1	1
532_200925031	Ambient	7	halo	Marine	0	0	1	1	1	0
532_200926041	SeaSweep	7	spherical	-	0	0	1	0	1	1
532_200927027	Ambient	7	spherical	Continental	0	0	1	1	1	1
532_200927104	Ambient	7	multi-clump	Continental	0	0	0	1	1	1
532_200927188	SeaSweep	7	spherical	-	0	0	1	0	1	1
532_201002006	Ambient	7	coated-cubic	Mixed	0	1	1	1	1	1
532_201002036	Ambient	7	multi-clump	Mixed	0	1	0	0	1	1
532_201002042	Ambient	7	irregular	Mixed	0	1	0	1	1	1
532_201002070	Seasweep	7	spherical	-	0	1	0	0	1	1
532_201003021	Ambient	7	irregular	Continental	0	0	0	1	1	1
532_201003048	Ambient	7	irregular	Continental	0	0	0	0	1	1
532_190909111	SML	8	oblong	-	1	1	0	0	0	0
532_190911040	SML	8	spherical	-	1	1	0	0	0	0
532_200927049	Ambient	8	spherical	Continental	1	1	0	0	0	0
532_200927098	Ambient	8	spherical	Continental	1	1	0	0	0	0
532_200927113	Ambient	8	spherical	Continental	1	0	0	0	0	0
532_201001023	SML	8	halo	-	1	1	0	1	0	0
532_201002103	Seasweep	8	oblong	-	1	1	0	1	0	0
532_210630021	SML	8	multi-clump	-	1	0	0	0	0	0
532_210630177	Seawater	8	multi-clump	-	1	1	0	0	0	0

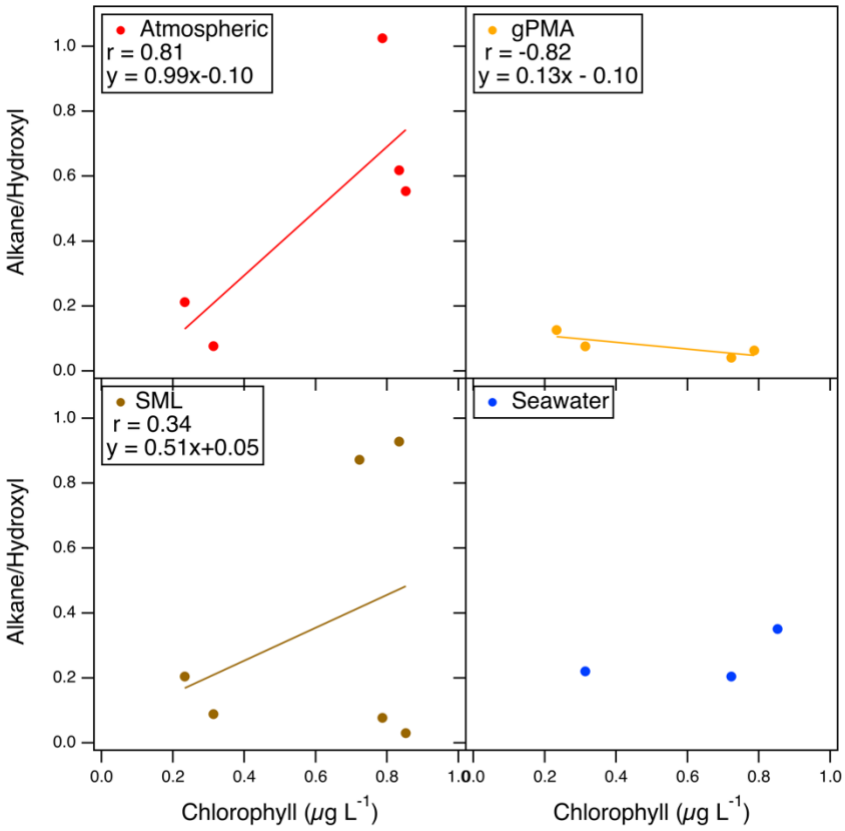

Figure 2.9: The alkane to hydroxyl ratio of concurrently sampled ambient (top left), SML (bottom left), Sea Sweep (top right), and seawater (bottom right) filters compared to 5 m in-line Chlorophyll A concentrations averaged to the ambient filter time. SML and ambient filters show much more alkane/hydroxyl variability and a positive slope whereas Sea Sweep and seawater samples exhibit relatively constant alkane/hydroxyl values resulting in a slope of ~0.

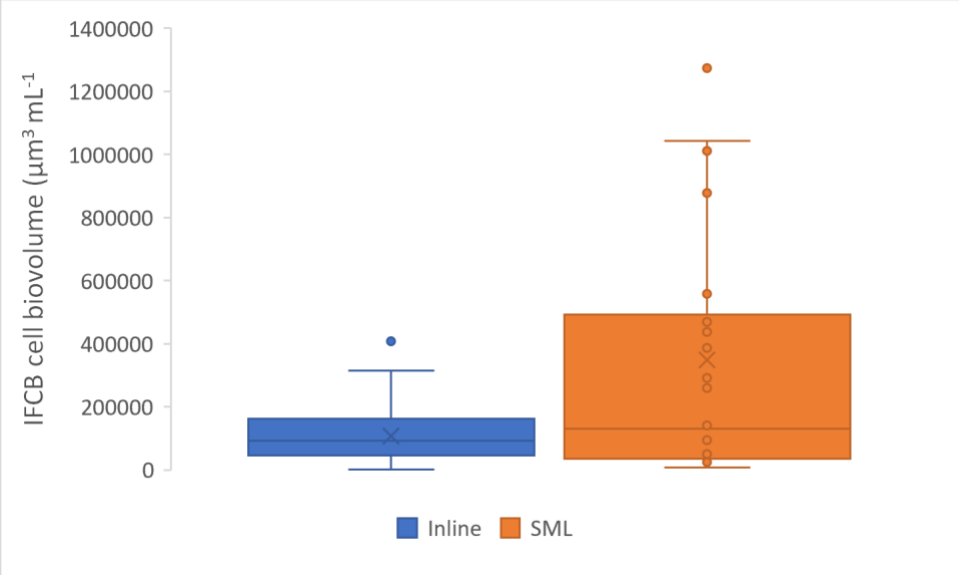

Figure 2.10: Box and whisker plot of IFCB cell biovolumes from 2 different sampling sources with median values of: 9.22 x 10^4 $\mu m^3 mL^{-1}$ (Inline, blue) and 1.29 x 10^5 $\mu m^3 mL^{-1}$ (SML, orange). The SML had a much more variable biovolume and was statistically distinct from the inline data ($p<0.05$).

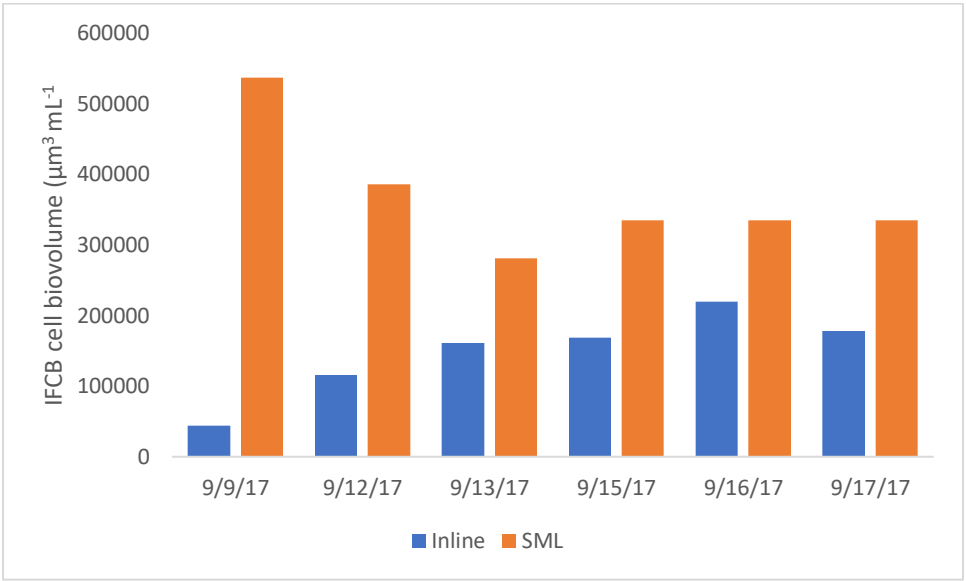

Figure 2.11: IFCB cell biovolume on 6 of the sample days during NAAMES 3 comparing inline data with SML data. The SML cell biovolume data is consistently larger than the inline data.

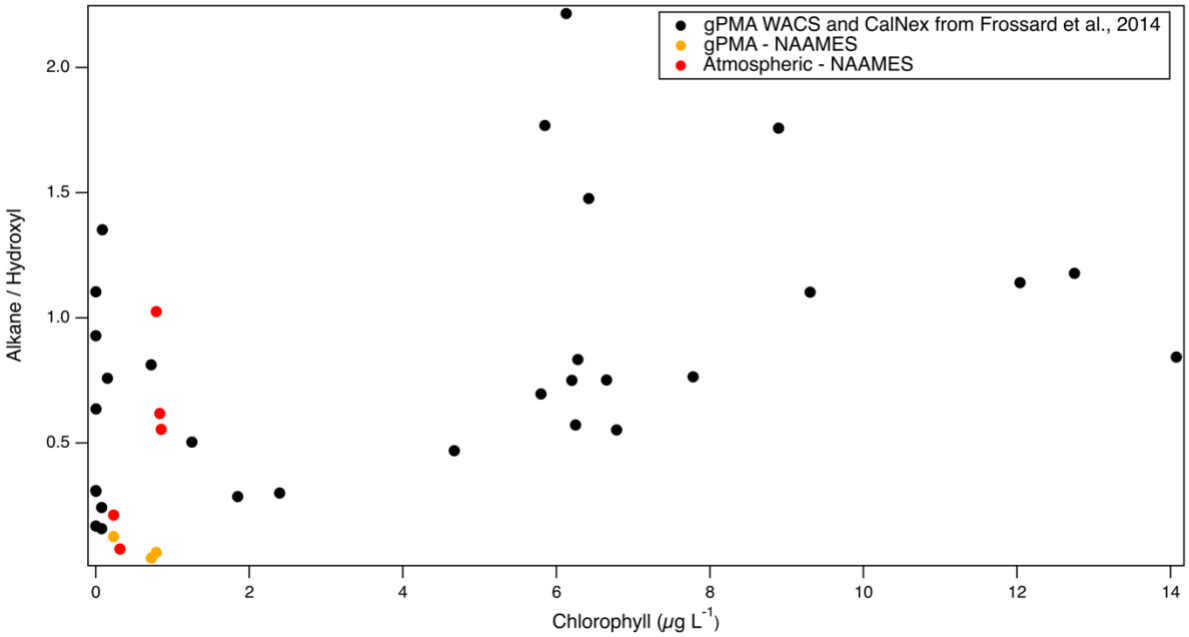

Figure 2.12: Alkane to hydroxyl ratios from 3 campaigns: NAAMES (red (ambient) and orange (gPMA) and a combined gPMA dataset of WACS and CalNex from Frossard et al., 2014. The gPMA data had a lower alkane / hydroxyl ratio that what was seen previously, possibly due to more tumultuous sampling conditions that inhibited the formation of the SML during sampling.

2.7 Acknowledgements

The authors would like to thank the dedicated officers and crew of the R/V *Atlantis*. The authors would also like to acknowledge Laura Ravelin, Chia-Li Chen, Raghu Betha, Derek Price, Maryam Askari Lamjiri, Derek Coffman, and Lucia Upchurch for their contributions to collecting and reducing data. The authors would also like to thank Nils Haëntjens for his help retrieving and processing the IFCB data. This work was funded by NASA grant NNX15AE66G and Savannah Lewis was supported by the National Science Foundation Graduate Research Fellowship. This is PMEL contribution number 5369.

Chapter 2, in full, has been submitted to *American Chemical Society: Earth and Space Chemistry.* Lewis, S.L, Russell L.M., Saliba, G., Quinn, P.K., Bates, T.S., Carlson, C.A., Baetge, N., Aluwihare, L.I., Boss, E., Frossard, A.A., Bell, T.G., and Behrenfeld, M.J., "Characterization of Sea Surface Microlayer and Marine Aerosol Organic Composition using STXM-NEXAFS Microscopy and FTIR Spectroscopy." The dissertation author was the primary investigator and author of this paper.

References

Aller, J. Y., Kuznetsova, M. R., Jahns, C. J., & Kemp, P. F. (2005). The sea surface microlayer as a source of viral and bacterial enrichment in marine aerosols. *Journal of Aerosol Science, 36*(5), 801-812. doi:https://doi.org/10.1016/j.jaerosci.2004.10.012

Aller, J. Y., Radway, J. C., Kilthau, W. P., Bothe, D. W., Wilson, T. W., Vaillancourt, R. D., . . . Knopf, D. A. (2017). Size-resolved characterization of the polysaccharidic and proteinaceous components of sea spray aerosol. *Atmospheric Environment, 154*, 331-347. doi:https://doi.org/10.1016/j.atmosenv.2017.01.053

Baetge, N., Behrenfeld, M. J., Fox, J., Halsey, K. H., Mojica, K. D. A., Novoa, A., . . . Carlson, C. A. (2021). The Seasonal Flux and Fate of Dissolved Organic Carbon Through Bacterioplankton in the Western North Atlantic. *Frontiers in Microbiology, 12*. doi:10.3389/fmicb.2021.669883

Bao, H., Niggemann, J., Luo, L., Dittmar, T., & Kao, S.-J. (2017). Aerosols as a source of dissolved black carbon to the ocean. *Nature Communications, 8*(1). doi:10.1038/s41467-017-00437-3

Bates, T. S., Quinn, P. K., Coffman, D. J., Johnson, J. E., Upchurch, L., Saliba, G., . . . Behrenfeld, M. J. (2020). Variability in Marine Plankton Ecosystems Are Not Observed in Freshly Emitted Sea Spray Aerosol Over the North Atlantic Ocean. *Geophysical Research Letters, 47*(1), e2019GL085938. doi:10.1029/2019GL085938

Bates, T. S., Quinn, P. K., Frossard, A. A., Russell, L. M., Hakala, J., Petaja, T., . . . Keene, W. C. (2012). Measurements of ocean derived aerosol off the coast of California. *Journal of Geophysical Research-Atmospheres, 117*. doi:10.1029/2012jd017588

Beaupré, S. R., Kieber, D. J., Keene, W. C., Long, M. S., Maben, J. R., Lu, X., . . . Bisgrove, J. (2019). Oceanic efflux of ancient marine dissolved organic carbon in primary marine aerosol. *Science Advances, 5*(10), eaax6535. doi:10.1126/sciadv.aax6535

Behrenfeld, M. J., Moore, R. H., Hostetler, C. A., Graff, J., Gaube, P., Russell, L. M., . . . Ziemba, L. (2019). The North Atlantic Aerosol and Marine Ecosystem Study (NAAMES): Science Motive and Mission Overview. *Frontiers in Marine Science, 6*(122). doi:10.3389/fmars.2019.00122

Blanchard, D. C. (1964). Sea-to-Air Transport of Surface Active Material. *Science, 146*(3642), 396. doi:10.1126/science.146.3642.396

Boss, E., Twardowski, M., & Herring, S. (2001). Shape of the particulate beam attenuation spectrum and its inversion to obtainthe shape of the particulate size distribution. *Appl. Opt., 40*(27), 4885--4893. doi:10.1364/AO.40.004885

Carlson, C. A., & Hansell, D. A. (2015). Chapter 3 - DOM Sources, Sinks, Reactivity, and Budgets. In D. A. Hansell & C. A. Carlson (Eds.), *Biogeochemistry of Marine Dissolved Organic Matter (Second Edition)* (pp. 65-126). Boston: Academic Press.

Carlson, D. J., & Mayer, L. M. (1980). Enrichment of dissolved phenolic material in the surface microlayer of coastal waters. *Nature, 286*(5772), 482-483. doi:10.1038/286482a0

Cetinić, I., Perry, M. J., Briggs, N. T., Kallin, E., D'Asaro, E. A., & Lee, C. M. (2012). Particulate organic carbon and inherent optical properties during 2008 North Atlantic Bloom Experiment. *Journal of Geophysical Research: Oceans, 117*(C6). doi:https://doi.org/10.1029/2011JC007771

Chance, R. J., Hamilton, J. F., Carpenter, L. J., Hackenberg, S. C., Andrews, S. J., & Wilson, T. W. (2018). Water-Soluble Organic Composition of the Arctic Sea Surface Microlayer and Association with Ice Nucleation Ability. *Environmental Science & Technology, 52*(4), 1817-1826. doi:10.1021/acs.est.7b04072

Chase, A. P., Kramer, S. J., Haëntjens, N., Boss, E. S., Karp-Boss, L., Edmondson, M., & Graff, J. R. (2020). Evaluation of diagnostic pigments to estimate phytoplankton size classes. *Limnology and Oceanography: Methods, 18*(10), 570-584. doi:10.1002/lom3.10385

Crilley, L. R., Ayoko, G. A., & Morawska, L. (2013). Analysis of organic aerosols collected on filters by Aerosol Mass Spectrometry for source identification. *Analytica Chimica Acta, 803*, 91-96. doi:https://doi.org/10.1016/j.aca.2013.07.013

Cunliffe, M., Engel, A., Frka, S., Gašparović, B., Guitart, C., Murrell, J. C., . . . Wurl, O. (2013). Sea surface microlayers: A unified physicochemical and biological perspective of the air–ocean interface. *Progress in Oceanography, 109*, 104-116. doi:https://doi.org/10.1016/j.pocean.2012.08.004

Cunliffe, M., & Wurl, O. (2014). Guide to best practices to study the ocean's surface. 19 - 31. doi:10.25607/OBP-1512

Drozdowska, V., Wrobel, I., Markuszewski, P., Makuch, P., Raczkowska, A., & Kowalczuk, P. (2017). Study on organic matter fractions in the surface microlayer in the Baltic Sea by spectrophotometric and spectrofluorometric methods. *Ocean Science, 13*(5), 633-647. doi:10.5194/os-13-633-2017

Engel, A., Bange, H. W., Cunliffe, M., Burrows, S. M., Friedrichs, G., Galgani, L., . . . Zäncker, B. (2017). The Ocean's Vital Skin: Toward an Integrated Understanding of the Sea Surface Microlayer. *Frontiers in Marine Science, 4*(165). doi:10.3389/fmars.2017.00165

Engel, A., & Galgani, L. (2016). The organic sea-surface microlayer in the upwelling region off the coast of Peru and potential implications for air–sea exchange processes. *Biogeosciences, 13*(4), 989-1007. doi:10.5194/bg-13-989-2016

Facchini, M. C., Rinaldi, M., Decesari, S., Carbone, C., Finessi, E., Mircea, M., . . . O'Dowd, C. D. (2008). Primary submicron marine aerosol dominated by insoluble organic colloids

and aggregates. *Geophysical Research Letters, 35*(17). doi:https://doi.org/10.1029/2008GL034210

Fox, J., Behrenfeld, M. J., Haëntjens, N., Chase, A., Kramer, S. J., Boss, E., . . . Halsey, K. H. (2020). Phytoplankton Growth and Productivity in the Western North Atlantic: Observations of Regional Variability From the NAAMES Field Campaigns. *Frontiers in Marine Science, 7*(24). doi:10.3389/fmars.2020.00024

Frossard, A. A., & Russell, L. M. (2012). Removal of Sea Salt Hydrate Water from Seawater-Derived Samples by Dehydration. *Environmental Science & Technology, 46*(24), 13326-13333. doi:10.1021/es3032083

Frossard, A. A., Russell, L. M., Burrows, S. M., Elliott, S. M., Bates, T. S., & Quinn, P. K. (2014). Sources and composition of submicron organic mass in marine aerosol particles. *Journal of Geophysical Research: Atmospheres, 119*(22), 12,977-913,003. doi:10.1002/2014JD021913

Gagosian, R. B., & Stuermer, D. H. (1977). The cycling of biogenic compounds and their diagenetically transformed products in seawater. *Marine Chemistry, 5*(4), 605-632. doi:https://doi.org/10.1016/0304-4203(77)90045-7

Garrett, W. D. (1967). The organic chemical composition of the ocean surface. *Deep Sea Research and Oceanographic Abstracts, 14*(2), 221-227. doi:https://doi.org/10.1016/0011-7471(67)90007-1

Gasparovic, B., Plavšić, M., Ćosović, B., & Reigstad, M. (2005). Organic matter characterization and fate in the sub-arctic Norwegian fjords during the late spring/summer period. *Estuarine, Coastal and Shelf Science, 62*, 95-107. doi:10.1016/j.ecss.2004.08.008

Hansell, D. A., Carlson, C. A., Repeta, D. J., & Schlitzer, R. (2009). Dissolved Organic Matter in the Ocean: A Controversy Stimulates New Insights. *Oceanography, 22*(4), 202-211.

Hasenecz, E. S., Kaluarachchi, C. P., Lee, H. D., Tivanski, A. V., & Stone, E. A. (2019). Saccharide Transfer to Sea Spray Aerosol Enhanced by Surface Activity, Calcium, and Protein Interactions. *ACS Earth and Space Chemistry, 3*(11), 2539-2548. doi:10.1021/acsearthspacechem.9b00197

Hawkins, L. N., & Russell, L. M. (2010). Polysaccharides, Proteins, and Phytoplankton Fragments: Four Chemically Distinct Types of Marine Primary Organic Aerosol Classified by Single Particle Spectromicroscopy. *Advances in Meteorology, 2010*, 14. doi:10.1155/2010/612132

Hayase, K., & Tsubota, H. (1983). Sedimentary humic acid and fulvic acid as surface active substances. *Geochimica et Cosmochimica Acta, 47*(5), 947-952. doi:https://doi.org/10.1016/0016-7037(83)90160-6

Hendrickson, B. N., Brooks, S. D., Thornton, D. C. O., Moore, R. H., Crosbie, E., Ziemba, L. D., . . . Alsante, A. N. (2021). Role of Sea Surface Microlayer Properties in Cloud Formation. *Frontiers in Marine Science, 7*. doi:10.3389/fmars.2020.596225

Hertkorn, N., Benner, R., Frommberger, M., Schmitt-Kopplin, P., Witt, M., Kaiser, K., . . . Hedges, J. I. (2006). Characterization of a major refractory component of marine dissolved organic matter. *Geochimica et Cosmochimica Acta, 70*(12), 2990-3010. doi:https://doi.org/10.1016/j.gca.2006.03.021

Hunter, K. A., & Liss, P. S. (1977). The input of organic material to the oceans: air—sea interactions and the organic chemical composition of the sea surface. *Marine Chemistry, 5*(4), 361-379. doi:https://doi.org/10.1016/0304-4203(77)90029-9

Kharbush, J. J., Close, H. G., Van Mooy, B. A. S., Arnosti, C., Smittenberg, R. H., Le Moigne, F. A. C., . . . Mohr, W. (2020). Particulate Organic Carbon Deconstructed: Molecular and Chemical Composition of Particulate Organic Carbon in the Ocean. *Frontiers in Marine Science, 7*. doi:10.3389/fmars.2020.00518

Knulst, J. C., Boerschke, R. C., & Loemo, S. (1998). Differences in Organic Surface Microlayers from an Artificially Acidified and Control Lake, Elucidated by XAD-8/XAD-4 Tandem Separation and Solid State 13C NMR Spectroscopy. *Environmental Science & Technology, 32*(1), 8-12. doi:10.1021/es9609819

Kuznetsova, M., Lee, C., & Aller, J. (2005). Characterization of the proteinaceous matter in marine aerosols. *Marine Chemistry, 96*(3), 359-377. doi:https://doi.org/10.1016/j.marchem.2005.03.007

Laskin, A., Moffet, R. C., Gilles, M. K., Fast, J. D., Zaveri, R. A., Wang, B., . . . Shutthanandan, J. (2012). Tropospheric chemistry of internally mixed sea salt and organic particles: Surprising reactivity of NaCl with weak organic acids. *Journal of Geophysical Research: Atmospheres, 117*(D15). doi:https://doi.org/10.1029/2012JD017743

Lewis, S. L., Saliba, G., Russell, L. M., Quinn, P. K., Bates, T. S., & Behrenfeld, M. J. (2021). Seasonal Differences in Submicron Marine Aerosol Particle Organic Composition in the North Atlantic. *Frontiers in Marine Science, 8*. doi:10.3389/fmars.2021.720208

Liss, P., and Duce, R. (1997). *The Sea Surface and Global Change* (P. S. Liss & R. A. Duce Eds.). Cambridge: Cambridge University Press.

Liu, J., Russell, L. M., Lee, A. K. Y., McKinney, K. A., Surratt, J. D., & Ziemann, P. J. (2017). Observational evidence for pollution-influenced selective uptake contributing to biogenic secondary organic aerosols in the southeastern U.S. *Geophysical Research Letters, 44*(15), 8056-8064. doi:https://doi.org/10.1002/2017GL074665

Maria, S. F., Russell, L. M., Turpin, B. J., & Porcja, R. J. (2002). FTIR measurements of functional groups and organic mass in aerosol samples over the Caribbean. *Atmospheric Environment, 36*(33), 5185-5196. doi:10.1016/s1352-2310(02)00654-4

Maria Steven, F., Russell Lynn, M., Gilles Mary, K., & Myneni Satish, C. B. (2004). Organic Aerosol Growth Mechanisms and Their Climate-Forcing Implications. *Science, 306*(5703), 1921-1924. doi:10.1126/science.1103491

Moberg, E. A., & Sosik, H. M. (2012). Distance maps to estimate cell volume from two-dimensional plankton images. *Limnology and Oceanography: Methods, 10*(4), 278-288. doi:10.4319/lom.2012.10.278

Obernosterer, I., Catala, P., Lami, R., Caparros, J., Ras, J., Bricaud, A., . . . Lebaron, P. (2008). Biochemical characteristics and bacterial community structure of the sea surface microlayer in the South Pacific Ocean. *Biogeosciences, 5*(3), 693-705. doi:10.5194/bg-5-693-2008

Quinn, P. K., Bates, T. S., Schulz, K. S., Coffman, D. J., Frossard, A. A., Russell, L. M., . . . Kieber, D. J. (2014). Contribution of sea surface carbon pool to organic matter enrichment in sea spray aerosol. *Nature Geoscience, 7*(3), 228-232. doi:10.1038/ngeo2092

Rahlff, J., Stolle, C., Giebel, H.-A., Brinkhoff, T., Ribas-Ribas, M., Hodapp, D., & Wurl, O. (2017). High wind speeds prevent formation of a distinct bacterioneuston community in the sea-surface microlayer. *FEMS microbiology ecology, 93*(5), fix041. doi:10.1093/femsec/fix041

Reinthaler, T., Sintes, E., & Herndl, G. J. (2008). Dissolved organic matter and bacterial production and respiration in the sea-surface microlayer of the open Atlantic and the western Mediterranean Sea. *Limnology and Oceanography, 53*(1), 122-136. doi:https://doi.org/10.4319/lo.2008.53.1.0122

Russell, L. M. (2003). Aerosol Organic-Mass-to-Organic-Carbon Ratio Measurements. *Environmental Science & Technology, 37*(13), 2982-2987. doi:10.1021/es026123w

Russell, L. M., Bahadur, R., Hawkins, L. N., Allan, J., Baumgardner, D., Quinn, P. K., & Bates, T. S. (2009). Organic aerosol characterization by complementary measurements of chemical bonds and molecular fragments. *Atmospheric Environment, 43*(38), 6100-6105. doi:10.1016/j.atmosenv.2009.09.036

Russell, L. M., Hawkins, L. N., Frossard, A. A., Quinn, P. K., & Bates, T. S. (2010). Carbohydrate-like composition of submicron atmospheric particles and their production from ocean bubble bursting. *Proceedings of the National Academy of Sciences of the United States of America, 107*(15), 6652-6657. doi:10.1073/pnas.0908905107

Russell, L. M., Maria, S. F., & Myneni, S. C. B. (2002). Mapping organic coatings on atmospheric particles. *Geophysical Research Letters, 29*(16), 26-21-26-24. doi:https://doi.org/10.1029/2002GL014874

Russell, L. M., Takahama, S., Liu, S., Hawkins, L. N., Covert, D. S., Quinn, P. K., & Bates, T. S. (2009). Oxygenated fraction and mass of organic aerosol from direct emission and atmospheric processing measured on the R/V Ronald Brown during

TEXAQS/GoMACCS 2006. *Journal of Geophysical Research: Atmospheres, 114*(D7). doi:10.1029/2008jd011275

Saliba, G., Chen, C.-L., Lewis, S., Russell, L. M., Quinn, P. K., Bates, T. S., . . . Behrenfeld, M. J. (2020). Seasonal Differences and Variability of Concentrations, Chemical Composition, and Cloud Condensation Nuclei of Marine Aerosol Over the North Atlantic. *Journal of Geophysical Research: Atmospheres, 125*(19), e2020JD033145. doi:10.1029/2020JD033145

Saliba, G., Sanchez, K. J., Russell, L. M., Twohy, C. H., Roberts, G. C., Lewis, S., . . . Toohey, D. W. (2021). Organic composition of three different size ranges of aerosol particles over the Southern Ocean. *Aerosol Science and Technology, 55*(3), 268-288. doi:10.1080/02786826.2020.1845296

Stein, S. E., & Scott, D. R. (1994). Optimization and testing of mass spectral library search algorithms for compound identification. *Journal of the American Society for Mass Spectrometry, 5*(9), 859-866. doi:10.1016/1044-0305(94)87009-8

Takahama, S., Gilardoni, S., Russell, L. M., & Kilcoyne, A. L. D. (2007). Classification of multiple types of organic carbon composition in atmospheric particles by scanning transmission X-ray microscopy analysis. *Atmospheric Environment, 41*(40), 9435-9451. doi:10.1016/j.atmosenv.2007.08.051

Takahama, S., Johnson, A., & Russell, L. M. (2013). Quantification of Carboxylic and Carbonyl Functional Groups in Organic Aerosol Infrared Absorbance Spectra. *Aerosol Science and Technology, 47*(3), 310-325. doi:10.1080/02786826.2012.752065

Takahama, S., Liu, S., & Russell, L. M. (2010). Coatings and clusters of carboxylic acids in carbon-containing atmospheric particles from spectromicroscopy and their implications for cloud-nucleating and optical properties. *Journal of Geophysical Research-Atmospheres, 115*(D01202). doi:10.1029/2009jd012622

Tseng, R.-S., Viechnicki, J. T., Skop, R. A., & Brown, J. W. (1992). Sea-to-air transfer of surface-active organic compounds by bursting bubbles. *Journal of Geophysical Research: Oceans, 97*(C4), 5201-5206. doi:https://doi.org/10.1029/91JC00954

van Pinxteren, M., Barthel, S., Fomba, K. W., Müller, K., von Tümpling, W., & Herrmann, H. (2017). The influence of environmental drivers on the enrichment of organic carbon in the sea surface microlayer and in submicron aerosol particles – measurements from the Atlantic Ocean. *Elementa: Science of the Anthropocene, 5*. doi:10.1525/elementa.225

Vedrinskii, R. V., Bugaev, L. A., Gegusin, I. I., Kraizman, V. L., Novakovich, A. A., Prosandeev, S. A., . . . Elango, M. A. (1982). X-ray absorption near edge structure (XANES) for KCl. *Solid State Communications, 44*(10), 1401-1407. doi:https://doi.org/10.1016/0038-1098(82)90019-9

Wan, K. X., Vidavsky, I., & Gross, M. L. (2002). Comparing similar spectra: From similarity index to spectral contrast angle. *Journal of the American Society for Mass Spectrometry, 13*(1), 85-88. doi:10.1016/S1044-0305(01)00327-0

Wurl, O., & Holmes, M. (2008). The gelatinous nature of the sea-surface microlayer. *Marine Chemistry, 110*(1), 89-97. doi:https://doi.org/10.1016/j.marchem.2008.02.009

Zäncker, B., Bracher, A., Röttgers, R., & Engel, A. (2017). Variations of the Organic Matter Composition in the Sea Surface Microlayer: A Comparison between Open Ocean, Coastal, and Upwelling Sites Off the Peruvian Coast. *Frontiers in Microbiology, 8*(2369). doi:10.3389/fmicb.2017.02369

Chapter 3 Sources and Composition of PM2.5 and PM10 Aerosol in the Oceano Dunes

The Oceano Dunes State Vehicular Recreation Area (ODSVRA) is a large natural source of wind-driven dust emissions that typically include nontoxic particle matter (PM) too large to be inhaled into alveoli. The San Luis Obispo County Air Pollution Control District (SLOAPCD) has targeted ODSVRA emissions to reduce exceedances of the state PM10 standard of 50 μg m^{-3} at a coastal monitoring site located 1 mile downwind of the dune area. To evaluate the potential effectiveness of this abatement strategy, five sets of measurements were collected during high-wind months (May and October) from 2019 to 2021 to quantify the organic and elemental composition of PM2.5 and PM10 samples. The five-campaign average afternoon PM2.5 composition relative to Beta Attenuation Monitor (BAM) concentrations included 14 ± 12% dust, 9 ± 9% sea salt, 4 ± 5% non-sea salt sulfate, and 8 ± 8% organic components, with the difference between BAM and the measured components contributing the remaining 66 ± 16% semivolatile/unidentified components. The high afternoon semivolatile/unidentified contribution was partially attributable to water, consistent with the increasing relative humidity during warm afternoons and in contrast to only a 3 ± 10% semivolatile/unidentified contribution for overnight samples. The organic functional group signature in FTIR for PM2.5 was closely related to previously reported ambient marine aerosol, consistent with a natural marine source for most of the organic mass concentration. For PM10, the dust fraction was 11 ± 8% of BAM PM10 concentration that increased up to 14 ± 10% of BAM PM10 concentration during days in which

hourly BAM PM10 concentration exceeded 140 µg m^{-3}. There was no statistically significant difference ($p>>0.05$) between dust, sea salt, sulfate, or organic fractions between weekend and weekday concentrations, consistent with most of these components being driven by natural processes. These results are consistent with national and state assessments of the good air quality of the region and provide evidence of semivolatile components causing differences between BAM and gravimetric mass concentrations for sampling times shorter than 24 hr. In addition, the results demonstrate that the regulatory dust abatement implemented at ODSVRA is misapplied and unlikely to improve downwind air quality significantly since ODSVRA and surrounding dunes contributes only 14% of BAM PM10, with no statistical difference between weekdays and weekends, and has not been shown to include toxic components.

3.1 Introduction

U.S. and California law and policy seeks to control particulate matter air pollution (PM) based on regulations that target two categories of PM that are defined by the size of the particles: PM10 and PM2.5. Nominally these limits are regulated independently of composition or source, restricting only the mass concentrations of PM2.5 and PM10 and not its components, but with the implicit objective of improving air quality by reducing manmade pollution (Apte, Brauer, Cohen, Ezzati, & Pope, 2018; Dockery et al., 1993; EPA, 2022b; Pope, Ezzati, & Dockery, 2009). In the decades since the introduction of national and state PM regulations, research has shown that the toxicity of the particles varies with their composition, making chemical speciation an important target for effective abatement (Duan, Tan, Wang, Hao, & Chail, 2012; Rogula-Kozłowska et al., 2014; Seagrave et al., 2006). Chemical speciation is also a simple way to identify many of the sources of pollution, since certain sources emit specific composition of particles (McMurry, Shepherd, & Vickery, 2003; Russell, Bahadur, & Ziemann, 2011). Solomon et al. (2014) provided the basis for identifying the components associated with specific sources in order to target reduction of specific industries. Identifying sources also provides a way to satisfy an implied tenet of the regulation of particle emissions, namely the targeting of manmade rather than natural sources, since pollution is defined as originating from human activities.

However, since neither the health effects nor the chemical attribution is required by the U.S. or California regulatory process, the cognizant government agencies can choose to regulate emissions without chemical speciation and without evidence of health effects. National standards for PM10 over 24 hour are 150 $\mu g\ m^{-3}$ and California standards are 50 $\mu g\ m^{-3}$, although the latter threshold is frequently exceeded because of natural sources (Motallebi, Taylor, & Croes, 2003), which are not subject to regulatory control. Oceano Dunes State Vehicular Recreation Area

(ODSVRA) is an example where mitigation was required of California State Parks and Recreation (hereafter "State Parks") to reduce sand dune dust without supporting chemical measurements of PM10 composition or of human contributions to dust (SLOAPCD, 2007, 2010; SOA, 2018). San Luis Obispo Air Pollution Control District (SLOAPCD) does not have the authority to regulate natural dust emissions but asserted that PM10 exceedances were attributable to OHV usage at ODSVRA (SOA, 2018, 2022). To demonstrate the effect of OHV activity on increasing dust emissions, measurements of dust lofting rates were collected and those show increased lofting in some OHV areas, although the connection of those increases on concentrations downwind was not quantified (Gillies, Furtak-Cole, Nikolich, & Etyemezian, 2022).

Oceano Dunes like many natural sandy areas is expected to be a wind-driven source of dust emissions, with natural emissions that are generally proportional to the exposed sand area (Bagnold, 1941). State Parks has reduced the exposed dunes to below the area that was historically-documented prior to OHV access, adding vegetation and artificial fences, nominally to address air quality concerns (Shuman, 2022). These landscape changes have cost in excess of $20 million of the revenue collected from fossil fuel taxes on vehicle use, which fund various expenditures related to vehicle usage including the operation and management of nine SVRAs (California Department of Parks and Recreation, 2021). These dust abatement measures have been justified as part of legal decisions for protecting public health (Shuman, 2022). However, there is little relevant evidence of PM10 from dune dust causing deleterious health effects. PM2.5 epidemiological studies that have shown harmful impacts on human health are largely based in urban areas in which anthropogenic emissions have high contributions from toxics, nanoparticles, and transition metals (Delfino, Sioutas, & Malik, 2005; Dockery et al., 1993;

Lighty, Veranth, & Sarofim, 2000). When rural and urban sites are evaluated separately, urban sites have higher toxicity (Duan et al., 2012; Rogula-Kozłowska et al., 2014; Seagrave et al., 2006). Seagrave et al. (2006) found the biological effects of intratracheal instillation varied as a function of both site and season, with urban sites having the most toxicity. These findings make it unlikely that dune dust has harmful health effects.

ODSVRA is one of the most visited of California's State Park and Recreation Areas, perhaps in part because it allows OHV usage, which was estimated to be bringing $243 million annually from visitors outside of San Luis Obispo County (Erickson, Mickel, & Rolloff, 2014; SMG Consulting, 2017). Pollution and other costs associated with vehicle usage are mitigated by collecting taxes on fuel usage, and the proceeds associated with OHV usage within State Parks are available to State Parks to mitigate health problems caused by OHVs. The State Parks are designed to preserve natural areas and support outdoors recreation (California Department of Parks and Recreation, 2022), making areas accessible to California citizens and visitors. OHV use of public lands has a near-century history at Oceano, providing high public access and park usage in an area with otherwise limited access. OHV enthusiasts tend to represent diverse communities (Cordell, Betz, Green, & Stephens, 2008), and their access to Park resources is restricted by reducing OHV usage at ODSVRA.

Here we present five sets of chemical measurements of PM10 and PM2.5 to assess the fraction contributed by dust and other components, providing clear evidence of a variety of PM sources that are from sources other than ODSVRA. The sampling approach initially targeted PM2.5 because of its health relevance, expanding in subsequent studies to show similar aspects of PM10. Chemical speciation included organic functional group measurements by FTIR spectroscopy and elemental species by XRF. BAM, gravimetric, and measured chemical species

were compared to assess the semivolatile/unidentified fraction. Elemental tracers and environmental conditions were used to attribute measured organic functional groups to sources. A combined assessment of these measurements shows the extent to which reducing dust emissions could improve air quality, which in turn reveals the how well measures taken by State Parks to restrict dune access and modify the dune landscape are an effective use of funds for reducing pollution.

3.2 Methods

PM2.5 and PM10 near the ODSVRA have been observed to be highest in the afternoons during high wind speeds, and May and October were targeted as the months with the highest average wind speeds (California Air Resource Board, 2022). The sampling site was located downwind of the southern edge of the at the California Department of Fire at Arroyo Grande (hereafter "CDF") (Oceano Dunes SVRA, 2022).This sampling used limited resources to target different aspects of PM2.5 and PM10, with a focus during the initial sampling from 14 May to 2 June 2019 and 23 September to 5 October 2019 on differences in PM2.5 composition at different times of day. These studies showed that afternoons were consistently the highest concentrations, reducing the need for overnight sampling. Comparisons of offline measured chemical components with online PM measurements indicated the need for gravimetric measurements, which were added for all subsequent studies starting with 27 April to 16 May 2020. PM10 chemical measurements were added for 28 September to 10 October 2020, and they were optimized for high-PM10 mass concentrations for 27 April to 24 May 2021. The local time during these sampling periods at CDF was PDT.

The temperatures, relative humidity, and wind speeds during sampling are shown in Table 3.1. Recreational vehicles were prohibited from access to the ODSVRA in May and October 2020 due to COVID shutdowns.

Table 3.1**:** The atmospheric sampling conditions during the collection of afternoon samples during the 5 campaigns reported as the average and standard deviation. The temperature, relative humidity, and wind speed are averaged over the filter sampling times. The sampling times in local time for each campaign, with sample number in parentheses are as follows: May 2019 [12:00-18:00 (11), October 2019 [10:00-18:00(4)], May 2020 [11:00-19:00 (17)], October 2020 [11:00-19:00 (6), 12:00-18:00 (7)].

	May 2019*	October 2019*	May 2020	October 2020	May 2021
Temperature (°C)	15 ± 1	18 ± 2	18 ± 3	19 ± 4	14 ± 1
Relative Humidity (%)	75 ± 3	69 ± 12	61 ± 13	72 ± 17	72 ± 7
Wind Speed (mph)	8 ± 3	9 ± 3	9 ± 3	7 ± 2	10 ± 3

*Measurements from nearby station, Nipomo – Oso Flaco Lake Road since temperature or relative humidity were not available at CDF for 2019.

3.2.1 Sample Collection

Aerosol particle sampling used sharp-cut cyclones operated with calibrated flows to collect particles for analysis at ambient diameters with a calibrated cut at 2.5 μm (SCC 2.229 operated at 7.5 L min^{-1}, BGI Inc., Waltham, MA) and a louvered PM10 sampling head (operated at 16.7 L min^{-1}) (Tolocka, Peters, Vanderpool, Chen, & Wiener, 2001).). PM2.5 sampling by SCC has been shown to have comparable 50% cutoff sizes and geometric standard deviations when following manufacturer calibrated flow rates (Du et al., 2020). October 2020 and May 2021 also measured PM10 directly after the PM10 sampling head, and in May 202**1** flows were split to improve accuracy at high concentrations (with expected loss

of data at low concentrations that were below detection), collecting 2 L min^{-1} for PM10 and 5 L min^{-1} for PM2.5. flow rates were calibrated at the beginning and end of each campaign, with recordings every 10 sec to document cyclone flow rates to ensure size cutoff performance.

37 mm Teflon filters (Pall Inc., 1 μm pore size) were used as substrates and have shown negligible adsorption of volatile organic compounds (VOCs) on duplicate back filters collected simultaneously with each sample (Gilardoni et al., 2007; Maria et al., 2003). Blank filters provided a measure of adsorption during sampling and contamination during handling and storage. Samples were quality-controlled with the following criteria: filter and cyclone flow rates were within 5% for the duration of sampling, filter pressure increased by >0.01 psi per m^3 air collected, and no anomalous readings in pressure, temperature, and relative humidity (as defined by the instrument specifications).

3.2.2 Mass Concentrations

BAM concentrations were measured nearly continuously during all sampling times by SLOAPCD at CDF. Hourly concentrations were obtained for both PM2.5 and PM10 from state records (California Air Resource Board, 2022); this database reports times as PST, which were converted to PDT. BAM concentrations below 5 μg m^{-3} were considered below detection, which represented 20% of the sample days reported here (Fig.1). Since SLOAPCD uses BAM to determine 24-hr PM2.5 and PM10 exceedances, we report here fractions of PM2.5 and PM10 relative to BAM concentrations. BAM concentrations that were below detection and ratios to those concentrations were not included in average values reported here. High-PM10 days were defined after collection as days in which CDF BAM PM10 measurements exceeded 140 μg m^{-3} for one or more reported hours. 97% of these high-PM10 days had an afternoon wind direction

greater than 270° (and less than 360°), which is a north-westerly direction with Oceano Dunes upwind of CDF.

For evaluation of BAM concentrations relative to federal standards, gravimetric analyses were completed for samples collected in 2020 and 2021 by Chester Labnet (Tigard, OR). These filters were weighed prior to sampling to provide filter-specific tare weights. After sampling, filters were weighed again, and the difference between the sampled weight and the tare was the reported gravimetric mass. The weighing procedure for samples used the PM2.5 federal reference method at 35±5% relative humidity for the 24-hour period (logged every 5 min), making the samples drier during weighing than the ambient conditions at which they were collected.

3.2.3 Organic Functional Groups from FTIR Spectroscopy

Samples were non-destructively analyzed by transmission FTIR spectroscopy. FTIR measurements of absorbance characterized the nonvolatile organic functional groups associated with major carbon bond types, including saturated aliphatic (alkane) groups, alcohol (used here to include phenol and polyol) groups, carboxylic acid groups, non-acidic carbonyl groups, and primary amine groups. The spectra were interpreted using an automated algorithm to perform baselining, peak-fitting, and integration with a revised version of the approach described previously (Maria, Russell, Turpin, & Porcja, 2002; Maria et al., 2003; Maria Steven, Russell Lynn, Gilles Mary, & Myneni Satish, 2004; Russell et al., 2009; Takahama, Johnson, & Russell, 2013), using calibrations revised for the Tensor 27 spectrometer with RT-DLATGS detector (Bruker Optics, Ettlingen, Germany) (Gilardoni et al., 2007). Complete sets of internal standards for organic components of the atmosphere are

not available, in part because the ambient particle composition is not fully known. The measured organic functional groups are summed to calculate organic mass (OM). Estimates of the accuracy, errors, and detection limits of this technique for ambient measurements are discussed in Russell (2003). Cosine similarity (dot-product cosine on normalized spectra) was used to quantify spectral similarity of FTIR spectra because it has been shown to be sensitive to small spectral differences in this type of chemical spectra (Frossard et al., 2014; J. Liu et al., 2017; Stein & Scott, 1994; Wan, Vidavsky, & Gross, 2002).

3.2.4 Dust, Sea salt, and Non-Sea Salt Sulfate from XRF Spectroscopy

Sample filters (and associated blank filters) were non-destructively analyzed by X-ray Fluorescence (XRF) measurements conducted by Chester LabNet (Tigard, OR) on the same filters used for gravimetric measurements. XRF analysis provided trace metal concentrations for elements Na and heavier (Maria et al., 2003). The following elements were above the detection limit for 50% or more of the PM2.5 afternoon samples and are used in the results reported here: Na, Mg, Al, Si, P, S, Cl, K, Ca, Ti, Mn, Fe, Ni, Zn, Br, Rb, and Sr. When Ba was above the detection limit (35% of the afternoon PM2.5 samples), it was used in the dust calculation and was zeroed out when below detection limit.

Mineral dust was measured above detection if Al and Si were above detection (defined as twice uncertainty), which was true for more than 86% of quality-controlled samples. The mass of dust was calculated from XRF metal concentrations, assuming dust consists of $MgCO_3$, Al_2O_3 and SiO_2 (in the form of Al_2SiO_5), K_2O, $CaCO_3$, TiO_2, Fe_2O_3, MnO, and BaO (Gilardoni et al., 2007; Jun Liu et al., 2018; Usher, Michel, & Grassian, 2003). This calculation increases the mass by an average factor of 2.14 to account for the O and C associated with the measured elements.

Because some elements are in both sea salt and mineral dust (K, Ca, Mg), the amount of those elements associated with the Na present was subtracted to avoid double-counting, resulting in ~2% less mass. The mineral dust contribution can also be estimated by calibration to a subset of elements, as discussed in the Supplement (Figure 3.8) (Frank, 2006; Hains, Chen, Taubman, Doddridge, & Dickerson, 2007; Malm, Sisler, Huffman, Eldred, & Cahill, 1994).

Sea salt was measured above detection when Na and Cl were above detection (defined as twice uncertainty). Atmospheric ambient sea salt concentrations were calculated using measured Cl and 1.47*Na concentrations to account for the possible depletion of Cl^- in the atmosphere, where 1.47 is the ratio of $(Na^+ + Mg^{2+} + Ca^{2+} + K^+ + SO_4^{2-} + HCO_3^-)/Na^+$ in seawater (Frossard et al., 2014; Holland, 1978). This sea-salt calculation represents an upper limit for sea-salt mass because the HCO_3^- would have been titrated before Cl^- was depleted significantly via acid displacement reactions. HCO_3^- is 0.3% of the mass of sea salt. Excluding HCO_3^- from the ratio, as a lower limit, the ratio of $(Na^+ + Mg^{2+} + Ca^{2+} + K^+ + SO_4^{2-})/Na^+$ is 1.45, instead of 1.47, making the sea salt mass calculated <2% lower than calculated here.

Non-sea salt sulfate (nss-sulfate) was calculated using measured S concentrations assuming S came from $(NH_4)_2\ SO_4$ and subtracting the amount of SO_4^{2-} associated with the Na present (Holland, 1978). The semivolatile/unidentified fraction was defined as the difference between filter sample time averaged BAM concentration and the sum of dust, sea salt, nss-sulfate, and organic mass concentrations.

3.3 Results and Discussion:

The time series of the collected measurements are shown in Figure 3.1, illustrating the episodic nature of the wind-driven high PM10 days. The time series also shows the variability in composition during each study, the frequency of high PM10 days, and the number of measurements collected.

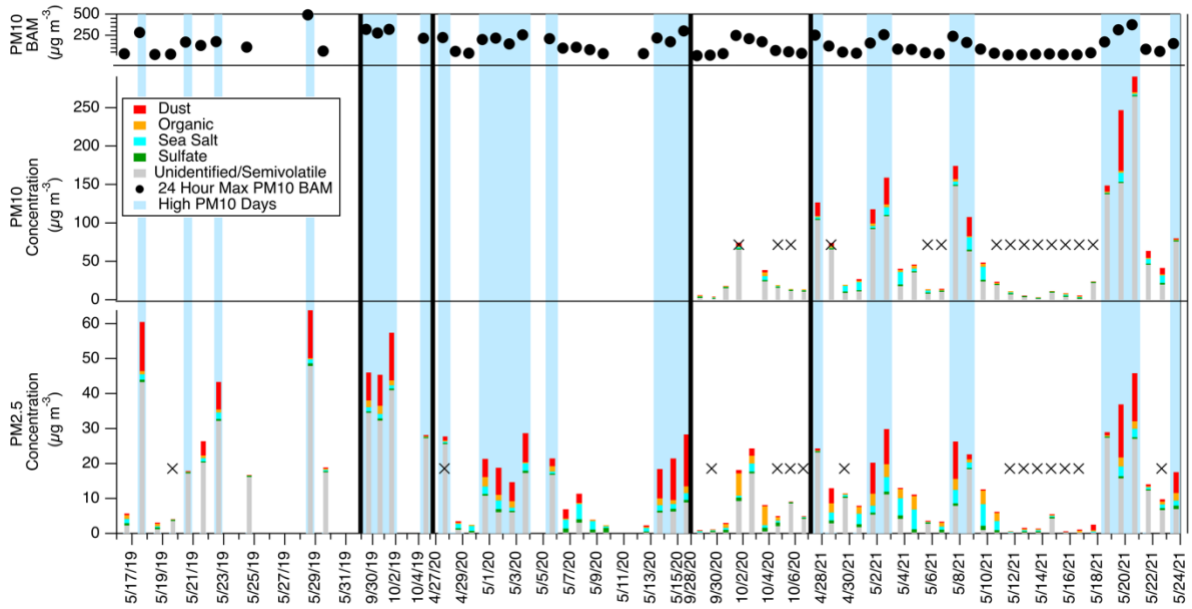

Figure 3.1**:** Time series of PM2.5 and PM10 CDF afternoon (11-18:00) mass concentrations (µg m^{-3}) with XRF mineral dust (red), sea salt (blue), sulfate (green), FTIR organic (orange), and the difference between BAM and measured components including dust, sea salt, sulfate, and organic (unidentified, grey). Samples that have gravimetric measurements below detection are denoted by a black "X". High-PM10 days, shown with light blue highlighting, are defined as days in which hourly BAM PM10 values exceeded 140 µg m^{-3} at least once during the sampling time. Black lines show divisions between the campaigns, which took place during 16 May – 1 June 2019, 29 September – 5 October 2019, 27 April – 16 May 2020, 28 September – 7 October 2020, and 27 April – 24 May 2021.

3.3.1 PM2.5 and PM10 Composition

The five-campaign composition measurements consistently showed that an average value of 14 ± 12% (4.8 ± 5.1 μg m^{-3}) of BAM PM2.5 and 11 ± 8% (11.6 ± 17.6 μg m^{-3}) of BAM PM10 can be attributed to mineral dust (Table 3.2). On high-PM10 days, this fraction increases to 22 ± 11% (8.1 ± 4.8 μg m^{-3}) of BAM PM2.5 and 14 ± 10% (23.2 ± 21.8 μg m^{-3}) of BAM PM10. Sea salt contributes 9 ± 9% (1.8 ± 1.4 μg m^{-3}) of BAM PM2.5 and 13 ± 14% (6.1 ± 5.3 μg m^{-3}) of BAM PM10 on average, which decreases on high-PM10 days to 4 ± 3% (1.6 ± 1.0 μg m^{-3}) of BAM PM2.5 and 4 ± 4% (5.8 ± 5.2 μg m^{-3}) of BAM PM10. Non-sea salt sulfate (nss-sulfate) contributes 4 ± 5% (0.7 ± 0.4 μg m^{-3}) of BAM PM2.5 and 3 ± 3% (1.0 ± 0.8 μg m^{-3}) of BAM PM10 on average, which decreases on high-PM10 days to 1 ± 1% (0.5 ± 0.3 μg m^{-3}) of BAM PM2.5 and 0.5 ± 1% (0.6 ± 0.7 μg m^{-3}) of BAM PM10 samples. These results indicate that mineral dust emissions from the Oceano Dunes account for on average 14% of BAM PM10 during the highest PM10 days in the windiest months of the year.

Table 3.2: Measurements from five campaigns pooled by size and location with the dust, sea salt, and OM fractions relative to BAM concentrations. High-PM10 days in gray. Number of samples indicated in parentheses. Only above detection afternoon samples were included, so the number of sampled days is different for each component and the two size cuts.

	Dust/ BAM (%)	Dust/ BAM (%)	Sea salt/ BAM (%)	Sea salt/ BAM (%)	$nssSO_4$/ BAM (%)	$nssSO_4$/ BAM (%)	OM/ BAM (%)	OM/ BAM (%)
CDF PM2.5	14 ± 12 (49)	22 ± 11 (26)	9 ± 9 (49)	4 ± 3 (26)	4 ± 5 (49)	1 ± 1 (26)	8 ± 8 (41)	4 ± 4 (25)
CDF PM10	11 ± 8 (23)	14 ± 10 (10)	13 ± 14 (23)	4 ± 4 (10)	3 ± 3 (23)	0.5 ± 1 (10)	16 ± 8 (4)	-

Organic mass contributes 8 ± 8% (1.9 ± 1.6 µg m^{-3}) of BAM PM2.5, which decreased on high-PM10 days to 4 ± 4% (1.5 ± 1.1 µg m^{-3}). The average PM2.5 composition consisted of 60 ± 13% hydroxyl groups, 28 ± 10% alkane groups, 11 ± 5% amine groups, and 1 ± 4% carboxylic acid groups relative to measured organic mass (Figure 3.2, Table 3.3). October 2020 PM10 organic mass, which was the only season organic mass was measured for PM10, contributes 16 ± 8% (2.4 ± 2.2 µg m^{-3}) of BAM PM10, and there were no high-PM10 days with detectable organic mass. The organic composition of PM10 for October 2020 consisted of 36 ± 12% hydroxyl groups, 34 ± 10% alkane groups, 21 ± 8% amine groups, and 9 ± 12% carboxylic acid groups relative to measured organic mass (Table 3.3).The PM10 organic fraction of 16% and the PM2.5 orgranic fraction of 18% in October 2020 are higher than the five campaign PM2.5 average (Table 3.1), likely due to biomass burning events which occurred during October 2020. This is supported by the enrichment in alkane and amine components in the PM10 organic fraction, which has been shown to be enhanced during wildfire events (Hawkins & Russell, 2010; Maudlin, Wang, Jonsson, & Sorooshian, 2015).

Table 3.3: The average and standard deviation of the organic functional group fractions relative to measured organic mass concentrations from the 5 campaigns (with the number of samples in parentheses). Above detection afternoon samples were included.

CDF PM25	May 2019 (1)	October 2019 (2)	May 2020 (6)	October 2020 (5)	May 2021 (13)	CDF PM10 Oct 2019 (8)
Hydroxyl	57	65 ± 3	61 ± 13	42 ± 9	65 ± 8	36 ± 12
Alkane	20	27 ± 2	29 ± 11	40 ± 8	23 ± 6	34 ± 10
Amine	21	8 ± 1	10 ± 5	18 ± 5	10 ± 3	21 ± 8
Acid	12	0	1 ± 2	0	2 ± 1	9 ± 12

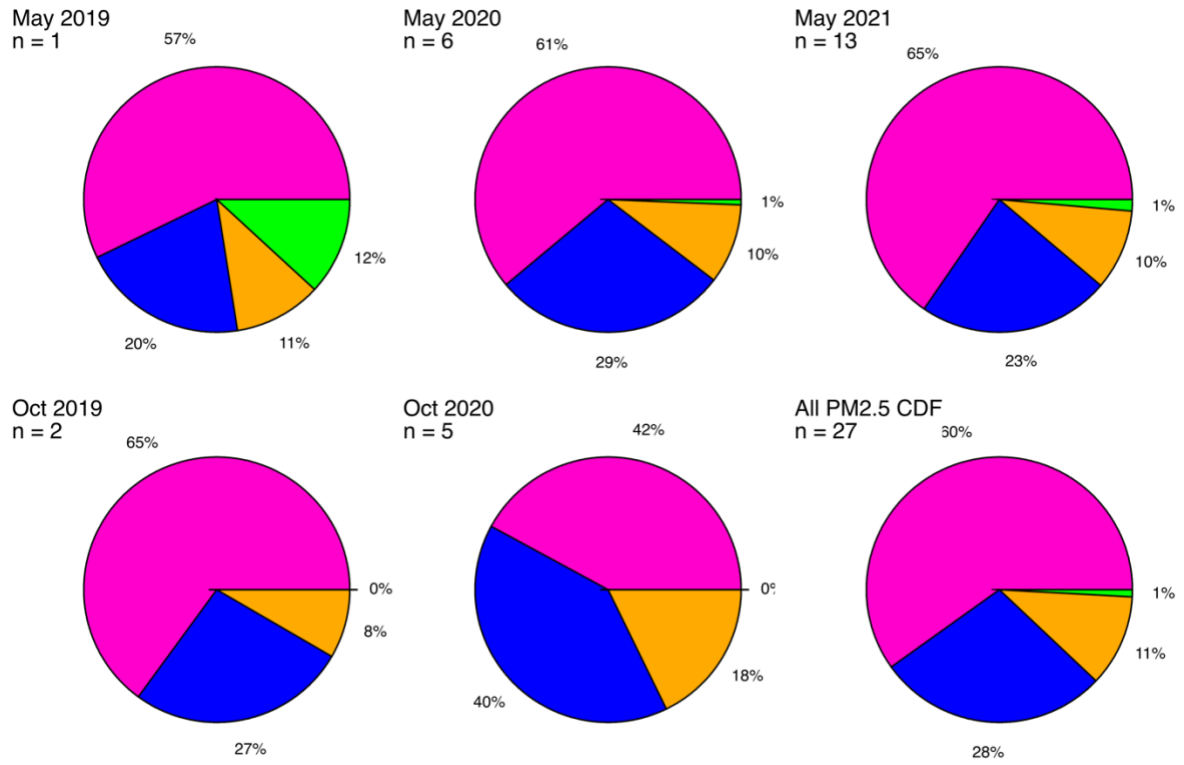

Figure 3.2**:** PM2.5 organic functional group composition of the 5 campaigns and the average of afternoon samples. Hydroxyl groups are pink, alkane groups are blue, amine groups are orange, and acid groups are green. The sampling times, in local time, were May 2020 – 11:00-19:00 (17); October 2020 – 11:00-19:00 (6), 12:00-18:00 (7); and May 2021 – 12:00-19:00 (30).

3.3.2 PM2.5 and PM10 Sources

Most of the measured dust is likely from the Oceano Dunes, although other nearby sources such as agricultural fields may also contribute. Dust accounted for averages of 22 ± 11 % of BAM PM2.5 during high-PM10 days for five campaigns and 14 ± 10% of BAM PM10 during high-PM10 days for October 2020 and May 2021. Dust mass concentration had a moderate correlation with wind speed (Figure 3.3, r = 0.65), as expected for a wind-driven source.

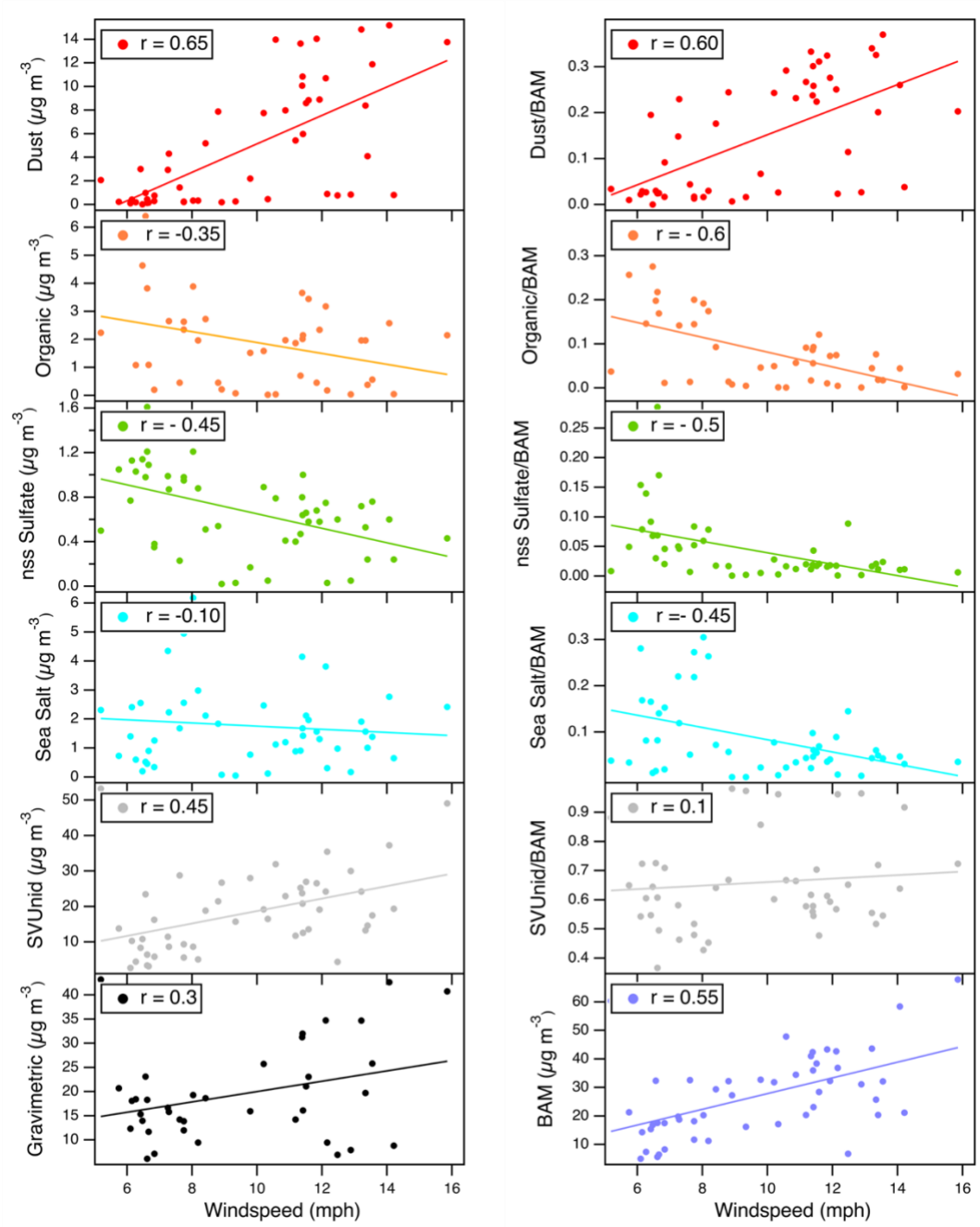

Figure 3.3**:** Comparison of PM2.5 afternoon mass concentrations (left, µg m^{-3}) and relative fractions (right) of dust (red), organic (orange), nss-sulfate (green), sea salt (teal), and semivolatile/unidentified (grey) to windspeed (mph). The gravimetric (black) and BAM (purple) concentrations (µg m^{-3}) are also shown. Above detection afternoon samples are included. Fit lines are shown and were significant ($p<0.05$) except for sea salt mass concentration ($p = 0.48$) and semivolatile/unidentified fraction ($p = 05$).

There was no statistical difference ($p>0.05$) between the weekend (Friday – Sunday, n = 21) and weekday (Monday – Thursday, n = 28) samples for the PM2.5 afternoon composition of dust ($p = 0.52$), sea salt ($p = 0.50$), organic ($p=0.58$), or sulfate ($p=0.81$) concentrations (Figure 3.4). The lack of a difference between weekend and weekday concentrations indicates that these sources are not significantly affected by human activities. The definition of weekend as Friday – Sunday, Saturday – Sunday, or Saturday – Monday did not affect this result (Figure 3.13).

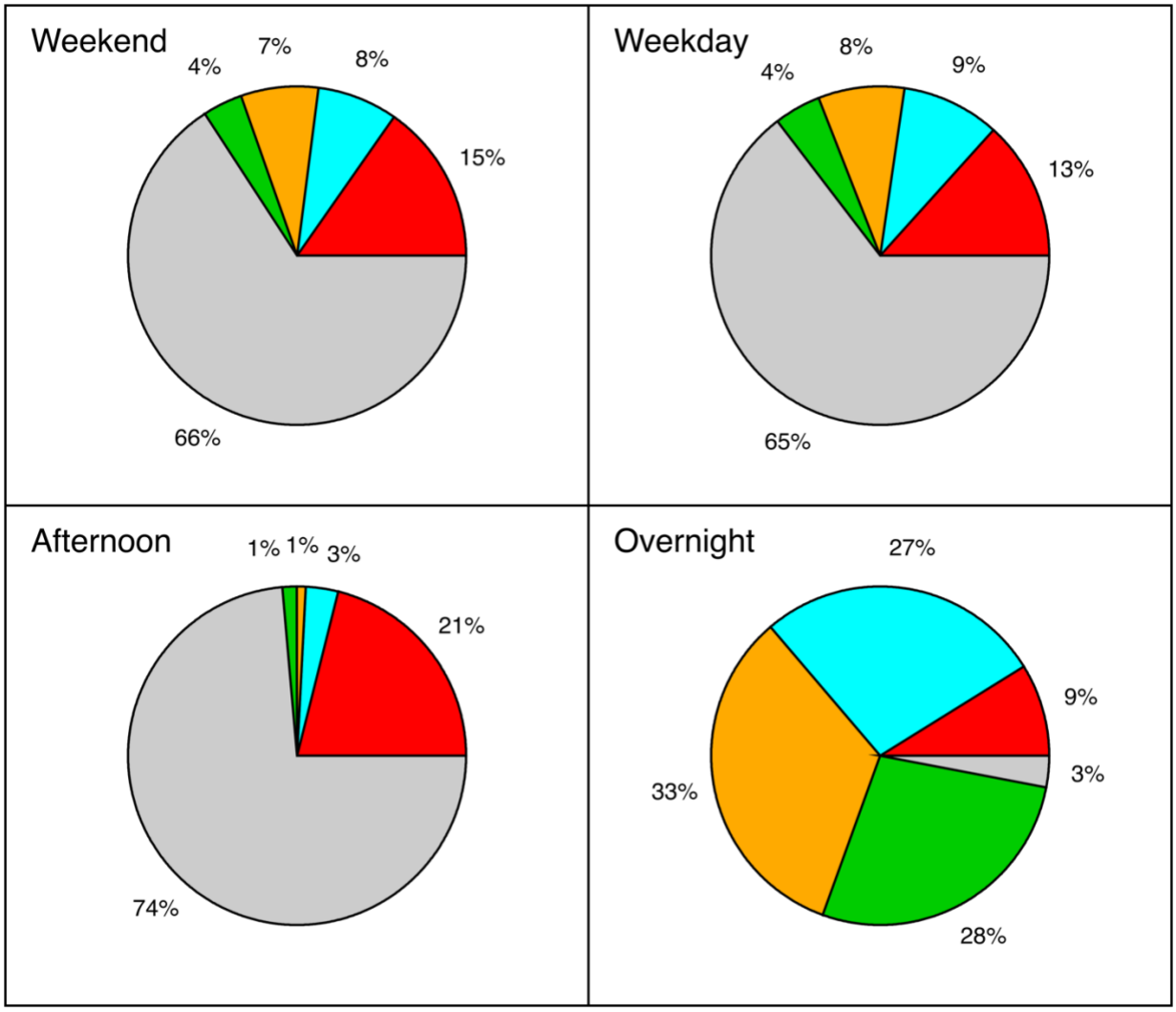

Figure 3.4: Chemical speciation of PM2.5 comparing weekends (Friday – Sunday, n = 21) and weekdays (Monday – Thursday, n = 28) with dust (red), sea salt (teal), organic (orange), nss-sulfate (green), and semivolatile/unidentified (grey) for all campaigns (May 2019, October 2019, May 2020, October 2020, and May 2021. There was no statistically significant difference ($p>0.05$) for any of the components between the weekend and weekday samples. Afternoon (n = 9, 12:00-18:00 local time) and overnight (n = 3, 18:00-6:00 local time) samples from May 2019 were compared as well following the same color scheme.

The source of sea salt is most likely from sea spray from the Pacific Ocean. Sea salt contributed 4 ± 3% of BAM PM2.5 during high-PM10 days and 4 ± 4% of BAM PM10 during high-PM10 days.

Organic mass (OM) concentration has been found to be associated with sea spray in many open-ocean campaigns, but coastal environments can sometimes include organic mass from local sources including biomass burning or other combustion sources (Gantt et al., 2011; Hawkins & Russell, 2010; Modini et al., 2015; Russell, Hawkins, Frossard, Quinn, & Bates, 2010). The FTIR OM measurements of PM2.5 afternoon samples showed spectra that were similar (cosine similarity value of 0.94) to those found for ambient marine aerosol composition measured in open ocean conditions (Frossard et al., 2014). The hydroxyl group is often associated with primary marine aerosol, which can consist of polysaccharides, monosaccharides, amino acids, and phytoplankton fragments (Lewis et al., 2021; Russell et al., 2010; Saliba et al., 2020). The hydroxyl groups in this study correlate with organic mass ($r = 0.75$) and sea salt ($r = 0.6$) and have no correlation with dust ($r = -0.1$), supporting the attribution of the measured nonvolatile OM as largely marine-derived. Carboxylic acid groups are only above detection during May, indicating that the acid groups are likely from photooxidation processes that are favored in spring over autumn (Fisseha et al., 2004; Lewis et al., 2021).

Potassium (K) is a common tracer for biomass burning emissions (Echalar, Gaudichet, Cachier, & Artaxo, 1995; Hawkins & Russell, 2010) and was correlated to both the October 2020 PM2.5 amine group concentration ($r = 0.7$) and the October 2020 PM10 amine group concentration ($r = 0.9$) (Figure 3.5). Multiple wildfires occurred in October 2020 with air quality warnings occurring on 1 October due to a local fire (Worsham, 2020). Along with the higher OM

fraction during this campaign, the association of the amine group with K demonstrates that a large fraction of the measured OM in October 2020 was from the nearby wildfires. In contrast, for above detection afternoon PM2.5 samples from the five campaigns, the correlation of K to amine group concentrations had $r<0.01$.

The organic fraction reported here provides an indication of the contributions from organic pollutants such as combustion, where the small fraction of alkane groups shows that the majority of chemically identified PM2.5 organic components are not associated with fossil-fuel combustion emissions (Chen et al., 2018; Xia et al., 2022). Further, the low contributions of Pb and Cd, which were below detection limit for 85% or more of the afternoon samples, shows that there is no evidence of sources associated with heavy metals (Maciejczyk, Chen, & Thurston, 2021; Zhang et al., 2014). The alkane group contribution could be associated with relatively recent emissions from highway or off-highway (recreational) vehicles (Chen et al., 2018; Xia et al., 2022), but the low contribution demonstrates that nearby vehicle emissions have negligible impacts on air quality at CDF. Consistent with the low contribution from vehicle emissions, the National Toxics Assessment for CDF (track identification 06079012304) shows a total cancer risk of 20 per million (50% lower than the US and California average of 30 per million) and total respiratory hazard quotient of 0.2 (half of the US and California respiratory hazard quotient average of 0.4) (EPA, 2022a). Of the total respiratory hazard quotient of 0.2, only 0.0003 is associated with non-road recreational sources such as ODSVRA, which is ten times lower than the background hazard quotient of 0.005. These values illustrate the good air quality in the area surrounding CDF, and the low levels of toxics associated with the ODSVRA.

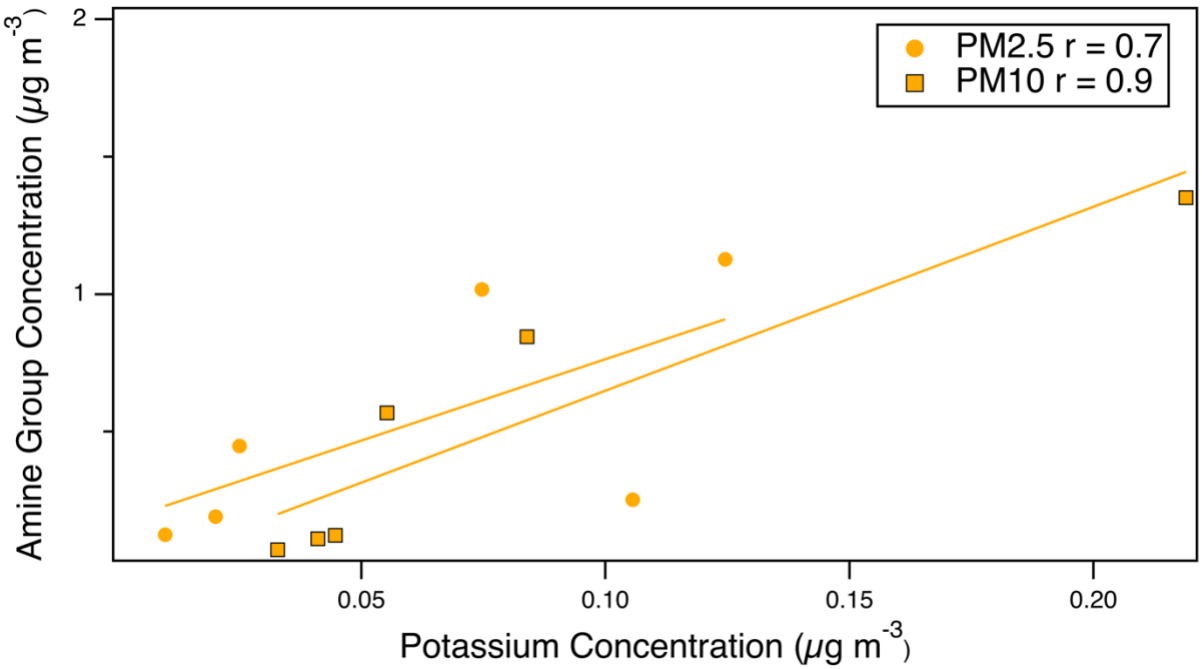

Figure 3.5: Comparison of amine group and potassium concentrations (µg m^{-3}) during a biomass burning event in October 2020 with both PM2.5 (circles) and PM10 (squares). Both the PM2.5 ($p = 0.07$) and PM10 fit are statistically significant ($p = 0.002$). Only afternoon samples were above detection.

Nss-sulfate is likely from photo-oxidation products of dimethyl sulfide (DMS), which has been shown to contribute a global sea-to-air flux of up to 39 x 10^{12} g sulfur per year (Andreae & Raemdonck, 1983; Charlson, Lovelock, Andreae, & Warren, 1987; Jaenicke, 1993). It contributed 1 ± 1% of BAM PM2.5 during high-PM10 days and 0.5 ± 1% of BAM PM10 during high-PM10 days.

3.3.3 Semivolatile Components

This project did not include direct measurements of ammonium nitrate, semivolatile organic compounds, or aerosol water, all of which may contribute to both BAM and gravimetric aerosol mass concentrations (Babila, Carlton, Hennigan, & Ghate, 2020; Nguyen, Zhang, Jimenez, Pike, & Carlton, 2016; Triantafyllou et al., 2016). The difference between BAM and

the measured component mass concentrations is largely attributable to these semivolatile components, although there are also minor contributions from other unmeasured components such as black carbon and nanoparticles which could include heavy metals, though most non-dust metals were below XRF detection limit (Motallebi et al., 2003). Hence, semivolatile/unidentified components are defined as the difference between BAM mass concentration and the sum of dust, sea salt, non-seasalt sulfate (nss-sulfate), and organic concentrations. The semivolatile/unidentified components accounted for 66 ± 16% (18.2 ± 11.4 μg m^{-3}) of BAM PM2.5 on average for the five-campaign average, increasing to 68 ± 15% (24.1 ± 8.5 μg m^{-3}) during high-PM10 days. Semivolatile/unidentified components accounted for 69 ± 18% (67.5 ± 69.1 μg m^{-3}) of BAM PM10 mass concentrations, which increased to 82 ± 14% (131.6 ± 58.3 μg m^{-3}) during high-PM10 days. The average PM2.5 semivolatile/unidentified fraction during most afternoons was quite consistent across the five campaigns (May 2019, October 2019, May 2020, October 2020, and May 2021), with a campaign-average range of 60 to 77% (Figure 3.6).

The composition differences between afternoon and overnight samples were compared for May 2019. The most notable difference was the semivolatile/unidentified fraction, which was 3% of the BAM PM2.5 mass concentration during the overnight samples (18:00 – 6:00) but 74% of the BAM PM2.5 mass concentration during the May 2019 afternoon samples (12:00 – 18:00) (Figure 4). The correlation between semivolatile/unidentified concentrations and windspeed (r = 0.45, Figure 3) may indicate that wind-driven sources like dune dust that are higher in the afternoons carry some semivolatile water with them. The higher semivolatile/unidentified contributions during the afternoons were likely associated with the increasing relative humidity and warmer temperature that occurs during the afternoon but not overnight. This difference also explains why 24-hr PM2.5 sampling would show lower semivolatile/unidentified contributions

(Chung et al., 2001; Gobeli, Schloesser, & & Pottberg, 2008; Hafkenscheid & Vonk, 2014; Hart, 2009), since averaging the high semivolatile/unidentified fractions in the afternoons with low fractions overnight would tend to hide the higher afternoon contributions.

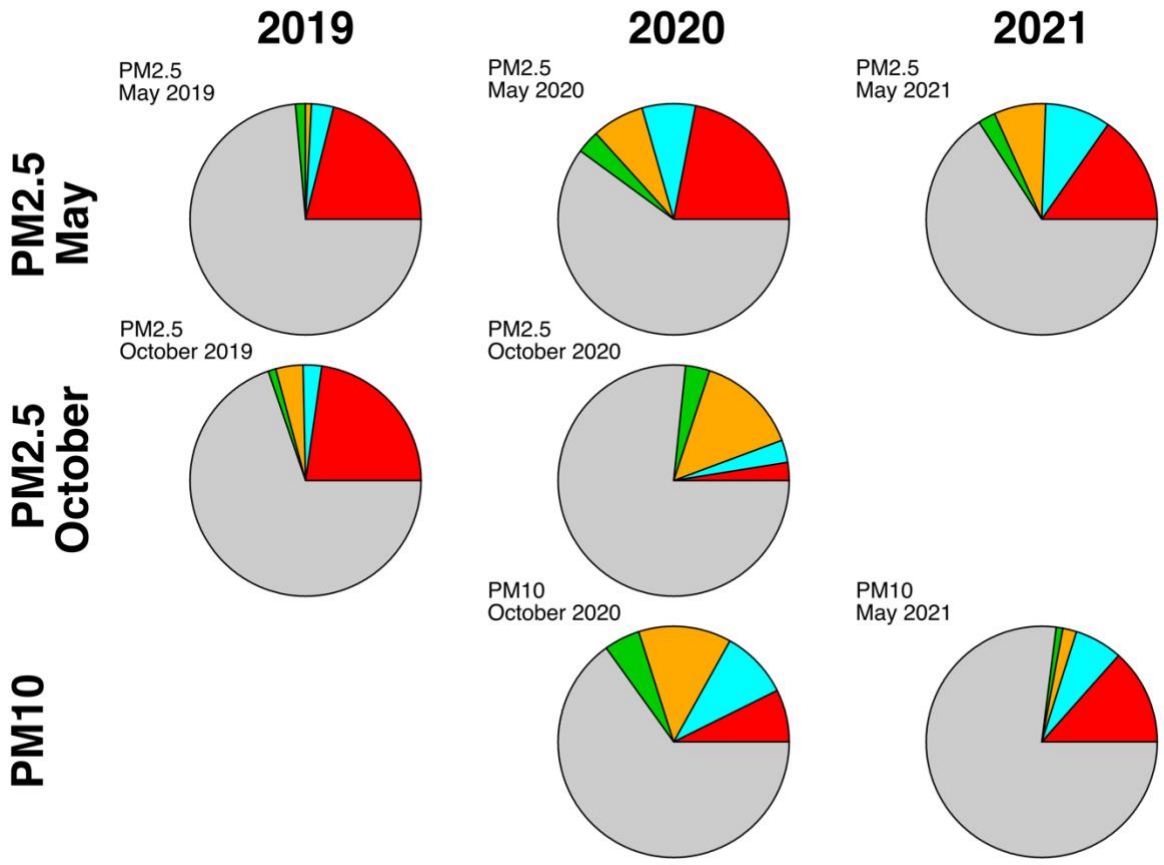

Figure 3.6: Composition of above detection afternoon PM2.5 and PM10 CDF mass concentrations (µg m^{-3}) with XRF mineral dust (red), sea salt (blue), sulfate (green), FTIR organic (orange), and semivolatile/unidentified (grey). The sampling times, in local time, were May 2019 – 12:00-18:00 (7); October 2019 – 10:00-18:00 (4); May 2020 – 11:00-19:00 (17); October 2020 – 11:00-19:00 (6), 12:00-18:00 (7); and May 2021 – 12:00-19:00 (30). For PM10 in May 2021, the organic concentration is from the average PM2.5 organic mass concentration for May 2021, since organic measurements were not collected for PM10 in May 2021.

The ranges of above detection BAM and gravimetric mass concentrations were similar, with gravimetric ranging from <10 to 45 µg m^{-3} and BAM from <10 to 70 µg m^{-3} for PM2.5 and gravimetric ranging from <10 to 250 µg m^{-3} and BAM from <10 to 290 µg m^{-3} for PM10 (Figure 3.3, Figure 3.14). However, there is a moderate correlation between ambient temperature and the BAM PM10 to gravimetric PM10 ratio. This correlation indicates that the warmer the outside temperature and the higher the specific humidity, the more BAM exceeds gravimetric results. This correlation provides additional evidence that the differences between BAM and gravimetric measurements are driven by semivolatile components, since temperature affects gas-to-particle partitioning (Figure 3.12). Since the gravimetric concentrations are measured at 35% RH and 21 °C, the outside temperature is likely adding water mass to the BAM concentrations. Semivolatile contributions to particle mass concentrations are expected to be reduced by the 24-hr equilibration of the gravimetric method at 35% RH. The BAM protocol is designed to provide similar conditions (Met One, 2016), but some semivolatile components can be captured by BAM if evaporation is incomplete (ECFR, 1971; C. Liu et al., 2013). This temperature dependence of the semivolatile/unidentified components is consistent with the comparison of PM2.5 afternoon and overnight sample composition, since the greater change in temperature during the afternoons would explain the larger semivolatile contribution (Figure 3.4). The larger organic fraction in the overnight samples than during the afternoons (although the concentration is higher for afternoons at 1.1 µg m^{-3} compared to 0.73 µg m^{-3} for overnight) is also consistent with semivolatile organic components accounting for some of the semivolatile/unidentified fraction.

Perhaps most revealing is the weak correlation of the specific humidity to the ratio of BAM PM2.5 to gravimetric PM2.5 concentrations compiled over three campaigns ($r = 0.4$, Figure 3.7), similar to previous findings in humid coastal areas (Triantafyllou et al., 2016). This

correlation was not evident for PM10 in May 2021 or October 2020, likely due to the more limited PM10 sampling and associated poor statistics. The weak, but statistically significant (p = 0.001), correlation for PM2.5 indicates that water is likely causing part of the difference between the BAM and gravimetric methods, but other semivolatile components such as ammonium nitrate may contribute to the BAM and gravimetric difference.

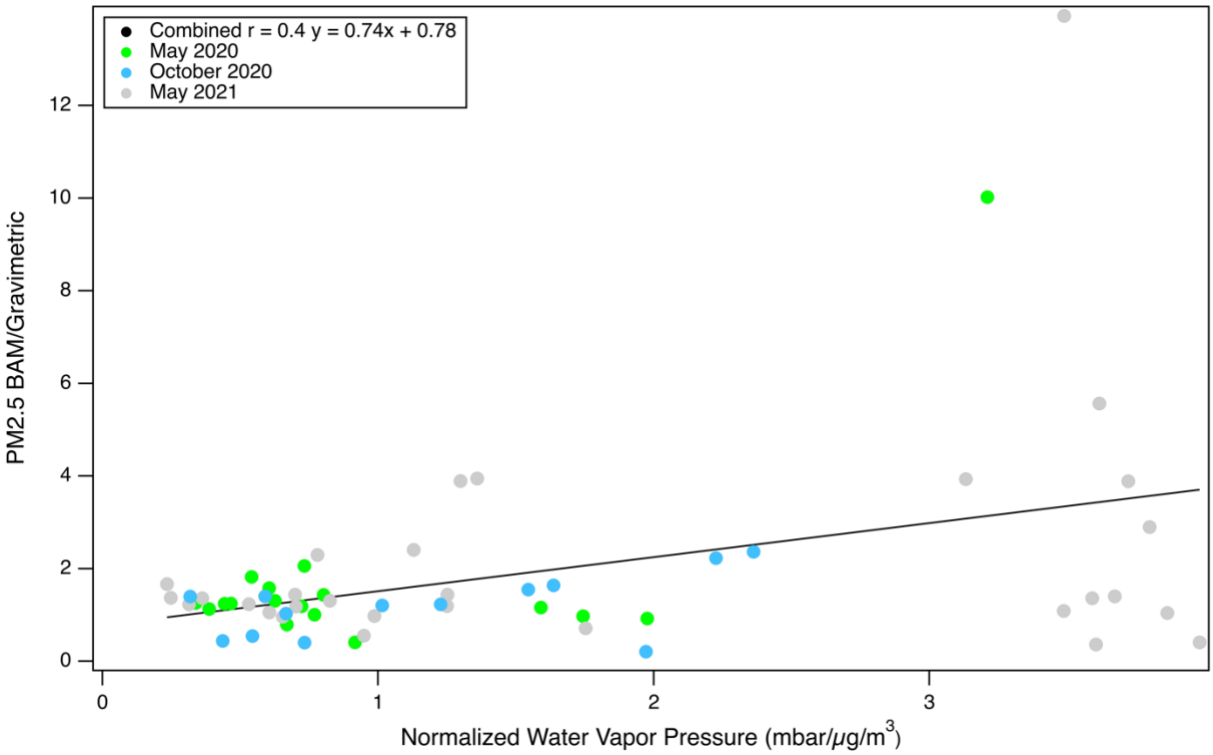

Figure 3.7**:** Dependence of the ratio of BAM PM2.5 to gravimetric PM2.5 concentrations on the water vapor pressure normalized by gravimetric mass concentration. The fit shown is the combined result of PM2.5 afternoon measurements from May 2020, October 2020, and May 2021 (p = 0.001). The correlation indicates the role of water in causing part of the difference between the two PM2.5 methods. The sampling times, in local time, were May 2020 – 11:00-19:00 (17); October 2020 – 11:00-19:00 (6), 12:00-18:00 (7); and May 2021 – 12:00-19:00 (30).

While water can account for part of the semivolatile contribution (Figure 3.7), it is likely that the semivolatile fraction includes ammonium nitrate, which may be emitted from vehicle emissions or agriculture (Jaenicke, 1993; McMurry et al., 2003). The moderate correlation of the semivolatile/unidentified concentration with dust (r = 0.49) and wind speed (r=0.45) (Figure 3.3) could suggest that water or other semivolatile gases are increased in the particle phase because of the higher surface area and volume associated with high PM concentrations (Liu et al., 2013). It is also possible that the heating required for evaporation of semivolatile/unidentified components during BAM measurements is insufficient as concentrations increase, since the semivolatile/unidentified contribution is nearly proportional and strongly correlated to BAM for both PM2.5 (r = 0.93) and PM10 (r = 0.97) (Figure 3.14). This could produce an artifact in BAM measurements that is larger at conditions above 50 µg m^{-3}, where few comparisons to gravimetric PM2.5 concentrations are available (Chung et al., 2001; Gobeli et al., 2008; Hafkenscheid & Vonk, 2014; Hart, 2009).

3.4 Conclusions

The chemical speciation of PM2.5 and PM10 from 3 years of sampling during high-wind months at CDF showed that the dust fraction of PM2.5 had an average contribution of 14 ± 12% to BAM PM2.5 and 11 ± 8% to BAM PM10. On days with hourly BAM PM10 exceeding 140 µg m^{-3}, the dust fraction increased to 22 ± 11% of BAM PM2.5 and 14 ± 10 % of BAM PM10. The remainder of PM2.5 and PM10 included sea salt, organic components that were largely from marine sources, ammonium sulfate, and semivolatile/unidentified components. The average sea salt contribution is smaller than dust at 9 ± 9% of BAM PM2.5 and 13 ± 14% of BAM PM10, which is consistent with other coastal locations (Modini et al., 2015). The average organic mass contribution was 8 ± 8% of BAM PM2.5 and 16 ± 8% of BAM PM10, and its composition was

consistent with ambient marine aerosol (Frossard et al., 2014). The semivolatile/unidentified contribution is substantial for afternoon samples at 66% for the five-campaign average but negligible overnight, indicating the needs for reducing sampling times below 24 hour and for quantifying aerosol water (Nguyen et al., 2016), semivolatile organic compounds, and ammonium nitrate (Chow et al., 2008).

The emission of mineral dust by natural winds over natural desert areas is a common feature of air quality in the western U.S. (Malm et al., 1994; Noll, Pontius, Frey, & Gould, 1985). Contributions of dust were low at CDF for PM10 at 14% on high PM10 days. This evidence of low dust contributions to PM10 along with a moderate wind correlation and negligible weekend/weekday difference show that the contribution of dune dust to high PM10 concentrations from Oceano Dunes is small and likely dominated by natural saltation processes associated with the indigenous geomorphological dune structure rather than by recreational activities. Since the dunes are the likely source of most of the dust, reducing or eliminating this unique geological feature of the local landscape could provide some marginal reductions in PM10. However, while reducing dust emissions by revegetation or fencing decreases PM10, there is no evidence that such reductions provide for improved air quality and thereby do not address the problem on which the expenditures are predicated.

In summary, (1) the amount of natural and man-made dust contributing to PM10 is 14% on average for high-PM10 days; (2) the amount of the dust attributable to OHV is some portion of that 14%, and the wind dependence and lack of weekday/weekend differences demonstrates that portion is negligible; (3) other sources, including ocean, agricultural, and highway vehicles, would need to be reduced to improve air quality significantly. Since reducing natural dust is not improving health outcomes, then air quality regulatory resources would be better applied

elsewhere. While PM10 and PM2.5 regulations are well-intentioned and overall quite effective strategies for reducing pollution for decades across much of the U.S., their implementation can be perversely applied if other socio-political motivations are at play to artificially justify restricting access to and modifying the natural landscape of State Parks. The requirements of reducing dunes area and limiting vehicle access constitutes a misapplication of PM regulations for purposes other than improving health, perhaps motivated by ethno-cultural bias against OHV enthusiasts (Cordell et al., 2008). Because the State Park system should be open to all residents of and visitors to the state of California, and because taxpayers deserve for fees collected for pollution reduction to be applied effectively to that end, the chemical speciation reported here should be used to ensure the appropriate application of air quality regulations to reduce potentially harmful pollution.

3.5 Appendix

3.5.1 Comparison of Dust Approximations

There are several estimates for crustal material from elemental composition that have been introduced. A classic estimate for the western U.S. (Malm, Sisler, Huffman, Eldred, & Cahill, 1994; Motallebi, Taylor, & Croes, 2003) based on five of the most prevalent elements (Al, Si, Ca, Fe, Ti) and was also used by San Luis Obispo Air Pollution Control District for its Nipomo Mesa Particulate Study (Phase 1) (SLOAPCD, 2007). A more comprehensive estimate was proposed to account for additional minerals from nine elements (Mg, Al, Si, K, Ca, Ti, Fe, Mn, Ba) (Usher, Michel, & Grassian, 2003), but needed to be corrected to avoid double counting of sea salt components (Mg, Ca, K) (Gilardoni et al., 2007). Figure 3.8 shows a comparison of PM2.5 dust at CDF during all 5 campaigns and that these three estimates are within ±7% of each other.

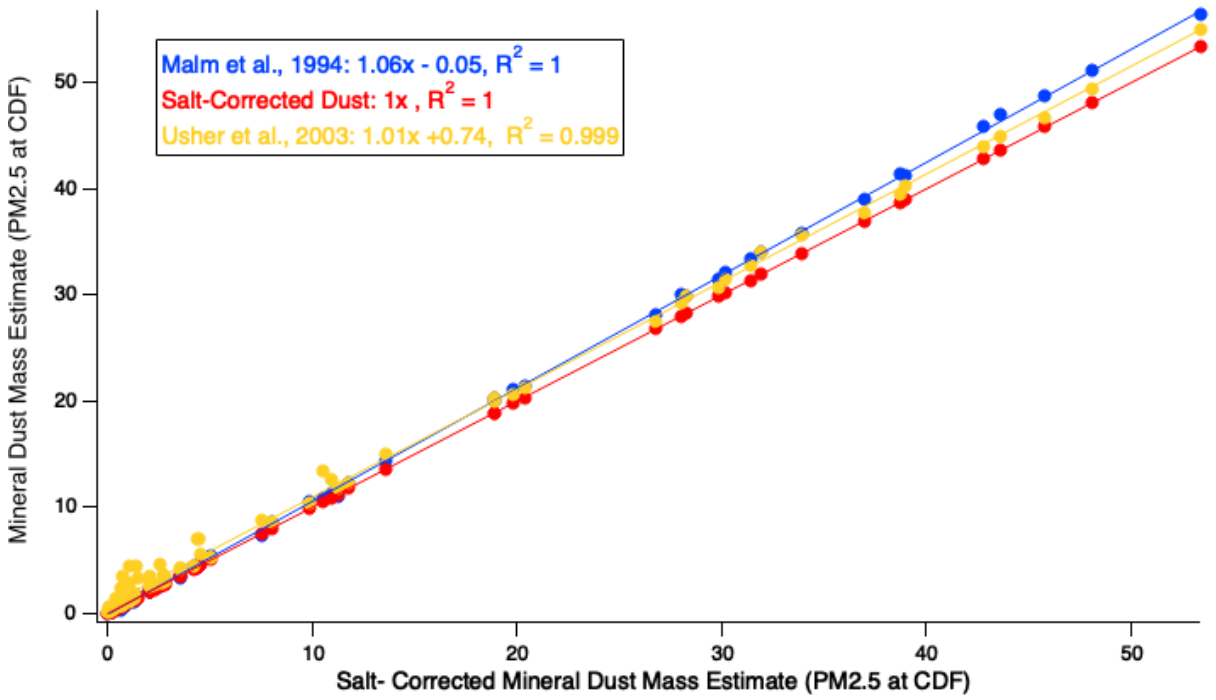

Figure 3.8: Mineral dust calculation comparison of Usher et al. (2003), after correction to exclude sea salt, and Malm et al. (1994), both without sea salt correction using PM2.5 samples collected at CDF for the five campaigns.

Using two methods, the elemental components of a limited number of samples were determined to estimate the mass of mineral dust. The first method is a standard approach based on the most common oxides for the non-sea salt (nss) elements measured and is named "nss dust" (Usher et al., 2003), while the second approach used aerosolized and size-separated PM generated in the laboratory from a bulk sample of surface dune sand collected adjacent to the S1 site. The collected dune sand was not dried prior to being aerosolized in the laboratory and so some water was retained. Salts that are present in sand (including NaCl, ammonium nitrate, and ammonium sulfate) will take up water once the relative humidity (RH) is high enough to exceed the solubility limit (deliquescence point) of the salt (Seinfeld et al., 2016;

Seinfeld & Pandis, 2006). The result is that when salts are in contact with humid air, some liquid water forms on the salts and becomes associated with the sand until it is dried out. Accordingly, this second method is named "wet dust." These two approaches provide estimates for the mineral component mass (nss dust) and for the higher mass that could be associated with dust at ambient relative humidity (wet dust). The comparison of the two approaches shown in Figure 4 from the February 2020 report (Scripps, 2020) indicates that the "wet dust" approach accounted for approximately 50% additional mass from water. This means that the two methods are consistent in terms of the amount of mass associated with specific measured elements. It also provides preliminary evidence that water could be a substantial fraction (50%) of both surface sand and lofted dust.

3.5.2 Evidence of Semivolatile Contribution to Differences between BAM and Gravimetric

Because temperature controls whether particles are in the gas phase or the particle phase for semivolatile components, showing the role of semivolatiles is clear from a consideration of temperature on the differences between the BAM and Gravimetric methods. The Scripps sampler was suspended on a building and the filters remained on the sampler for only the 7-8 hr of sampling in the afternoon. In this sense, the sampling and the filters were at ambient temperature. In contrast, the BAM was located inside the SLOAPCD shelter at CDF, which is temperature controlled to maintain 20-30ºC continuously. This temperature was typically warmer than ambient during May 2021, resulting in a heating of air as it was sampled and then a further heating inside the instrument for the purpose of reducing the relative humidity to below 30%. While the temperature inside the instrument is not recorded, the temperature inside the instrument room is recorded.

To illustrate why the conditions are different for afternoon sampling than for a 24-hr sample, the temperature, wind speed, and ambient relative humidity for the 3 campaigns in which gravimetric data were obtained are displayed in Figures 3.9-3.11.

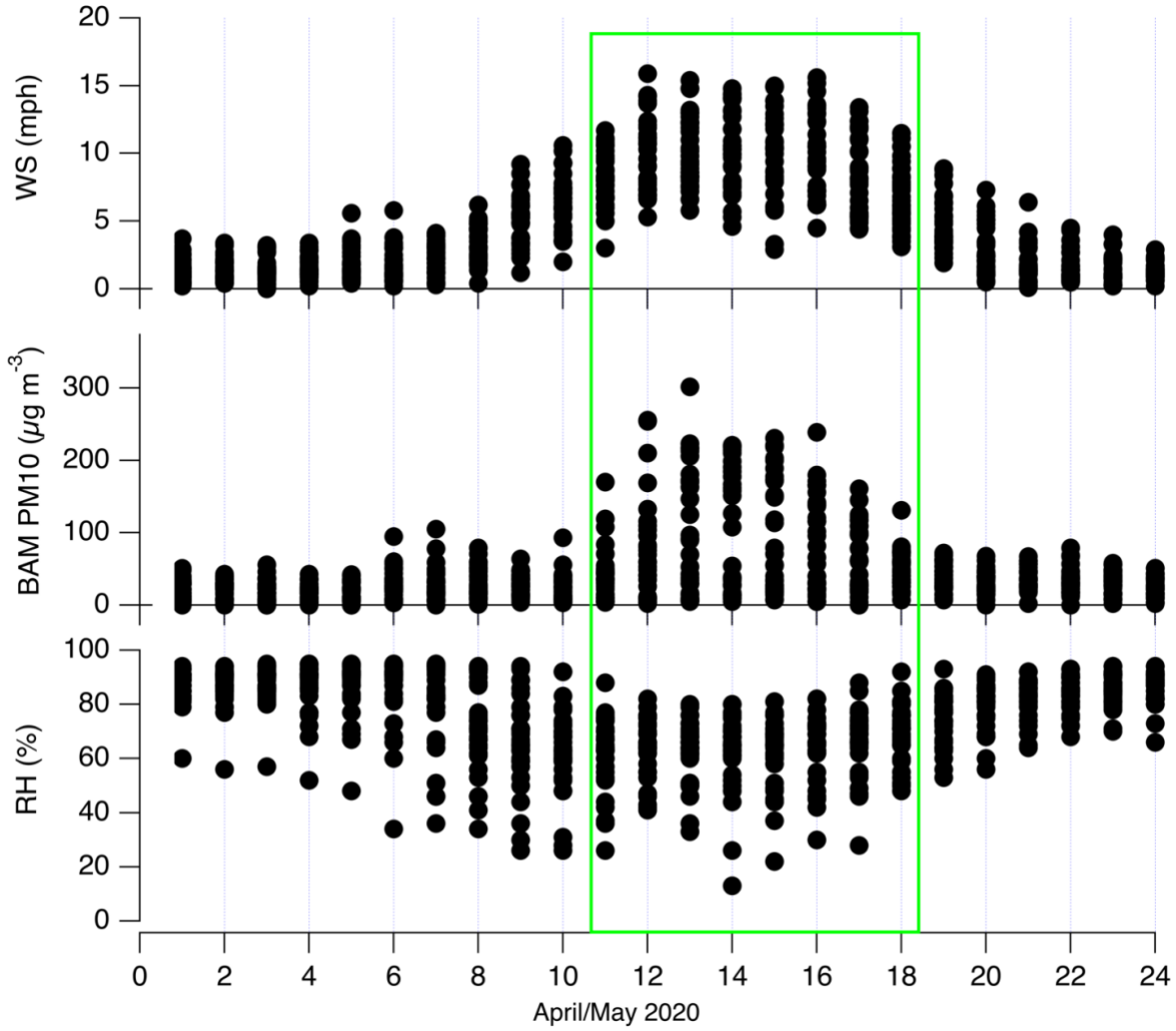

Figure 3.9: Daily time series (local) of wind speed (top), BAM PM10 (middle), and ambient relative humidity (bottom) from 27 April to 17 May 2020. Filter sampling times are indicated by the highlighted boxes with 1 sampling time (local): 11:00-19:00 (green,16 samples).

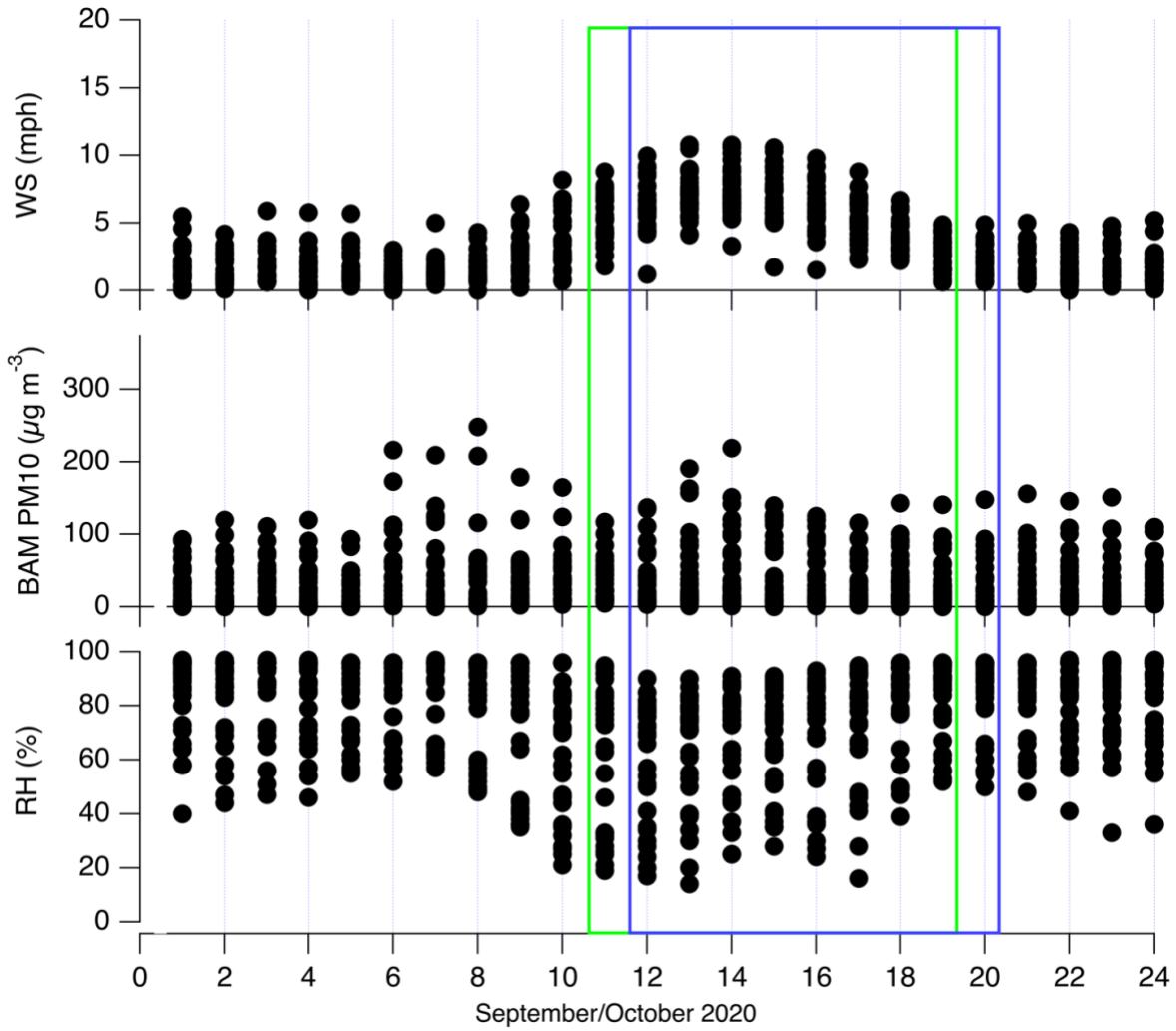

Figure 3.10: Daily time series (local) of wind speed (top), BAM PM10 (middle), and ambient relative humidity (bottom) from 28 September to 10 October 2020. Filter sampling times are indicated by the highlighted boxes with 2 sampling times (local): 11:00-19:00 (green, 3 samples) and 12:00-18:00 (blue, 1 sample).

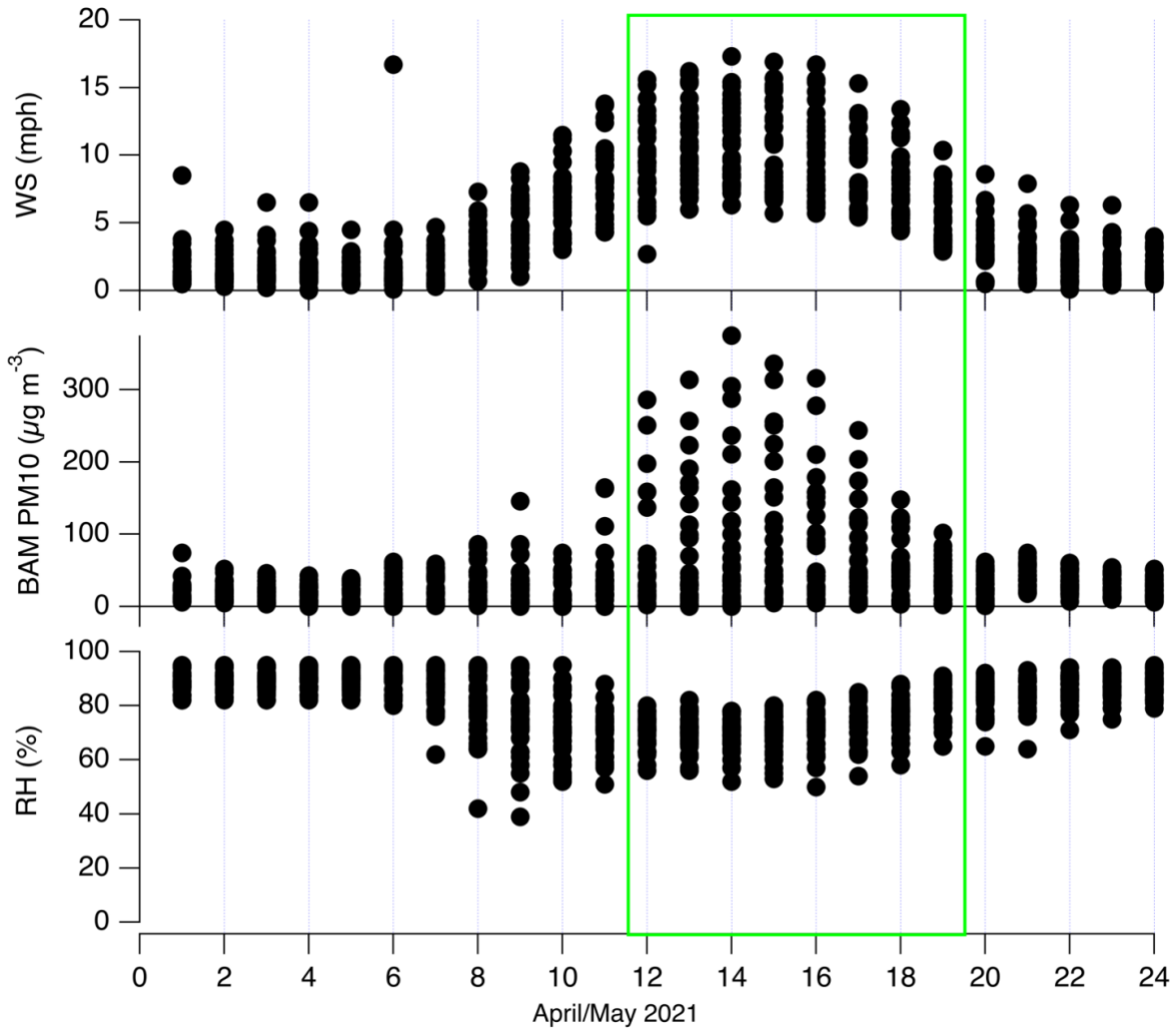

Figure 3.11**:** Daily time series of wind speed (top), BAM PM10 (middle), and ambient relative humidity (bottom) from 27 April to 26 May 2021. Filter sampling times are indicated by the highlighted box in local time: 12:00-19:00 (green, 19 samples).

If there were no contributions from semivolatile components, then there would be no effect of temperature or water on either the BAM or Gravimetric results. However, as shown in Figure 3.12, there is a moderate correlation (r=0.53) between the ratio of BAM to Gravimetric and the ambient temperature. This indicates that the warmer the outside temperature, the more BAM exceeded gravimetric. This is consistent with the fact that the saturation pressure of water and other semivolatile components increase with temperature, allowing air to "hold" more in the vapor phase that is then available to condense onto particles (and filter substrates, especially for

glass and quartz filters typically used in the BAM). This effect is especially important downwind of the ocean, where air is often near 100% relative humidity.

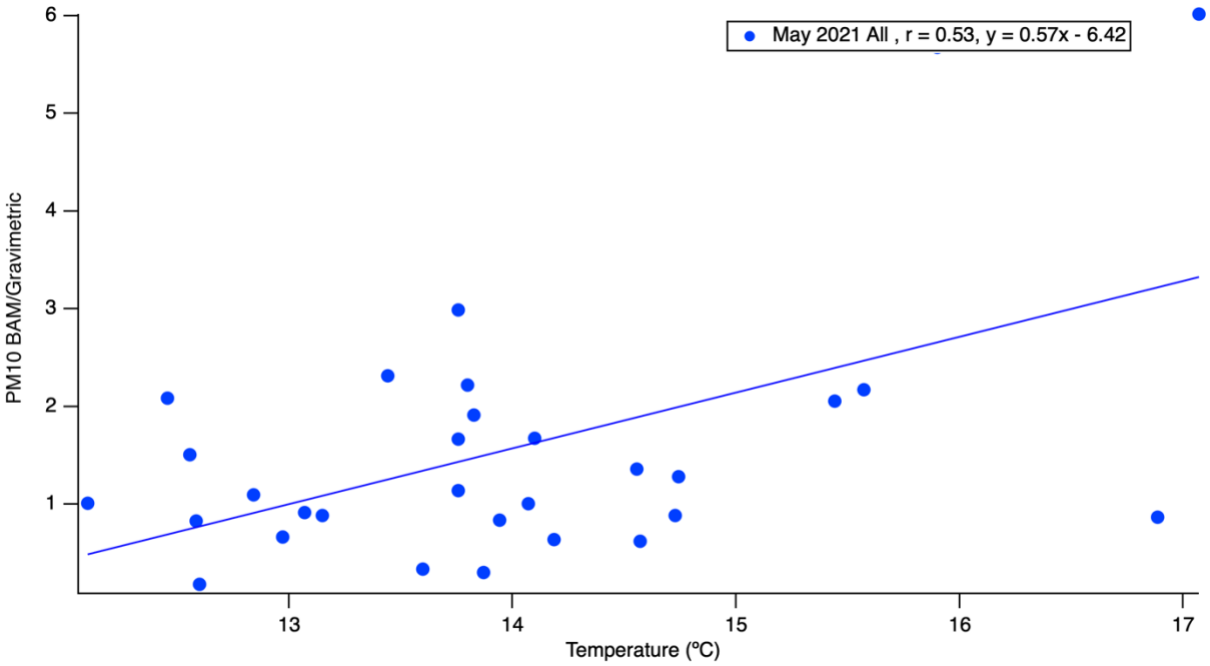

Figure 3.12: Relationship between the ratio of SLOAPCD BAM PM10 to Scripps gravimetric mass concentrations with the average ambient temperature at CDF during the afternoon samples in May 2021. The correlation indicates the larger role of gas uptake and evaporation in causing the larger difference between the two PM10 methods at higher temperatures. CDF PM10 measurements from October 2020 were not included because of the lack of high wind days. To maximize the number of samples available for this analysis, gravimetric mass concentrations that were below the detection limit (20 µg), were replaced with half of the detectable concentration (10 µg divided by the volume of air sampled on the filter).

3.5.3 Comparison of Weekend Definitions

To thoroughly investigate whether there was evidence of anthropogenic influence on aerosol composition at CDF, three different weekend definitions were tested: 1.) Friday through Sunday (in main text), 2.) Saturday through Sunday, and 3.) Saturday through Monday. The difference between weekend and weekday composition for all three iterations were tested using a two sided t test for every aspect of composition (dust, sea salt, organic, sulfate, semivolatile, and unidentified) and the null hypothesis could not be rejected for any ($p>0.05$).

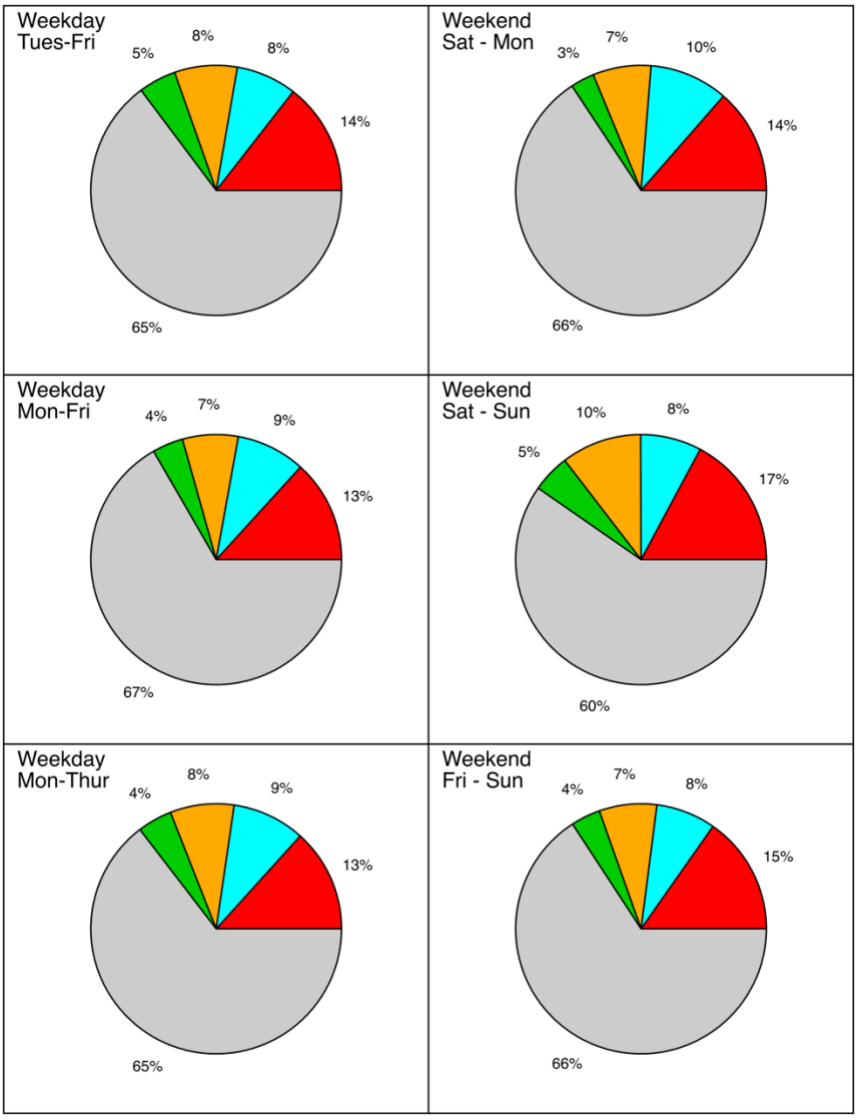

Figure 3.13: Composition of afternoon (11-18:00) PM2.5 weekend and weekday mass concentrations (µg m^{-3}) with XRF mineral dust (red), sea salt (blue), sulfate (green), FTIR organic (orange), semivolatile (grey), and unidentified (brown). Regardless of how the weekend was defined, there was no statistical difference ($p > 0.05$) between the individual components between the weekend and weekday samples.

3.5.4 Comparison of Gravimetric and BAM Concentrations for PM2.5 and PM10

The BAM and gravimetric mass concentrations show that gravimetric is consistently smaller than BAM (Figure 3.14). BAM has been shown to be higher than gravimetric measurements, particularly during warmer seasons with increased aerosol water (Chung et al., 2001; Gobeli et al., 2008; Hafkenscheid & Vonk, 2014; Hart, 2009) and conditions with high acid gas-adsorption (Liu et al., 2013).

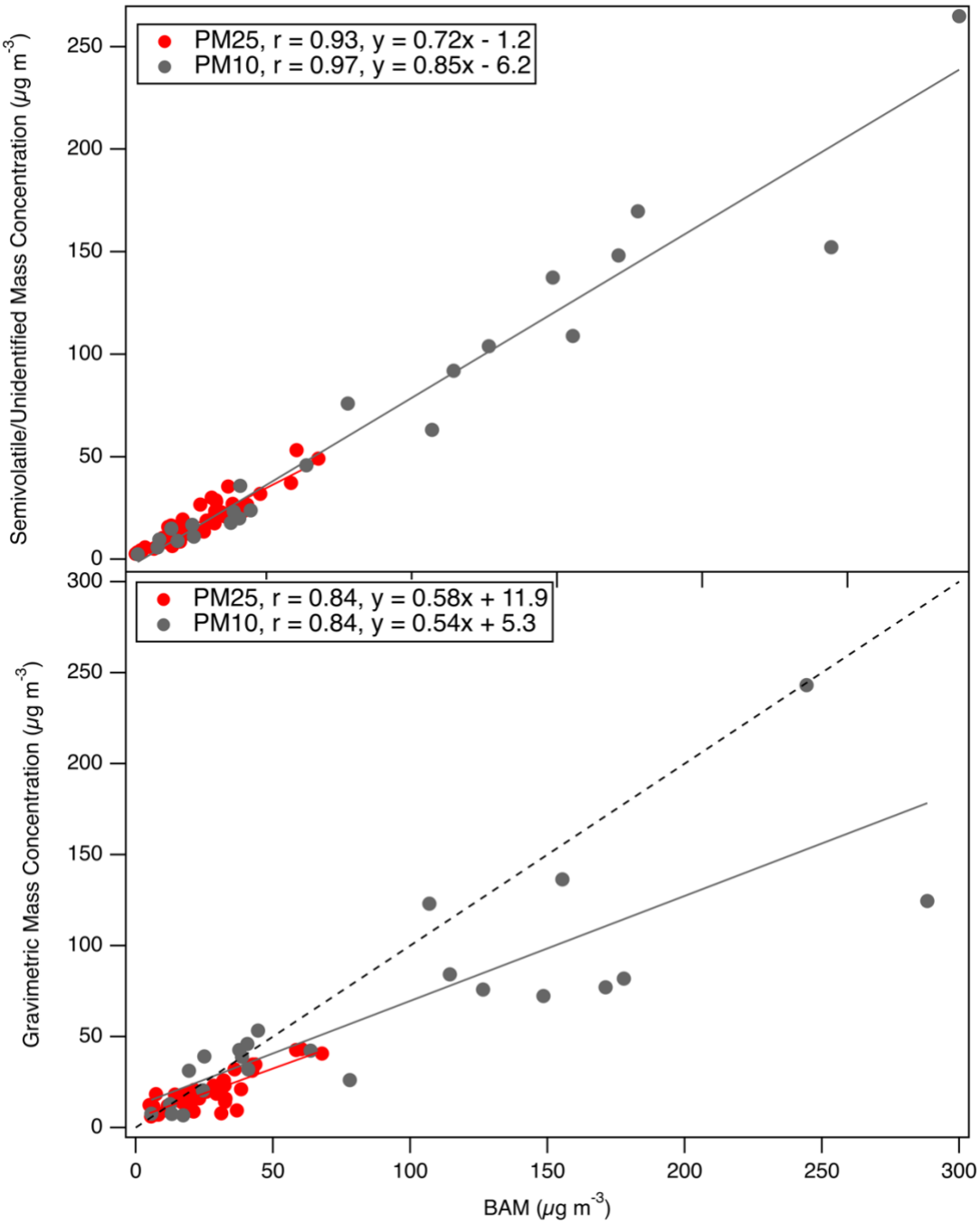

Figure 3.14: Comparison of semivolatile/unidentified mass concentration (top) and gravimetric mass concentration (bottom) to BAM mass concentration (µg m^{-3}) for both PM2.5 (red) and PM10 (grey) filters. The one-to-one line is shown with a dashed black line.

3.6 Acknowledgements

The authors would like to thank Jinghan Li, Melissa Lopez, Abigail Haynam, Kyle La Fever, and Randall Baxter for their contributions to preparing and collecting data. This work was funded by the California Parks and Recreation Contract C18V0003/FS#26915.

Chapter 3, in full, is currently being prepared for submission for publication of the material in *Atmospheric Environment.* Lewis, S.L.; Russell, L.M.; McKinsey, J.A., Harris, W.J. (2022) *Atmospheric Environment* "Contributions of Dust and Other Chemical Components to PM2.5 and PM10 Concentrations at Oceano Dunes". The dissertation author was the primary researcher and author of this material.

References

Andreae, M. O., & Raemdonck, H. (1983). Dimethyl Sulfide in the Surface Ocean and the Marine Atmosphere: A Global View. *Science, 221*(4612), 744-747. doi:10.1126/science.221.4612.744

Apte, J. S., Brauer, M., Cohen, A. J., Ezzati, M., & Pope, C. A. (2018). Ambient PM2.5 Reduces Global and Regional Life Expectancy. *Environmental Science & Technology Letters, 5*(9), 546-551. doi:10.1021/acs.estlett.8b00360

Babila, J. E., Carlton, A. G., Hennigan, C. J., & Ghate, V. P. (2020). On Aerosol Liquid Water and Sulfate Associations: The Potential for Fine Particulate Matter Biases. *Atmosphere, 11*(2). doi:10.3390/atmos11020194

Bagnold, R. A. (1941). *The Physics of Blown Sand and Desert Dunes*: Springer Dordrecht.

California Air Resource Board. (2022). AQMIS2 Meteorological Data. Retrieved from https://www.arb.ca.gov/aqmis2/display.php?report=SITE31D&site=3762&year=2020&mon=4&day=28&hours=all&param=WINSPD&units=012&statistic=HVAL&ptype=met

California Department of Parks and Recreation. (2021). Air Quality Expenses at Oceano Dunes District. Retrieved from https://ohv.parks.ca.gov/pages/1140/files/08-26-2021-Item%203-OHV%20Trust%20Fund%20Update%20(2021%20Fiscal%20Year%20Budget%20Report).pdf

California Department of Parks and Recreation. (2022). Mission Statement. Retrieved from https://www.parks.ca.gov/?page_id=91#:~:text=Our%20Mission,for%20high%2Dquality%20outdoor%20recreation.

Charlson, R. J., Lovelock, J. E., Andreae, M. O., & Warren, S. G. (1987). Oceanic phytoplankton, atmospheric sulphur, cloud albedo and climate. *Nature, 326*(6114), 655-661. doi:10.1038/326655a0

Chen, C. L., Chen, S., Russell, L. M., Liu, J., Price, D. J., Betha, R., . . . Cappa, C. D. (2018). Organic Aerosol Particle Chemical Properties Associated With Residential Burning and Fog in Wintertime San Joaquin Valley (Fresno) and With Vehicle and Firework Emissions in Summertime South Coast Air Basin (Fontana). *Journal of Geophysical Research: Atmospheres, 123*(18), 10,707-710,731. doi:10.1029/2018jd028374

Chester LabNet. (2018). Methods. Retrieved from https://chesterlab.net/methods/

Chow, J. C., Doraiswamy, P., Watson, J. G., Chen, L.-W. A., Ho, S. S. H., & Sodeman, D. A. (2008). Advances in Integrated and Continuous Measurements for Particle Mass and Chemical Composition. *Journal of the Air & Waste Management Association, 58*(2), 141-163. doi:10.3155/1047-3289.58.2.141

Chung, A., Chang, D. P. Y., Kleeman, M. J., Perry, K. D., Cahill, T. A., Dutcher, D., . . . Stroud, K. (2001). Comparison of Real-Time Instruments Used To Monitor Airborne Particulate Matter. *Journal of the Air & Waste Management Association, 51*(1), 109-120. doi:10.1080/10473289.2001.10464254

Cordell, K. H., Betz, C. J., Green, G. T., & Stephens, B. (2008). *Off-Highway Vehicle Recreation in the United States and its Regions and States: A National Report from the National Survey on Recreation and the Environment (NSRE)*. Retrieved from https://www.fs.fed.us/recreation/programs/ohv/IrisRec1rpt.pdf

Delfino, R. J., Sioutas, C., & Malik, S. (2005). Potential Role of Ultrafine Particles in Associations between Airborne Particle Mass and Cardiovascular Health. *Environmental Health Perspectives, 113*(8), 934-946. doi:doi:10.1289/ehp.7938

Dockery, D. W., Pope, C. A., Xu, X., Spengler, J. D., Ware, J. H., Fay, M. E., . . . Speizer, F. E. (1993). An Association between Air Pollution and Mortality in Six U.S. Cities. *New England Journal of Medicine, 329*(24), 1753-1759. doi:10.1056/nejm199312093292401

Du, P., Liu, J., Gui, H., Zhang, J., Yu, T., Wang, J., . . . Chen, C. (2020). Development of a static test apparatus for evaluating the performance of three PM2.5 separators commonly used in China. *Journal of Environmental Sciences, 87*, 238-249. doi:https://doi.org/10.1016/j.jes.2019.06.008

Duan, J. C., Tan, J. H., Wang, S. L., Hao, J. M., & Chail, F. H. (2012). Size distributions and sources of elements in particulate matter at curbside, urban and rural sites in Beijing. *Journal of Environmental Sciences, 24*(1), 87-94. doi:10.1016/s1001-0742(11)60731-6

ECFR. (1971). Part 50 - National Primary and Secondary Ambient Air Quality Standards. Retrieved from https://www.ecfr.gov/current/title-40/chapter-I/subchapter-C/part-50

Echalar, F., Gaudichet, A., Cachier, H., & Artaxo, P. (1995). Aerosol emissions by tropical forest and savanna biomass burning: Characteristic trace elements and fluxes. *Geophysical Research Letters, 22*(22), 3039-3042. doi:https://doi.org/10.1029/95GL03170

EPA. (2022a). 2017 AirToxScreen Mapping Tool.

EPA. (2022b). Summary of the Clean Air Act. Retrieved from https://www.epa.gov/laws-regulations/summary-clean-air-act

Erickson, E., Mickel, A. E., & Rolloff, D. B. (2014). Attendance Study 2012-2013. Retrieved from https://ohv.parks.ca.gov/pages/25010/files/ohmvr-attendance-study-report-2014.pdf

Fisseha, R., Dommen, J., Sax, M., Paulsen, D., Kalberer, M., Maurer, R., . . . Baltensperger, U. (2004). Identification of Organic Acids in Secondary Organic Aerosol and the Corresponding Gas Phase from Chamber Experiments. *Analytical Chemistry, 76*(22), 6535-6540. doi:10.1021/ac048975f

Frank, N. H. (2006). Retained Nitrate, Hydrated Sulfates, and Carbonaceous Mass in Federal Reference Method Fine Particulate Matter for Six Eastern U.S. Cities. *Journal of the Air & Waste Management Association, 56*(4), 500-511. doi:10.1080/10473289.2006.10464517

Frossard, A. A., Russell, L. M., Burrows, S. M., Elliott, S. M., Bates, T. S., & Quinn, P. K. (2014). Sources and composition of submicron organic mass in marine aerosol particles. *Journal of Geophysical Research: Atmospheres, 119*(22), 12,977-913,003. doi:10.1002/2014JD021913

Gantt, B., Meskhidze, N., Facchini, M. C., Rinaldi, M., Ceburnis, D., & O'Dowd, C. D. (2011). Wind speed dependent size-resolved parameterization for the organic mass fraction of sea spray aerosol. *Atmos. Chem. Phys., 11*(16), 8777-8790. doi:10.5194/acp-11-8777-2011

Gilardoni, S., Russell, L. M., Sorooshian, A., Flagan, R. C., Seinfeld, J. H., Bates, T. S., . . . Worsnop, D. R. (2007). Regional variation of organic functional groups in aerosol particles on four U.S. east coast platforms during the International Consortium for Atmospheric Research on Transport and Transformation 2004 campaign. *Journal of Geophysical Research: Atmospheres, 112*(D10). doi:10.1029/2006jd007737

Gillies, J. A., Furtak-Cole, E., Nikolich, G., & Etyemezian, V. (2022). The role of off-highway vehicle activity in augmenting dust emissions at the Oceano Dunes State Vehicular Recreation Area, Oceano, CA. *Atmospheric Environment: X, 13*, 100146. doi:https://doi.org/10.1016/j.aeaoa.2021.100146

Gobeli, D., Schloesser, H., & & Pottberg, T. (2008). Met One Instruments BAM-1020 Beta Attenuation Mass Monitor US-EPA PM2.5 Federal Equivalent Method Field Test Results. *Air and Waste Management Association.*

Hafkenscheid, T. L., & Vonk, J. (2014). *Evaluation of equivalence of the MetOne BAM-1020 for the measurement of PM2.5 in ambient air*. Retrieved from https://www.rivm.nl/bibliotheek/rapporten/2014-0078.pdf

Hains, J. C., Chen, L. W. A., Taubman, B. F., Doddridge, B. G., & Dickerson, R. R. (2007). A side-by-side comparison of filter-based PM2.5 measurements at a suburban site: A closure study. *Atmospheric Environment, 41*(29), 6167-6184. doi:https://doi.org/10.1016/j.atmosenv.2007.04.008

Hart, D. (2009). What is the Difference Between the New BAM-1020 PM2.5 FEM and Older BAM-1020 Monitors? In: Met One Technical Bulletin.

Hawkins, L. N., & Russell, L. M. (2010). Oxidation of ketone groups in transported biomass burning aerosol from the 2008 Northern California Lightning Series fires. *Atmospheric Environment, 44*(34), 4142-4154. doi:10.1016/j.atmosenv.2010.07.036

Holland, H. D. (1978). *The chemistry of the atmosphere and oceans*. New York: Wiley.

Jaenicke, R. (1993). Chapter 1 Tropospheric Aerosols. In P. V. Hobbs (Ed.), *International Geophysics* (Vol. 54, pp. 1-31): Academic Press.

Lewis, S. L., Saliba, G., Russell, L. M., Quinn, P. K., Bates, T. S., & Behrenfeld, M. J. (2021). Seasonal Differences in Submicron Marine Aerosol Particle Organic Composition in the North Atlantic. *Frontiers in Marine Science, 8*. doi:10.3389/fmars.2021.720208

Lighty, J. S., Veranth, J. M., & Sarofim, A. F. (2000). Combustion aerosols: Factors governing their size and composition and implications to human health. *Journal of the Air & Waste Management Association, 50*(9), 1565-1618. doi:10.1080/10473289.2000.10464197

Liu, C., Awasthi, A., Hung, Y., Gugamsetty, B., Tsai, C., Wu, Y., & Chen, C. (2013). Differences in 24-h average PM2.5 concentrations between the beta attenuation monitor (BAM) and the dichotomous sampler (Dichot). *Atmospheric Environment, 75*, 341-347. doi:https://doi.org/10.1016/j.atmosenv.2013.04.062

Liu, J., Dedrick, J., Russell, L. M., Senum, G. I., Uin, J., Kuang, C., . . . Lubin, D. (2018). High summertime aerosol organic functional group concentrations from marine and seabird sources at Ross Island, Antarctica, during AWARE. *Atmospheric Chemistry and Physics, 18*(12), 8571-8587. doi:10.5194/acp-18-8571-2018

Liu, J., Russell, L. M., Lee, A. K. Y., McKinney, K. A., Surratt, J. D., & Ziemann, P. J. (2017). Observational evidence for pollution-influenced selective uptake contributing to biogenic secondary organic aerosols in the southeastern U.S. *Geophysical Research Letters, 44*(15), 8056-8064. doi:https://doi.org/10.1002/2017GL074665

Maciejczyk, P., Chen, L.-C., & Thurston, G. (2021). The Role of Fossil Fuel Combustion Metals in PM2.5 Air Pollution Health Associations. *Atmosphere, 12*(9). doi:10.3390/atmos12091086

Malm, W. C., Sisler, J. F., Huffman, D., Eldred, R. A., & Cahill, T. A. (1994). Spatial and seasonal trends in particle concentration and optical extinction in the United States. *Journal of Geophysical Research: Atmospheres, 99*(D1), 1347-1370. doi:https://doi.org/10.1029/93JD02916

Maria, S. F., Russell, L. M., Turpin, B. J., & Porcja, R. J. (2002). FTIR measurements of functional groups and organic mass in aerosol samples over the Caribbean. *Atmospheric Environment, 36*(33), 5185-5196. doi:10.1016/s1352-2310(02)00654-4

Maria, S. F., Russell, L. M., Turpin, B. J., Porcja, R. J., Campos, T. L., Weber, R. J., & Huebert, B. J. (2003). Source signatures of carbon monoxide and organic functional groups in Asian Pacific Regional Aerosol Characterization Experiment (ACE-Asia) submicron aerosol types. *Journal of Geophysical Research: Atmospheres, 108*(D23). doi:https://doi.org/10.1029/2003JD003703

Maria Steven, F., Russell Lynn, M., Gilles Mary, K., & Myneni Satish, C. B. (2004). Organic Aerosol Growth Mechanisms and Their Climate-Forcing Implications. *Science, 306*(5703), 1921-1924. doi:10.1126/science.1103491

Maudlin, L. C., Wang, Z., Jonsson, H. H., & Sorooshian, A. (2015). Impact of wildfires on size-resolved aerosol composition at a coastal California site. *Atmospheric Environment, 119*, 59-68. doi:https://doi.org/10.1016/j.atmosenv.2015.08.039

McMurry, P., Shepherd, M., & Vickery, J. (2003). *Particulate matter science for policy makers: A NARSTO assessment* (EPRI Report 1007735). Retrieved from Pasco, WA:

Met One. (2016). BAM 1020 Particulate Monitor Operation Manual. Retrieved from https://metone.com/wp-content/uploads/2019/05/BAM-1020-9800-Manual-Rev-W.pdf

Modini, R. L., Frossard, A. A., Ahlm, L., Russell, L. M., Corrigan, C. E., Roberts, G. C., . . . Leaitch, W. R. (2015). Primary marine aerosol-cloud interactions off the coast of California. *Journal of Geophysical Research-Atmospheres, 120*(9), 4282-4303. doi:10.1002/2014jd022963

Motallebi, N., Taylor, C. A., & Croes, B. E. (2003). Particulate Matter in California: Part 2—Spatial, Temporal, and Compositional Patterns of PM2.5, PM10–2.5, and PM10. *Journal of the Air & Waste Management Association, 53*(12), 1517-1530. doi:10.1080/10473289.2003.10466323

Nguyen, T. K. V., Zhang, Q., Jimenez, J. L., Pike, M., & Carlton, A. G. (2016). Liquid Water: Ubiquitous Contributor to Aerosol Mass. *Environmental Science & Technology Letters, 3*(7), 257-263. doi:10.1021/acs.estlett.6b00167

Noll, K. E., Pontius, A., Frey, R., & Gould, M. (1985). Comparison of Atmospheric Coarse Particles at an Urban and Non-urban Site. *Atmospheric Environment, 19*(11), 1931-1943. doi:10.1016/0004-6981(85)90019-8

Oceano Dunes SVRA. (2022). Map Area of SVRA. Retrieved from http://ohv.parks.ca.gov/?page_id=1208

Pope, C. A., Ezzati, M., & Dockery, D. W. (2009). Fine-Particulate Air Pollution and Life Expectancy in the United States. *New England Journal of Medicine, 360*(4), 376-386. doi:10.1056/nejmsa0805646

Rogula-Kozłowska, W., Klejnowski, K., Rogula-Kopiec, P., Ośródka, L., Krajny, E., Błaszczak, B., & Mathews, B. (2014). Spatial and seasonal variability of the mass concentration and chemical composition of PM2.5 in Poland. *Air Quality, Atmosphere & Health, 7*(1), 41-58. doi:10.1007/s11869-013-0222-y

Russell, L. M. (2003). Aerosol Organic-Mass-to-Organic-Carbon Ratio Measurements. *Environmental Science & Technology, 37*(13), 2982-2987. doi:10.1021/es026123w

Russell, L. M., Bahadur, R., & Ziemann, P. J. (2011). Identifying organic aerosol sources by comparing functional group composition in chamber and atmospheric particles. *Proceedings of the National Academy of Sciences, 108*(9), 3516. doi:10.1073/pnas.1006461108

Russell, L. M., Hawkins, L. N., Frossard, A. A., Quinn, P. K., & Bates, T. S. (2010). Carbohydrate-like composition of submicron atmospheric particles and their production from ocean bubble bursting. *Proceedings of the National Academy of Sciences of the United States of America, 107*(15), 6652-6657. doi:10.1073/pnas.0908905107

Russell, L. M., Takahama, S., Liu, S., Hawkins, L. N., Covert, D. S., Quinn, P. K., & Bates, T. S. (2009). Oxygenated fraction and mass of organic aerosol from direct emission and atmospheric processing measured on the R/V Ronald Brown during TEXAQS/GoMACCS 2006. *Journal of Geophysical Research: Atmospheres, 114*(D7). doi:10.1029/2008jd011275

Saliba, G., Chen, C.-L., Lewis, S., Russell, L. M., Quinn, P. K., Bates, T. S., . . . Behrenfeld, M. J. (2020). Seasonal Differences and Variability of Concentrations, Chemical Composition, and Cloud Condensation Nuclei of Marine Aerosol Over the North Atlantic. *Journal of Geophysical Research: Atmospheres, 125*(19), e2020JD033145. doi:10.1029/2020JD033145

Seagrave, J., McDonald, J. D., Bedrick, E., Edgerton, E. S., Gigliotti, A. P., Jansen, J. J., . . . Mauderly, J. L. (2006). Lung Toxicity of Ambient Particulate Matter from Southeastern U.S. Sites with Different Contributing Sources: Relationships between Composition and Effects. *Environmental Health Perspectives, 114*(9), 1387-1393. doi:doi:10.1289/ehp.9234

Shuman, M. (2022). Can State Parks close 130 acres of Oceano Dunes to off-road riding? Here's what judge ruled. Retrieved from https://www.sanluisobispo.com/news/local/environment/article260387202.html

SLOAPCD. (2007). Nipomo Mesa Particulate Study (Phase 1). Retrieved from https://storage.googleapis.com/slocleanair-org/images/cms/upload/files/Phase1PMStudyReport2.pdf

SLOAPCD. (2010). South County Phase 2 Particulate Study. Retrieved from https://www.slocleanair.org/air-quality/oceano-dunes-efforts/south-county-phase2-particulate-matter-studyphp.php

SMG Consulting. (2017). Oceano Dunes Economic Impact Analysis Report 2016-2017. Retrieved from https://ohv.parks.ca.gov/pages/1170/files/Final-Oceano_Dunes_SVRA_2016_2017_3-5-18.pdf

SOA. (2018). *Stipulated Order of Abatement 17-01* Control District Hearing Board, April 30, 2018. Retrieved from https://ohv.parks.ca.gov/pages/1140/files/07-28-2021-5C-Stipulated%20Order%20of%20Abatement.pdf

SOA. (2022). Scientific Basis for Possible Revision of the Stipulated Order of Abatement (SOA). Retrieved from https://ohv.parks.ca.gov/pages/1140/files/Memo%20Scientific%20Basis%20for%20Possible%20Revision%20of%20the%20Stipulated%20Order%20of%20Abatement%20(SOA).pdf

Solomon, P. A., Crumpler, D., Flanagan, J. B., Jayanty, R. K. M., Rickman, E. E., & Mcdade, C. E. (2014). U.S. National PM2.5 Chemical Speciation Monitoring Networks—CSN and IMPROVE: Description of networks. *Journal of the Air & Waste Management Association, 64*(12), 1410-1438. doi:10.1080/10962247.2014.956904

Stein, S. E., & Scott, D. R. (1994). Optimization and testing of mass spectral library search algorithms for compound identification. *Journal of the American Society for Mass Spectrometry, 5*(9), 859-866. doi:10.1016/1044-0305(94)87009-8

Takahama, S., Johnson, A., & Russell, L. M. (2013). Quantification of Carboxylic and Carbonyl Functional Groups in Organic Aerosol Infrared Absorbance Spectra. *Aerosol Science and Technology, 47*(3), 310-325. doi:10.1080/02786826.2012.752065

Tolocka, M. P., Peters, T. M., Vanderpool, R. W., Chen, F.-L., & Wiener, R. W. (2001). On the Modification of the Low Flow-Rate PM10 Dichotomous Sampler Inlet. *Aerosol Science and Technology, 34*(5), 407-415. doi:10.1080/02786820119350

Triantafyllou, E., Diapouli, E., Tsilibari, E. M., Adamopoulos, A. D., Biskos, G., & Eleftheriadis, K. (2016). Assessment of factors influencing PM mass concentration measured by gravimetric & beta attenuation techniques at a suburban site. *Atmospheric Environment, 131*, 409-417. doi:https://doi.org/10.1016/j.atmosenv.2016.02.010

Usher, C. R., Michel, A. E., & Grassian, V. H. (2003). Reactions on Mineral Dust. *Chemical Reviews, 103*(12), 4883-4940. doi:10.1021/cr020657y

Wan, K. X., Vidavsky, I., & Gross, M. L. (2002). Comparing similar spectra: From similarity index to spectral contrast angle. *Journal of the American Society for Mass Spectrometry, 13*(1), 85-88. doi:10.1016/S1044-0305(01)00327-0

Worsham, K. (2020). Air Quality Alert issued for SLO County due to smoky skies. Retrieved from https://www.ksby.com/weather/fire-watch/air-quality-alert-issued-for-slo-county-due-to-smoky-skies

Xia, K., Mei, S.-S., Liu, C.-C., Liu, H., Yuan, R., & Liu, S. (2022). Characterization of the organic functional group composition and sources of summertime aerosols in an eastern city of China. *Atmospheric Environment, 277*, 119078. doi:https://doi.org/10.1016/j.atmosenv.2022.119078

Zhang, W., Tong, Y., Wang, H., Chen, L., Ou, L., Wang, X., . . . Zhu, Y. (2014). Emission of Metals from Pelletized and Uncompressed Biomass Fuels Combustion in Rural Household Stoves in China. *Scientific Reports, 4*(1), 5611. doi:10.1038/srep05611

Conclusions

Ambient atmospheric and generated primary marine aerosol particles collected over five field studies were characterized using complementary instrumentation to identify the sources and composition of aerosol particles within the marine boundary layer. The first chapter focused on the seasonality of primary marine aerosol in the North Atlantic. The second chapter investigates the evolution of the chemical composition from seawater particle composition to atmospheric aerosol particle composition using a combination of FTIR and STXM-NEXAFS. The third chapter identifies sources and both organic and inorganic composition of aerosol particles in the Oceano Dunes. The objective of these studies is to understand the variability in organic composition of marine aerosol as it relates to seasonality and location.

The first chapter used measurements during the 2015-2018 North Atlantic Aerosol and Marine Ecosystem Study (NAAMES). This study was designed to identify how the seasonal changes in marine ecology affect atmospheric chemistry. The four cruises encountered a wide range of biological and meteorological conditions, however the atmospheric primary marine aerosol (aPMA) had similar composition which was 78% hydroxyl, 10% alkane, 6% amine, and 7% carboxylic acid functional groups, which is consistent with previous marine studies. The organic mass (OM) concentrations from each season were compared and were not statistically different ($p>0.01$). The seasonal averages of gPMA OM/Na showed negligible differences, however more pronounced seasonal differences were seen in higher latitudes (>47°N).

The second chapter used measurements from the Autumn 2017 and Late Spring 2018 NAAMES campaigns. This study was designed to identify how the organic composition of particles changed as they traveled from the seawater, through the microlayer, and ultimately ejected into the atmosphere. Scanning transmission X-ray microscopy with near-edge absorption

fine structure (STXM-NEXAFS) measurements were collected to investigate the organic evolution in bulk (FTIR) and individual particles (STXM-NEXAFS). Hydroxyl and alkane functional groups were identified by both instruments with hydroxyl groups comprising 50-90% of the quantified OM. The sea-surface microlayer and ambient atmospheric aerosol show a much larger range in alkane/hydroxyl group ratios than seawater and gPMA samples. The sea-surface microlayer and ambient atmospheric aerosol alkane/hydroxyl group ratios also showed weak positive correlations with biological tracers that were not present for seawater and gPMA samples, suggesting that the SML was an important contributor of atmospheric aerosol particles. A variety of particle types were identified with eight STXM-NEXAFS clusters, with no cluster containing only one sample source, other than an outlier cluster, Csalt, which was only found in one sample.

The third chapter used observations from the Oceano Dunes from May 2019 to May 2021 with measured PM2.5 and PM10 particle composition. The focus of this study was to chemically speciate the PM2.5 aerosol, which are relevant to human health and regulated federally, to inform the California Parks Department. Up to 14% of the PM2.5 composition during the five-campaign average was comprised of dust with the remaining components being sea salt (9%), non-sea salt sulfate (4%), organic mass (8%), and unidentified/semivolatile (66%) relative to BAM PM2.5. There was no statistical difference ($p>0.05$) between any of the PM2.5 measured components during the week or weekend, suggesting that the sources are mostly natural, as was further supported by the moderate correlation of both dust and semivolatile/unidentified components to windspeed (0.65 and 0.45). Overall, these results suggest the air quality in the region has mostly natural sources which have not been shown to include toxic components.

The measurements presented in this dissertation contribute to a better characterization of the contribution of organic aerosol composition in both the North Atlantic and coastal Pacific marine boundary layer and the transfer of said organics to the marine boundary layer. These measurements can help provide a better constraint on modeling aerosol-cloud interactions, kappa calculations, and the climactic impact these particles play.

There are several ways in which additional measurements could be made to disentangle some of the topics addressed in this dissertation. One experiment, likely in a wave flume, would be to analyze sea-surface microlayer samples while simultaneously sampling ambient air in order to disentangle secondary processing, including photo-oxidation, that could be contributing to the heterogeneity observed in both atmospheric ambient samples and sea-surface microlayer samples that could not be constrained in the field. An additional study to ascertain the relationship between marine ecology and atmospheric aerosols could be conducted in a remote environment, possibly the Labrador Sea or the Southern Ocean, and utilize a Lagrangian course. This would aid in the number of 'marine' air samples, due to the remote location, and enable the measured air to be more related to the biology sampled, whereas a more conventional cruise track is sampling air from a wide variety of sources that may be un-related to the biology measured at the ship. This would be even better implemented if the biology measured was using flow cytometry and other real-time methods towards the top of the water column. Dimethyl sulfide remains one of the clearest links between phytoplankton activity and both aerosol composition and CCN activity. Simultaneous DMS and DMSP measurements in both the seawater and the MBL would facilitate a clearer comparison between the ocean ecology and atmospheric chemistry. This information could be used to constrain the complex relationships between the dissolved and

particulate matter in the ocean that is transferred to the marine boundary layer and how these relationships will be impacted because of climate change.